A Layered Approach to Artifact Rejection in Neural Stimulation and Recording

A thesis submitted by

Hailey DiSpirito

in partial fulfillment of the requirements for the

degree of

Master of Science

in

Biomedical Engineering

Tufts University

[August 2015]

Adviser: Sameer Sonkusale

Abstract

Neural stimulation is a developing treatment to several disorders. The neural response is recorded to monitor the patient's response. The field goal is to create an adaptable, closed-loop system. The stimulation pulse creates an artifact that interferes with the recording by causing amplifier saturation, making it hard to observe the neural response. This makes it hard to create a closed-loop system. Means of artifact reduction are currently researched, none of which are ideal. This thesis examines a layered approach to artifact rejection, combining techniques: blanking, lowered amplifier gain, and high dynamic range. This method was tested using a custom circuit board and compared to a commercially available recording amplifier, to find that the layered approach recovered to record 2x faster than commercial amplifier. The method was implemented on a smaller scale using an integrated circuit recording amplifier, with recovery time of 2ms, which is enough time to record the neural response.

Acknowledgements

Thank you to my fiancé, Daniel Jordan, for supporting me and encouraging me during my Master's work. Thank you to my parents for providing me with support and guidance throughout my education, and for being strong role models. Thank you to John Lachapelle for your valuable expertise and guidance during my thesis work. Thank you to my advisors at Tufts University, Professor Sameer Sonkusale and Professor Mark Cronin-Golomb, for providing feedback and advice. Finally, thank you to C.S. Draper Laboratory for providing me with the unique opportunity to learn and grow as a part of the Draper Laboratory Fellowship Program.

Table of Contents

List of tables

List of figures

1 Introduction

1.1 Neural stimulation and recording

The goal of neural stimulation is to treat disorders of the nervous system by modulating neural activity using electrical stimulation (Anikeeva, et al., 2013). The implementation of neural stimulation as a disease treatment and therapy is a developing solution to several disorders. As part of ongoing research in neural stimulation, it is common to record how neurons respond to electrical stimulation with a goal of examining how the The neural response to the stimulation is recored with a goal of examining it to see how the treatment is affecting the patient in order to adjust stimulation parameters (Lo & Liu, 2013).

The overall goal in the field of neural stimulation and recording is to use these two techniques together in order to create a closed loop, adaptable, implantable system, as shown in **Figure 1** (Harrison, et al., 2007). This type of system would be fully implantable. A stimulation pulse would be sent to the electrodes near the targeted neurons, and would evoke a neural response. The response would then be recorded, and the stimulation parameters would be adapted based on this response. The parameters of interest include but are not limited to pulse amplitude and duration, frequency, and number of pulses in a train.

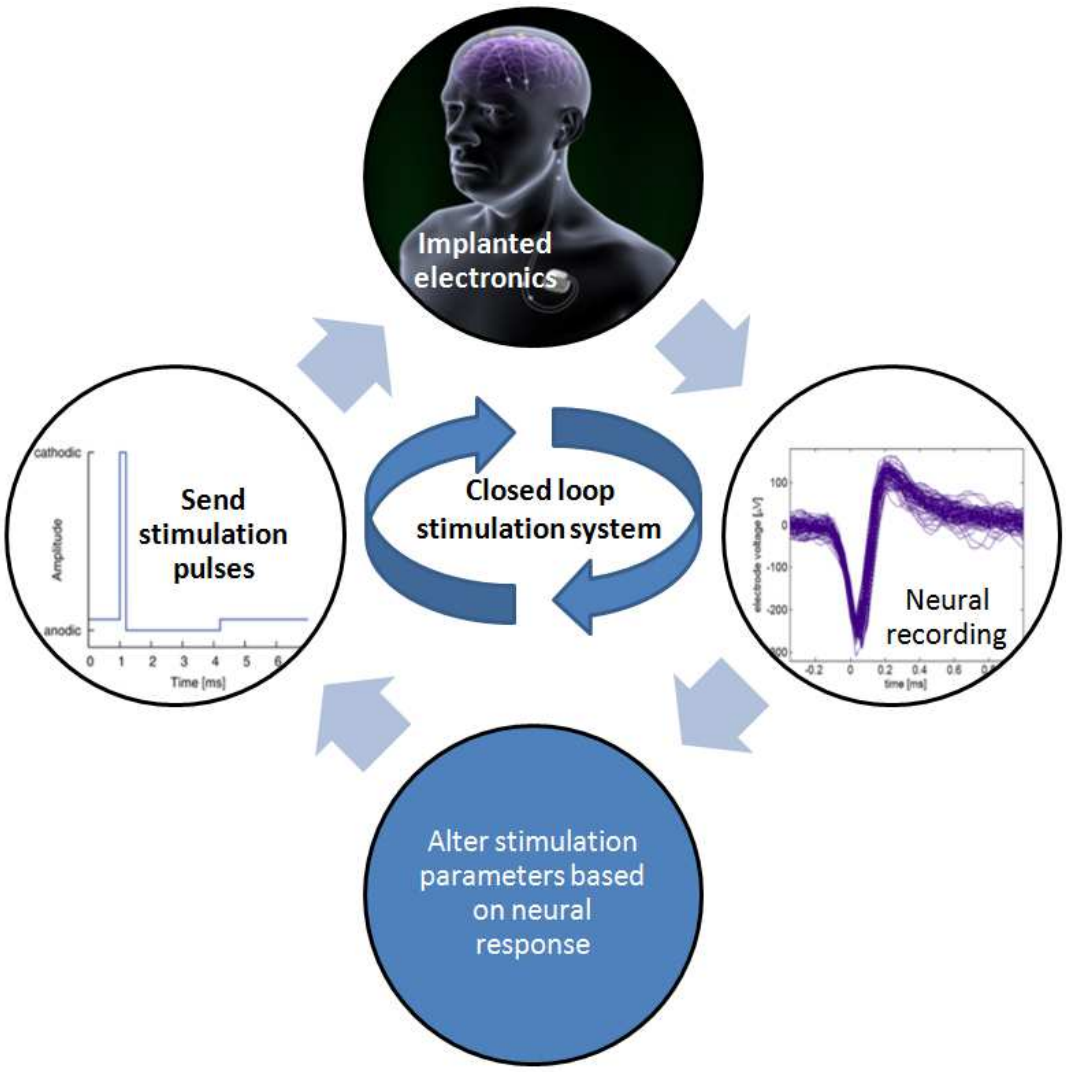

Figure 1: Closed loop neural stimulation and recording system which is fully implantable because the pulse parameters adapt based on the neural response (Hofmann, Ebert, Tass, & Hauptmann, 2011) (alzforum.org)(Intan Technologies, LLC, 2014).

Although neural stimulation and recording are currently researched for disease treatment, they are not perfect techniques. The stimulation pulse creates an artifact that can interfere with the neural recording by causing amplifier saturation, making it hard to observe the neural response to stimulation. In turn, this makes it hard to create a closed loop system. Researchers currently are examining different methods, none of which are ideal, to reduce the stimulation

artifact in order to better observe the neural response. The goal of this thesis is to provide increased artifact reduction by using a layered approach, or a combination of several techniques to reduce the artifact, instead of a single technique on it's own.

1.2 Chapters of the thesis

In Chapter 2, the current research in the field of neural stimulation and recording is discussed in more detail, as well as the problems encountered when using these techniques. Chapter 3 describes the approaches researchers are taking to eliminate these problems, along with a further description of my approach and how it is improved upon current research methods. The materials and methodology I used to implement my approach are introduced in Chapter 4. Chapter 5 includes the results of my experimentations and success of my approach, and Chapter 6 is the conclusion to my work.

2 Neural Stimulation and Recording

2.1 Uses of neural stimulation and recording

2.1.1 Diseases and disorders being treated

The implementation of neural stimulation as disease treatment or therapy is a developing solution to several problems such as depression and Parkinson's disease, as seen in **Figure 2**.

A biphasic stimulation voltage or current is applied to an implanted electrode in the brain for symptom reduction, such as tremor, in patients with Parkinson's Disease (Temel, et al., 2004). This treatment is known as Deep Brain

Stimulation (DBS). It involves a system made up of an electrode (implanted in either the globus pallidus interna or subthalamic nucleus), an implantable pulse generator (IPG), and extension wires (connection between the electrodes and IPG). DBS is an example of cortical stimulation.

Neural stimulation is also currently being used in cochlear implants to examine the auditory response to an electrical stimulus. In retinal prosthesis that are used to treat degenerative disorders of the eye, electrical stimulation is used to evoke a response to light(Weiland, et al., 2003). Electrical stimulation of the muscles is also used as a form of physical therapy and rehabilitation for athletes, which is minimally invasive and an example of peripheral stimulation.

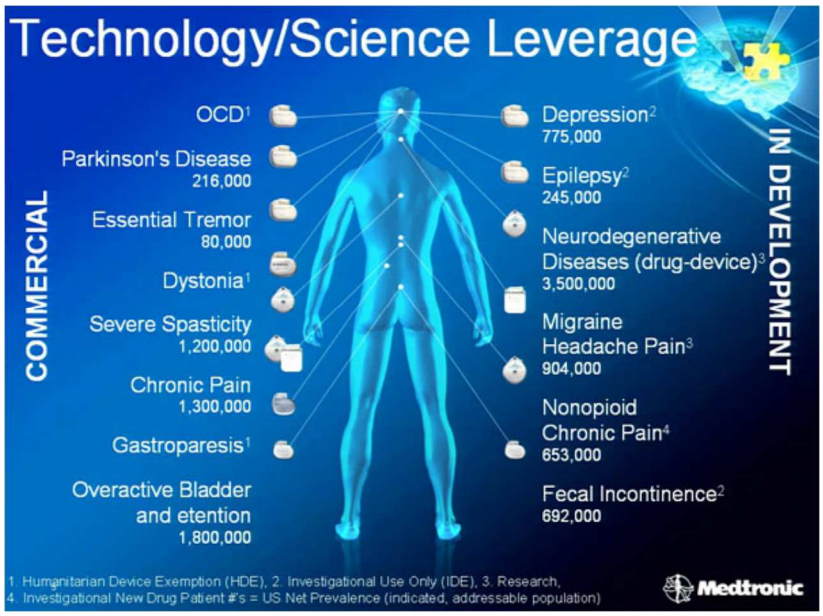

Figure 2: Electrical stimulation can be used to treat a variety of conditions, including but not limited to the disorders mentioned in the figure.

2.1.2 Signals of interest during recording

Neural recording is used to examine two types of signals: action potentials, or spikes, and local field potentials (LFP). Neural spikes are higher frequency signals, with a typical range of 300-600Hz. The spikes are recorded to examine a single unit firing. LFPs are low frequency signals, typically between 1-200Hz. These signals are recorded in order to examine information and firing patterns of a group of neurons as opposed to a single neuron (Lopez, Prodanov, Braeken, & Gligorijevic, 2012).

2.1.3 Field goal: simultaneous stimulation and recording to achieve closed loop system

In order to learn more about how this technique works to treat diseases, and to create a closed loop system, researchers are working to determine the physiology behind stimulation (Blum, Ross, Das, Brown, & DeWeerth, 2004). There is ongoing research to simultaneously stimulate and record at different locations in the body, including but not limited to the retina, cochlea, and brain (Gosselin, 2011). Simultaneously stimulating and recording the brain gives insight into the neural response to an electrical pulse (Limnuson, Lu, Chiel, & Mohseni, 2013). The recordings also allow for a deeper understanding of how the electrical stimulation is successfully treating medical conditions (Waddell, Porr, Pratt, & Ewing, 2009).

Simultaneous stimulation and recording could allow for development of a closed-loop, implantable device that stimulates the patient and records the neural response (Nurmikko, 2015). Based on the recording, the stimulation parameters would be automatically altered to meet the patient's needs. An adaptable system

would be beneficial to patients with long term implants, so that the stimulation pulses could automatically be altered to fit their current needs at any given moment.

2.2 Artifacts: problems faced in neural stimulation and recording

Although neural stimulation is currently researched for disease treatment, it is not a perfect technique. The use of electrical stimulation is currently limited because the underlying mechanisms are not completely understood (McConnell, So, Hilliard, Lopomo, & Grill, 2012). This makes it so that it is hard to determine the correct stimulation parameters (Kuncel & Grill, 2004).

The reason for this is that there are several types of noise present during simultaneous stimulation and recording. The noise seen in the recorded unfiltered signal may include but is not limited to 60 Hz noise, device 1/f noise, muscle movement noise from an electromyographic signals (EMG), and a stimulation artifact (Junghofer, Elbert, Tucker, & Rockstroh, 2000) (Yazicioglu, Merken, Puers, & Van Hoof, 2007). These different types of noise encountered in a neural recording are displayed with typical amplitudes and frequencies in a plot in **Figure 3.**

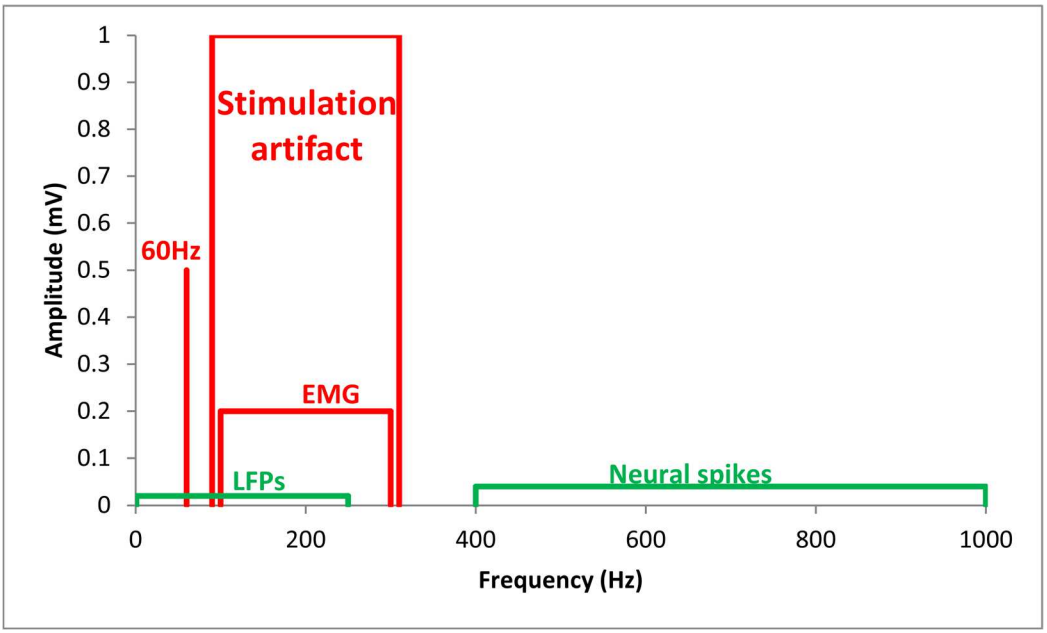

Figure 3: A plot showing the wide range of overlapping frequencies and amplitudes of the noise experienced during neural recording (red) and the signals of interest (green) (Yoshida & Stein, 1999).

2.2.1 The presence of the stimulation artifact

For my thesis, I will be focusing on the presence of the stimulation artifact. A stimulation artifact results from the stimulation and is picked up on the neural recording (Brown E. A., 2008). The artifact has a large amplitude of up to 1V, while the neural response to stimulation has an amplitude of only a few µV, as shown in **Figure 4** (McGill, et al., 1982).

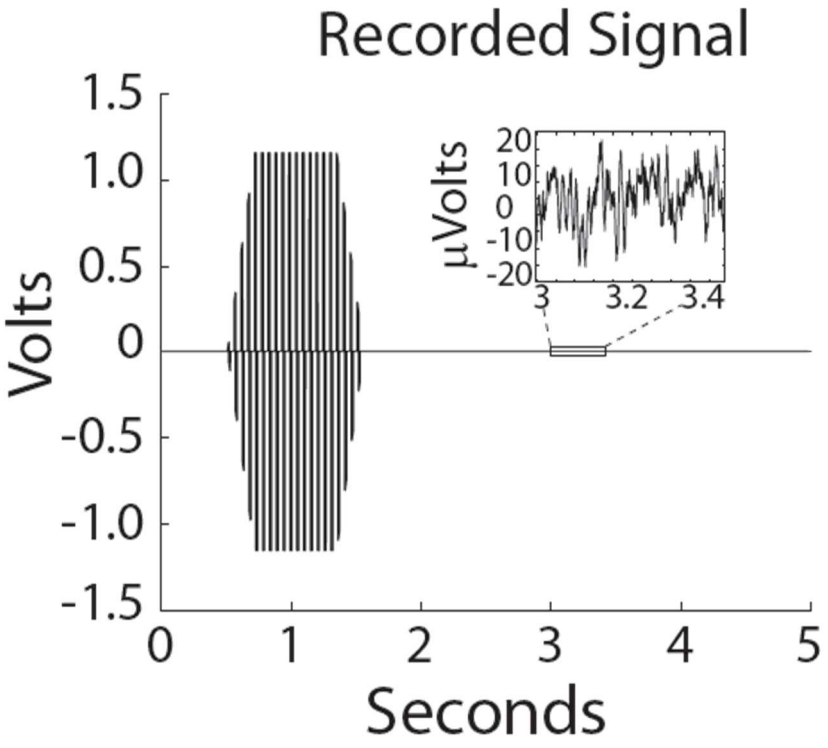

Figure 4: The demonstration of the size difference between the artifact and the neural signal: artifact is up to 1V, while the recorded neural response is only about 10 µV.

Since the stimulation artifact is larger than the recorded signal, it is hard to distinguish between the two (Al-ani, Cazettes, Palfi, & Lefaucheur, 2011). Because of the orders of magnitude in the difference in size between the two signals, it is hard to record right after the stimulation, making it difficult to understand how the stimulation is working to produce a physiological response (Nam, Brown, Ross, Blum, Wheeler, & SP, 2009).

This size difference can also cause amplifier saturation (Andrews, Kermani, Cascio, & Nagle, 1994) (Nikolic, Popovic, Stein, & Kenwell, 1994). The recording amplifier is typically set up to record small neural signals, yet the stimulation

artifact is many orders of magnitude larger than these signals so it can saturate the input to the amplifier, resulting in an unreadable signal.

The stimulus artifact can vary even when the stimulation signal amplitude and duration remains the same (Nowicki, Benabid, & Aksenova, 2007). The artifact can also vary during each pulse in a train of stimulation pulses (Nowicki, Piallat, Benabid, & Aksenova, 2008). There are several techniques that are being developed for artifact removal, each with its own set of benefits and problems, which will be discussed in the next chapter.

3 Current methods of artifact rejection

Several methods of artifact reduction are presented in research papers. These techniques reduce the artifact, but are not perfect. Often times, the removal takes place during post-processing of the data. This would not work for a real-time closed loop system. Also, this type of removal does not eliminate amplifier saturation. The three main methods of artifact rejection include filtering, template subtraction, and artifact blanking. The goal of this thesis is to use a layered approach instead of a single approach to artifact rejection, in order to further reduce the artifact.

3.1 Filtering the artifact

Filtering the stimulation artifact from the recorded neural response is the most common method of artifact rejection (Libbus & Boon, 2012) (Aksenova, Nowicki, & Benabid, 2008). This method is most successful when there is a separation in time between the stimulus artifact and the recording. In the case of

a time overlap between the artifact and recorded signal, filtering may result in distortion of the recorded signal (Nagel, 2000). In the same instance, if the signal is completely preserved, parts of the stimulus artifact might be left over (Nagel, 2000). The artifact is filtered after the recordings are completed, using a type of post-processing software, such as MATLAB. An example of a filter applied to recorded date can be seen in **Figure 5.**

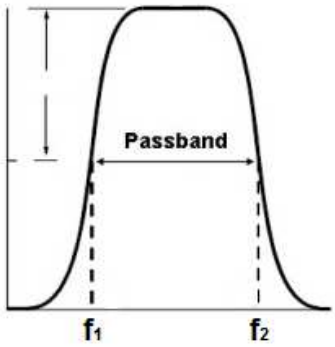

Figure 5: Example of a filter that could be used to remove artifacts from neural recordings.

3.2 Template subtraction

Template subtraction is a second method used for artifact rejection. The artifact shape is required knowledge in order to perform template subtraction. In order to determine the artifact shape, the artifact is recorded and averaged to be used to remove the artifact (Montgomery, Gale, & Huang, 2005). The template subtraction method has been used for artifact removal at stimulation frequencies of up to 1 kHz (Zhang, Miller, Robinson, Abbas, & Hu, 2007)(Miller, Abbas, Robinson, Rubinstein, & Matsuoka, 1991). At stimulation frequencies as high as 5 kHz, template subtraction fails to completely remove the artifact from the recorded signal because the neural response is overlapping the stimulation

parameters (Heffer & Fallon, 2008). Digital filtering may be useful in this case to remove the remnants of the artifact (Heffer & Fallon, 2008).

Template subtraction can be applied to the signal during post-processing, after the recording is completed (Hashimoto, Elder, & Vitek, 2002). Since this technique is used during post-processing, the artifact can still saturate the amplifier inputs. It also would not work in a closed loop system, because it would not be real time. The data would need to be recorded and stored, then artifact removal would take place after the process (Wichmann & Devergnas, 2011).

Zhang et al. predicted the shape of the artifact to use as a template in a research paper regarding auditory recordings (Zhang, Miller, Robinson, Abbas, & Hu, 2007). In order to predict the artifact shape, Zhang et al. used a threshold spike amplitude detection to find recorded signals that did not include neural responses (Zhang, Miller, Robinson, Abbas, & Hu, 2007). Several of these traces were averaged to create the template used for subtraction. Another option for generating an artifact template involves template optimization. This method is not as practical because it increases the computational time. The increase in computation time occurs because template optimization requires data to be collected during each stimulus signal. This data is then averaged to create the optimal template for each stimulation signal (Heffer & Fallon, 2008). When analyzing with large amounts of recorded data, predicting the template prior to recording was found to be more efficient method of template subtraction (Heffer & Fallon, 2008).

3.3 Artifact blanking

The sample and hold method, or blanking, is another option for stimulus artifact rejection. In this method, the recording circuitry is set to "hold" mode, where the inputs are turned off by being shorted to ground, before stimulation takes place, as seen in **Figure 6** (O'Keeffe, Lyons, Donnelly, & Byrne, 2001). This prevents the amplifier from recording the artifact and saturating the amplifier inputs.

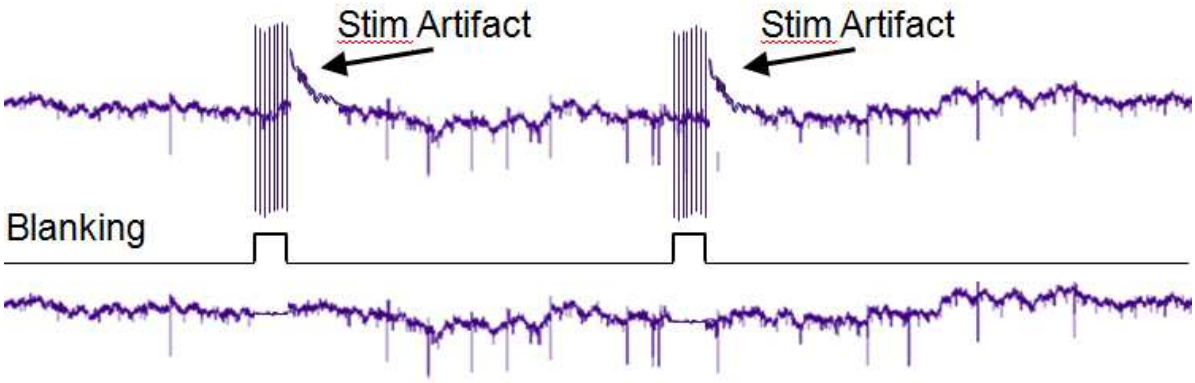

Figure 6: Blanking technique for artifact rejection, illustrated in a commercially available neural recording amplifier chip. The top is showing how the stimulation artifact is recorded without blanking; the middle shows the trigger to enable blanking; the bottom shows what the recording would ideally look like with blanking (no artifact or recovery time).

Once the stimulation signal is sent, the recording circuitry is changed back to "sample" mode, and records the neural response to the stimulus (Heffer & Fallon, 2008). This method has been found to work when the artifact and the recorded signal are not overlapping in time. The problem with this method is that if the artifact signal is overlapping the neural response, part of the neural response will be lost while the circuit is set to blank, or "hold." Another similar issue is that

if the duration of the blanking period is too long, the neural response to the stimulation may not be recorded at all (Heffer & Fallon, 2008). On the other hand, if the duration of the hold is too short, artifacts will remain in the recorded signal (Heffer & Fallon, 2008). The blanking technique is applied to the signal during the recording process, at the first stage of amplification.

3.4 General problems with these methods for artifact rejection

Many of the currently available techniques for artifact rejection take place during post-processing, after all of the data has been collected. This type of artifact removal causes the following problems:

1. The artifact, with amplitude of around 1V, is several orders of magnitude larger than the recorded neural signal. This causes amplifier saturation during recording (Brown, Ross, Blum, Nam, Wheeler, & DeWoorth, 2008).
2. Artifact removal after all of the recording has taken place does not allow for adaptive, closed-loop stimulation and recording because the amplifier saturation from the artifact makes it hard to examine the neural response.

3.5 Thesis technique: a layered approach to artifact rejection

In order to address the previously mentioned problems and to improve the ability to reduce artifacts, a layered approach to artifact rejection was examined. The artifact removal takes place over the course of the recording, and would include removal in the spatial domain, the frequency domain, and the time

domain, as seen in **Figure 7.** The goal of this process is to avoid amplifier saturation during recording in order to examine the neural response to a stimulation pulse or pulse train. There are several components of the layered approach to artifact rejection, including electrode placement, lowering amplifier gain, increasing dynamic range, and blanking. Each step theoretically would reduce the artifact along the way. Together, these steps would work to stop the artifact from saturating the amplifier, and decrease the recovery time after stimulating in order to observe the direct neural response to stimulation.

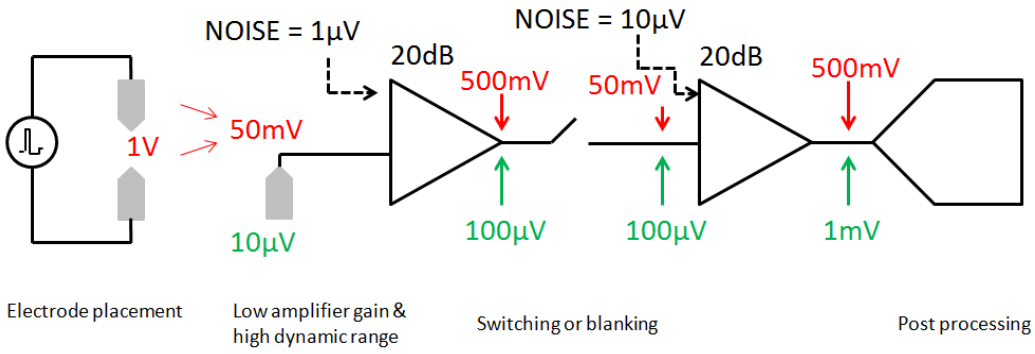

Figure 7: A layered approach to artifact rejection takes place throughout the recording process in the spatial domain, frequency domain, and time domain. The theoretical artifact reduction throughout the process is shown above as well. Green is the neural signal level and red is the artifact level throughout the process.

3.5.1 Electrode placement

Beginning artifact rejection in the spatial domain, electrode placement and bipolar stimulation are key components to reducing the artifact to less than 100 mV before the initial recording stage, as seen in **Figure 7**. This would help to eliminate amplifier saturation. As seen in **Figure 8**, when the recording electrode

is placed in the middle of the two stimulation electrodes (set up in a bipolar configuration) the maximum artifact can be reduced to around 10mV, which is about a 20dB drop in amplitude. This occurs because the electrode placement creates a dipole, which effectively reduces the artifact level.

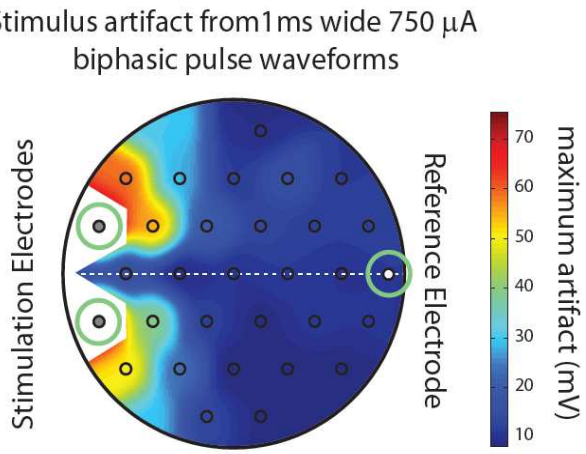

Figure 8: Bipolar stimulation and recording setup shows that the reference electrode is ideally placed in the middle of the stimulation electrode and the return electode (Data collected by Jesse Wheeler, Draper Labs).

3.5.2 High dynamic range and low gain amplifiers

The layered approach also includes using low first stage gain and parts with a high dynamic range. Reducing amplifier gain improves artifact processing, at a small cost of an increase in power for a reduction in second stage noise. A small decrease of amplifier gain in the first and second stages allows linear processing of neural signals mixed with artifacts. Lowering amplifier gain to reduce artifacts is successful if the amplifier has a low noise floor or if the neural signal is greater in magnitude than the noise floor. This is important because when the noise interferes with the neural signals, they can become unrecognizable since the noise

has a much greater magnitude. Additionally, the ADC used for processing needs to have improved noise when the amplifier gain is decreased. In addition to reduction in amplifier gain, increased dynamic range allows linear processing of both wanted signals and artifacts. If the dynamic range is large, artifact signals would not be as likely to saturate the amplifier.

3.5.3 Enhanced artifact blanking

Finally, the layered technique incorporates blanking at the input of the second stage amplifier. The low gain and high dynamic range on the first stage amplifier make it so that the blanking can occur on the second stage without the stimulation artifact saturating the first stage inputs. As previously mentioned, blanking occurs when the inputs to the amplifier are shorted to ground during a stimulation pulse, and then are opened back up to record when the stimulation is over. Blanking can result in a separate artifact that is the recovery time of the recording.

4 Methods/Materials

In order to examine a layered approach to artifact rejection in neural stimulation and recording, several steps were necessary. This chapter describes the methodology behind the experiments of the thesis. The first experimentation was examining a stimulation artifact in vitro in order to better understand what the characteristics are. Next, a stimulation and recording board was designed using a commercially available neural amplifier with built in blanking for artifact rejection. This board was tested in vivo in order to evaluate

the degree of artifact reduction. Another board was designed using commercially available operational amplifiers in order to implement the layered approach to artifact rejection to collect data and see if this rejection technique improved upon artifact reduction. Finally, the layered approach was implemented on a much smaller scale on an integrated circuit. This integrated circuit was placed on a board and tested in vitro and in vivo to determine the level of success of the layered approach to artifact rejection.

4.1 Initial Artifact Data Collection in Vitro

In order to gather some initial data and examine artifact variation with stimulation pulse amplitude, a saline tank setup was used to stimulate and record. The saline used for all testing was phosphate buffered saline with calcium chloride and magnesium chloride. The electrodes used in the saline tank were deep brain stimulation electrodes. Saline is commonly used as a "phantom brain" for in vitro testing because it has similar conductivity to the brain (Chew, Sudirman, Seman, & Yong, 2013). In vitro artifacts were collected using a fully differential amplifier from Texas Instruments. The CSI021 stimulator integrated circuit (IC) designed by Cactus Semiconductor was used to send stimulation pulses. The pulses that this chip generates were designed so that the anodal portion was delivered first. The amplitude of the stimulation pulse was programmable using LABVIEW. A stimulation pulse with constant duration pulse of 500 µs was used, and stimulation amplitudes tested were 1 mA, 2 mA, and 10 mA. A diagram of the saline tank setup with approximate electrode placement is shown in **Figure 9.**

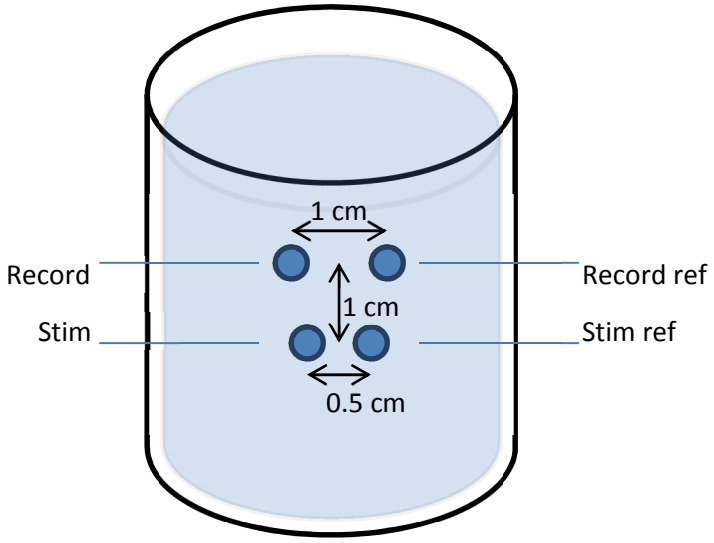

Figure 9: In vitro stimulation and recording setup using separate electrodes for stimulation and recording.

4.2 Stimulation and recording board using a commercially available neural recording amplifier

A stimulation and recording board was built for in vivo testing at Mass General Hospital (MGH). **The goal of this testing was to examine artifacts recorded in vivo using a commercially available amplifier chip that had blanking as an artifact rejection technique.** The board was designed using Mentor Graphics, and the finished product is shown in Appendix A.

4.2.1 Board design and in vitro testing

The stimulation integrated circuit used on the board was CSI021 (Cactus Semiconductor), and the recording chip was the RHD2216. The RHD2216 has 16 differential recording amplifiers, and a built in method for artifact rejection. The artifact rejection is a “fast settle” (or blanking) button, which sets the recording

amplifier up for blanking for the duration of stimulation. This rejection is hardware triggered, and shorts the inputs of the first stage amplifiers to ground.

The board was built with jumpers to allow the first 4 amplifier channels to be configured to perform single-ended recording. The jumpers act like a multiplexer on the first four channels of the amplifier. They are set up to give the user the option to manually change them to set the channel as either fully differential recording, single ended recording, stimulation, or a stimulation reference. The other 12 channels are brought directly out to a header that can be connected to the electrodes in order to keep the size of the board down.

The board was setup for bench top testing in saline to verify functionality before in vivo testing. The Intan evaluation board was used to control the RHD2216. The evaluation board has an Opal Kelly FPGA on board, and comes with software that was used to record. The software allows for bandwidth selection and the addition of a notch filter. The software also gives the user the ability to select how the fast settle is triggered.

For the stimulation side of the board, the Atmel XMEGA-E5 XPLAINED evaluation board was connected to control the CSI021. The user interface was designed to be straightforward. It allowed the user to select the amplitude of stimulation, the pulse width, the frequency, and the pulse count. The user also had the option to select a blanking pre-delay and post-delay, as well as enable blanking for the entire stimulation train or over each individual pulse. In order for the fast settle trigger to work, a connection was made between the output of the

Atmel evaluation board and the Intan evaluation board. The software user interface for controlling the CSI021 is shown in Appendix A.

4.2.2 In vivo rodent testing at Mass General Hospital

After in vitro testing using saline, the board was tested in rodents at MGH to verify functionality and examine artifacts. The rodents used for testing had chronically implanted deep brain stimulation electrodes. The electrodes had two contacts that were connected to the amplifier channels, and the third contact was a ground electrode. The testing setup is shown in Appendix A. Sixteen different tests were conducted on the board, including recording, stimulation, and combinations of both. The test specifications are shown in Appendix A. Upon arrival at the testing location, it was noted by MGH staff that the electrode connections were not 100% reliable because they had been implanted for a long period of time. The board was plugged into the implanted electrodes using a custom connector. The rodent was placed on a table and allowed to move freely during testing. All recordings were done at a sampling rate of 20kS/s, and the stimulation pulse width was never greater than 300µs.

4.2.3 In Vivo Non Human Primate Testing at Mass General Hospital

The stimulation and recording board that was previously tested at MGH in rodents was brought back for in vivo testing in Non Human Primates (NHP). The NHP used had a chronically implanted deep brain stimulation electrode that had been implanted for almost three years. The electrode had eight contacts total, but it was noted that some of the contacts on the electrode were broken, and the

MGH staff were unsure of which ones. A diagram of the implanted electrode is shown in Appendix A. The amplifier channels that each electrode was connected to are labeled. No amplifier channel was connected to contact 3 of the electrode because prior to testing, it was noted by MGH staff that this electrode was most likely damaged.

The board was setup and connected to the implanted electrode using an ADTECH connector that was modified on one end to plug into the board. The NHP was head fixed and was focusing on a touch screen. He was performing a task of selecting certain circles on the touch screen, and was rewarded with juice. All recordings were done at a sampling rate of 20kS/s. The digital 60Hz notch filter during recording which was selected on the Intan software was used for all testing. The different tests completed are detailed in the Appendix and the stimulation parameters used in the NHP are shown in Appendix A.

Some impedance tests were performed on the implanted electrodes and their respective connections to the stimulation and recording board. The impedance measurements were made using equipment readily available at MGH.

4.2.3.1 Electrode Impedance Measurements

In order to verify that electrodes used in vivo were acceptable to use for stimulation and recording and did not have broken contacts, impedance measurements were taken. The Intan chip has the ability to perform these measurements, and the procedure is detailed in the following paragraph. Impedance testing was performed on electrodes and resistors with known

impedances in order to verify the functionality of the impedance measurement feature.

The RHD2216 has the ability to perform impedance measurements on connected electrodes. The chip can be configured to measure the impedance when the electrode is connected to the positive or negative amplifier inputs, but the software only supports measurements made on the positive amplifier inputs. The impedance measurements are made by the software generating a small AC sine wave current and injecting this into the electrode. The resulting voltage waveform is measured by the amplifier on the RHD2216 that the electrode is connected to.

The ADTECH connector was modified so that only positive channels of the amplifier were connected to the electrode contacts. This modification made it so that the impedance of all eight electrode contacts could be measured at the same time. Before performing impedance tests on the electrodes at MGH, measurements were made on resistors, as well as a four-contact platinum iridium electrode in saline. The electrode contacts were 2mm in diameter, and the distance between the center of one contact to the center of another contact was 1 cm. The electrode used is shown in Appendix A.

For the testing, CH0 of the 16 channel differential Intan amplifier was used. A resistor was connected between the positive input and ground, and the negative input was grounded. The evaluation board software was used to take the measurement and to vary the frequency. Five resistors with different values were

measured at each of the following frequencies: 500Hz, 1kHz, 2kHz, and 5kHz. The impedance of the electrode was measured at 1kHz. According to the datasheet for the Intan evaluation board, the standard frequency for measuring neural recording electrode impedances is 1kHz (Intan Technologies, LLC, 2014). The datasheet also mentions that the best accuracy is obtained at a sample rate of 20kS/s with the measurement frequency set to no higher than 2kHz [7] At this sampling rate, impedances cannot be measured at any lower frequencies than 19.6 Hz using the Intan software.

After verifying that the impedance measurements made with the RHD2216 were accurate, the measurements were made on the electrode implanted in the NHP at MGH. The mapping of amplifier channels to electrode contacts is shown in Appendix A. Electrode impedances were measured three times at each of the following frequencies: 19.6Hz, 50Hz, 100Hz, 500Hz, 1000Hz, and 5000Hz.

4.3 Layered approach to artifact rejection recording board

After the collection of initial stimulation artifact data, a recording board with a high resolution analog to digital converter (ADC) was designed using DipTrace (DipTrace, 2015). Appendix B has block diagrams of the board and parts used. **The goal of this PCB was to implement the layered approach to artifact rejection and to collect data in order to compare this method to a commercially available neural recording amplifier with a single artifact rejection method**.

4.3.1 Board design specifications

The board had two amplifiers in order to have a pre-amplification stage and a second amplification stage. This made it so that artifact rejection could be performed in between stages to minimize the amount of the artifact amplified. The main board was built without the amplifiers, and instead had two separate stages where there were headers to plug in an amplifier so that different amplifiers could be tested if necessary. The board also had a high dynamic range ADC, LTC2378-20, on board in order to transfer the recorded data to the computer. The serial peripheral interface (SPI) connections for the ADC was brought out to headers on the board so that a microcontroller could be used to program them.

A low pass filter was designed between the output of the second amplifier stage and the input to the ADC stage of the board. The purpose of this filter was to set the upper limit of the recording bandwidth to about 5kHz. The calculation to determine appropriate part values to create this cutoff frequency is shown in the equation below, and the filter design is shown in Appendix B.

$$fc = 1 \div (2 \times \pi \times R \times C)$$

$$\sim 5kHz = 1 \div \left(2 \times \pi \times 2\, x\, 30.9\Omega \times \left(\frac{1\mu F}{2} + 1nF\right)\right)$$

Two separate amplifier boards were built to plug in to the main board, one for the first amplification stage and one for the second. Both were 0.7 by 0.9 inches. The amplifier chosen for the first low gain stage was the LTC6087 (Linear

Technology). The input offset current of this amplifier was 0.5pA. This amplifier was single ended, and met the following requirements:

- Rail to rail inputs and outputs
- Low input noise voltage density (12nV/rtHz)
- Low input bias current (1pA)
- Low input capacitance (2.7pF)

The low noise is necessary for neural recordings because the signals are small in amplitude, and if the noise floor of the amplifier was too high, it would corrupt the signal (Blum, Ross, Brown, & DeWeerth, 2007). A high pass filter was created using the capacitive feedback on this board in order to create the lower end of the bandwidth. The cutoff frequency was set to about 530Hz. The calculation to determine appropriate part values to create this frequency is shown below.

$$\sim 530Hz = 1 \div (2 \times \pi \times 30M\Omega \times 10pF)$$

The amplifier chosen for the second board was the OPA1632 (Texas Instruments) which is fully differential. This amplifier was chosen based on its high input impedance of 34 MΩ and low noise of 1.3 nV/rtHz. This board was designed with resistive feedback to have a gain of 10 in order to further amplify the signal before the ADC stage.

Switches were also placed on the board at the inputs to the second stage amplifier to implement blanking. The first amplifier stage had a low gain of 10 to prevent the artifact from saturating the inputs. The low gain is possible if the

neural signal is large enough to stay above the amplifier's noise floor. Another way this low gain is possible is if the noise floor of the amplifier is low, making it so that smaller neural signals will still be above the noise floor. This is important because when the noise interferes with the neural signals, they can become unrecognizable.

The bandwidth of the amplifiers was set to 500-5kHz, which is the typical bandwidth for recording neural spike activity. This bandwidth could be adjusted and lowered to accommodate low frequency potential recording if desired. It also filtered out any signals in unwanted frequency bands.

The microcontroller used to program the SPI is the ATXMEGA32E5 from Atmel. The microcontroller used was on an evaluation board, the Atmel XMEGA-E5 XPLAINED. This allowed for easy SPI connections between the evaluation board and the main amplifier board. The type of SPI used to communicate with the ADC on the main amplifier board was UART. The XMEGA board has a USB connection for power, and this is also used to transmit information back to the computer via another UART port.

In order to program the XMEGA board to read the data from the ADC on the main board, the program Atmel Studio 6.2 was used. Interrupts were used in the program in order to continuously poll the ADC for new conversions. The sampling rate used was 20kS/s. The same program was used to read the data from the XMEGA board over the USB to the computer. After some initial testing, it was determined that the XMEGA alone was not fast enough to record data at the

desired 20kS/s rate, so an FTDI breakout board was used as an intermediary between the XMEGA board and the computer. The program Realterm was used to save the recorded data as a binary file on the computer. MATLAB was used to plot the data and perform analysis and processing. Figure 10 is a picture of the test setup with saline solution and supporting circuitry for stimulation.

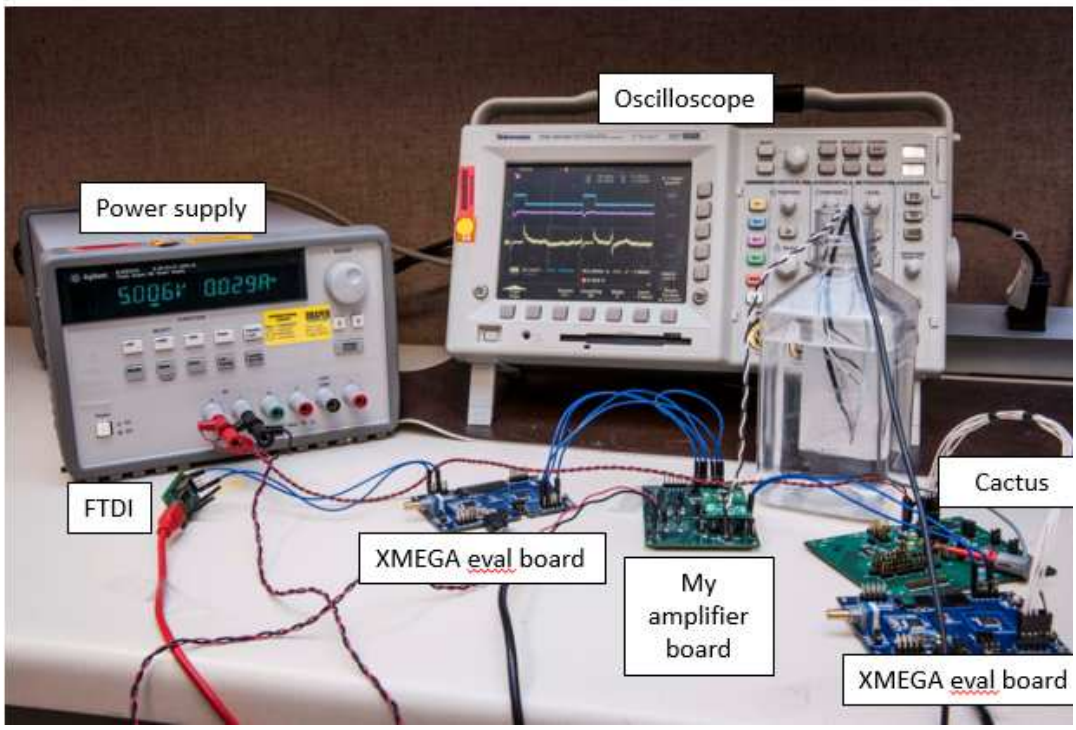

Figure 10: Artifact rejection board general test setup.

4.3.2 Artifact rejection board and intan recovery time comparison

The artifact rejection board blanking recovery time was compared to the blanking of the Intan in order to determine if the layered approach improved the recovery time of artifact blanking to allow for faster recording. In both cases, a software trigger for blanking was used that was based on the timing of the

stimulation pulse. This comparison was made to examine the different recovery times at similar bandwidths. The main difference is that the blanking with the Intan occurs at the first stage amplifier, while the blanking with the artifact rejection board is at the input to the second gain stage. The bandwidth of the artifact rejection board was set to 50Hz to 5kHz, and the bandwidth of the Intan was set to the same. The artifact rejection board was set up in saline with a single stimulation pulse and no neural signals. The stimulation pulse parameters were 1mA, 0.3ms duration. The single pulse was sent 20 times. The board was set up for blanking during the stimulation pulse. The four-contact platinum iridium electrode used for stimulation and recording is shown in Appendix B. The electrode contacts were 2mm in diameter, and the distance between the center of one contact to the center of another contact was 1 cm.

This test was repeated 20 times using the Intan board. The data was saved to MATLAB and statistically analyzed. The mean recovery times and standard deviations were plotted, and the statistical significance of the difference in recovery times between first and second stage blanking was examined.

4.3.3 Lowered gain testing

In order to test the lowered gain portion of the layered approach to artifact rejection, I reduced the first stage gain to 4.5. This made it so that the cascade gain decreased from 100 to 45. These changes were made on amplifier plug in boards, so I could swap out the stage and test using the gain of 10, and

repeat the test using the gain of 4.5. I changed the gain by changing the feedback of the amplifier.

The test setup for this portion of testing, including electrode placement, is shown in Appendix B. The stimulation current was sent into the saline using the Cactus stimulation chip. The stimulation current was increased until the amplifier was saturating. The first stage amplifier was swapped off of the main board and replaced with the amplifier with a gain of 4.5, making the total gain 45 instead of 100. The saturating current was applied to this amplifier to examine if the same current would saturate the amplifier with lower gain. The stimulation current was then increased until saturation was reached. During this testing, pre-recorded neural signals composed of both spikes and LFPs were played into the saline using an altered audio cable. The neural signals had been saved as an audio file.

4.4 Layered approach to artifact rejection amplifier IC testing

An artifact rejection amplifier IC was fabricated at Draper Laboratory. The amplifier had artifact rejection on the second stage, along with total low gain of 50, and a high dynamic range. **The goal of the amplifier IC was to implement the layered approach to artifact rejection on a smaller scale that might eventually be implantable.** The artifact rejection board was reworked to incorporate the amplifier IC instead of off the shelf amplifier parts.

4.4.1 In vitro testing using saline

The amplifier was tested in vitro using saline and the Cactus stimulation IC to send constant stimulation pulses. The amplifier output was viewed on an

oscilloscope, saved as a spreadsheet file, and plotted in Microsoft Excel. A 40µF capacitor was placed on the switching power supply on the cactus IC board to minimize 80Hz noise propagating on the stimulation output. The negative recording input was grounded, the positive recording input was connected to an electrode in saline, and the ground of the board was also connected to an electrode in the saline. The electrodes used were tungsten microelectrodes with a diameter of 90mm and an impedance of 500k-1MΩ. A function generator was used in all cases to output a sine wave into the saline solution. A diagram of the general test setup is shown in Appendix B.

Three cases were tested in saline; **case 1** was with stimulation and recording connected to the same electrode, with artifact rejection (blanking) enabled, **case 2** was with stimulation and recording connected to separate, adjacent electrodes with artifact rejection enabled, and **case 3** was with stimulation and recording connected to the same electrode with artifact rejection disabled. Stimulation parameters and sine wave parameters are shown in **Table 1.**

Table 1: Stimulation and sine wave parameters used for testing the artifact rejection amplifier IC.

Case	Stimulation parameters			Sine wave parameters	
	amplitude	width	frequency	amplitude	frequency
1	12 µA	0.3mS	10Hz	1Vpp	2.5kHz
2	12 µA	0.3mS	10Hz	200mVpp	2.5kHz
3	12 µA	0.3mS	10Hz	600mVpp	2.5kHz

4.4.2 In vivo testing at Boston University

The amplifier was tested in vivo recording from an anesthetized bird at Boston University. The neural signals being recorded from the bird were around 200µV in amplitude. Several spikes were recorded and later overlayed and plotted in MATLAB. The recording configuration was connecting the negative input to ground and the reference electrode, and connecting the positive input to a recording electrode.

5 Results

5.1 Initial artifact data collection in vitro

The saline used for all testing was phosphate buffered saline with calcium chloride and magnesium chloride. The electrodes used were platinum iridium and had four contacts. The diameter of each contact was 2 mm and the distance between the centers of two contacts was 1 cm.

The Labview recordings of the different sized artifacts were overlaid in order to compare amplitudes. The recordings show that the amplitude of the artifact does increase with increasing stimulation amplitude, as shown in **Figure 11**. The artifact resembles a decay of the stimulation pulse. A 1mA stimulation pulse produces an artifact that is about 0.4mV peak to peak. The cathode, or the small amplitude, long duration portion of the pulse, is not apparent in the artifact resulting from stimulation amplitude of 1mA. It becomes more apparent as the amplitude is increased. The 2mA stimulation pulse results in an artifact amplitude of about 0.7mV peak to peak, and the 10mA stimulation results in an artifact

amplitude of about 1.3V peak to peak. These artifacts are much larger than neural signals, which only have amplitudes of a few hundred microvolts at most. Looking at the artifacts in vivo verifies the need for artifact rejection in neural recording.

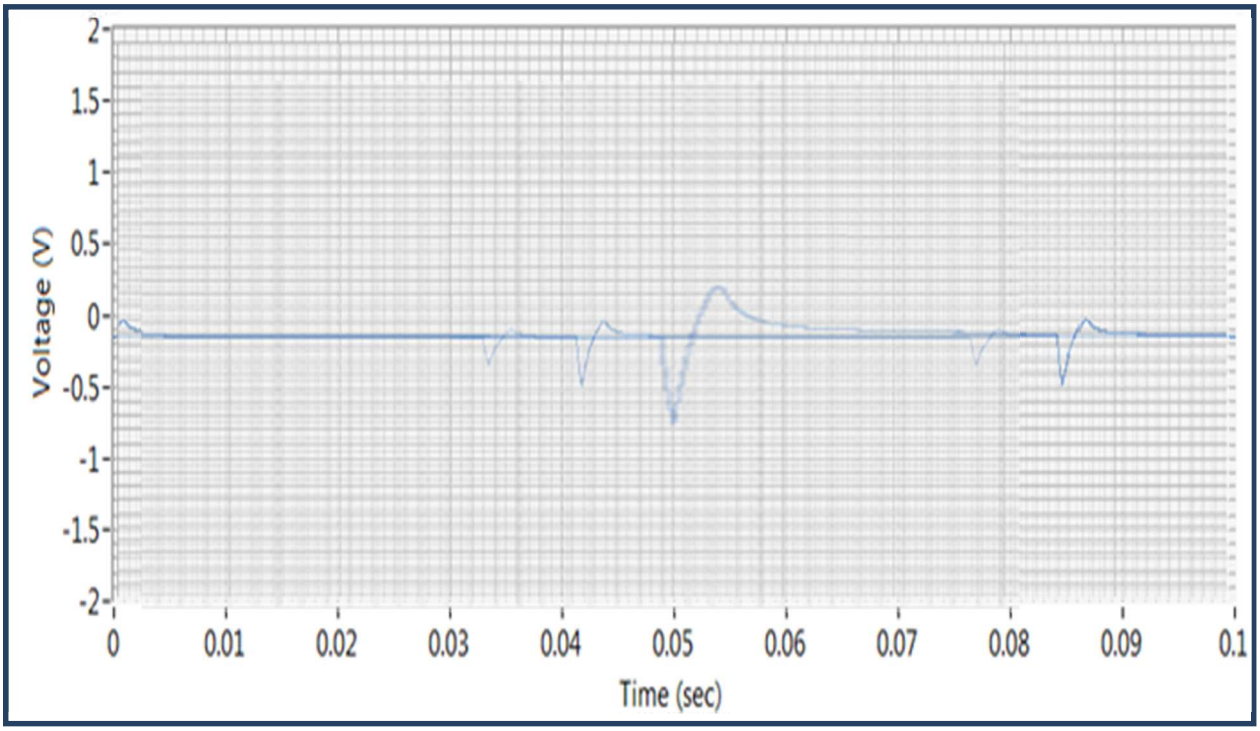

Figure 11: Artifacts recorded in vitro overlaid to show increasing amplitude with increasing stimulation amplitude. This recording was done using off the shelf parts to examine the artifact in an in vitro environment.

5.2 Stimulation and recording board using a commercially available neural recording amplifier

5.2.1 In vivo rodent testing at Mass General Hospital

Through testing in rodents, it was determined that blanking over each individual stimulation pulse with a frequency of 200Hz was not possible because the Intan did not recover in time between each pulse to record any data, as shown in **Figure 12 and Figure 13**. In this situation, blanking over the entire pulse train is

necessary, as shown in **Figure 14**. Blanking over the entire pulse train is not a perfect solution because it results in its own recovery time. The recovery time after blanking the entire pulse train is about 100ms. A solution with a shorter blanking recovery time is addressed in the design of my amplifier PCB. The recording was made at a bandwidth of 1Hz to 7.5kHz to detect LFPs. This artifact rejection method makes it so that one cannot examine the neural response to a single stimulation pulse, because the amplifier does not recover in time from the blanking artifact to record the response and blank over individual pulses.

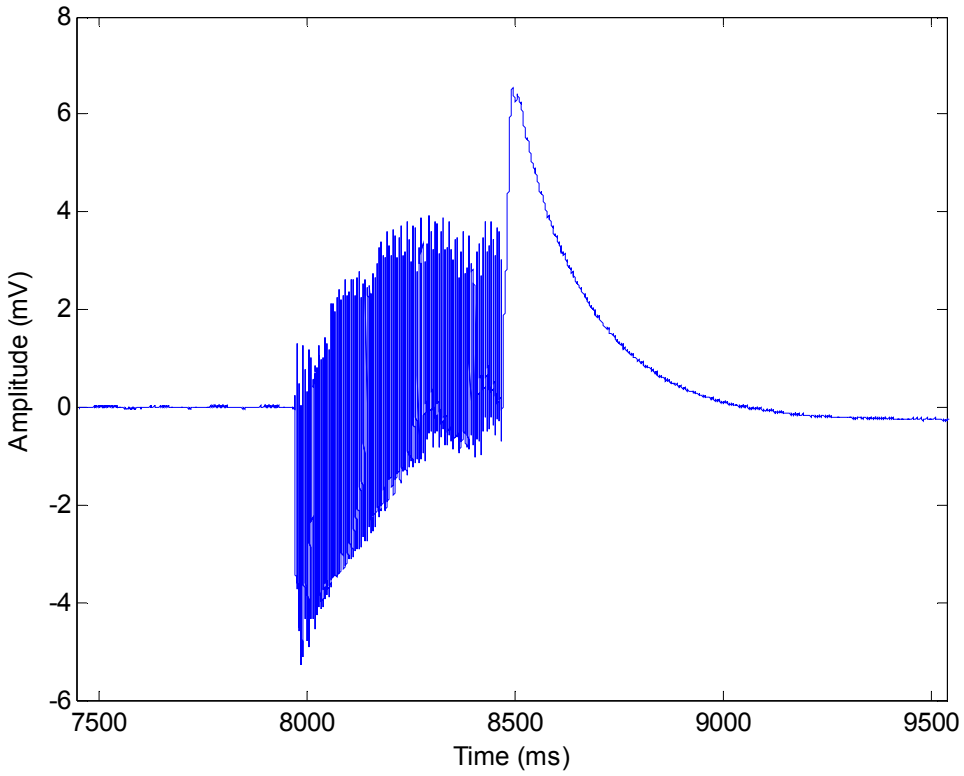

Figure 12: MATLAB plot of input referred recording showing that blanking over each individual pulse does not work because the recovery time is too long. The area between 8000 ms and 8500 ms is when blanking was taking place over each individual pulse. The spikes are the result of blanking, and the amplifier does

not fully recover in time to blank the next stimulation pulse, or to record in between each stimulation pulse.

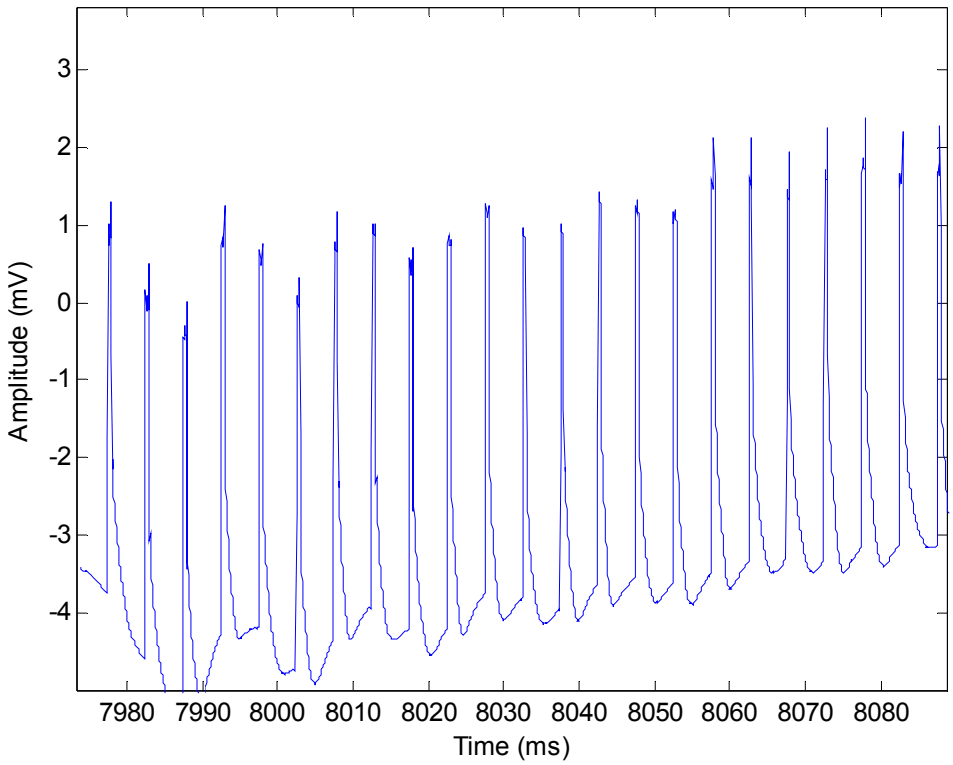

Figure 13: A zoomed in MATLAB plot of input referred recording showing that blanking over each individual pulse does not work because the recovery time is too long. The spikes are the result of blanking, and the amplifier does not fully recover (back to 0mV) in time to blank the next stimulation pulse, or to record in between each stimulation pulse.

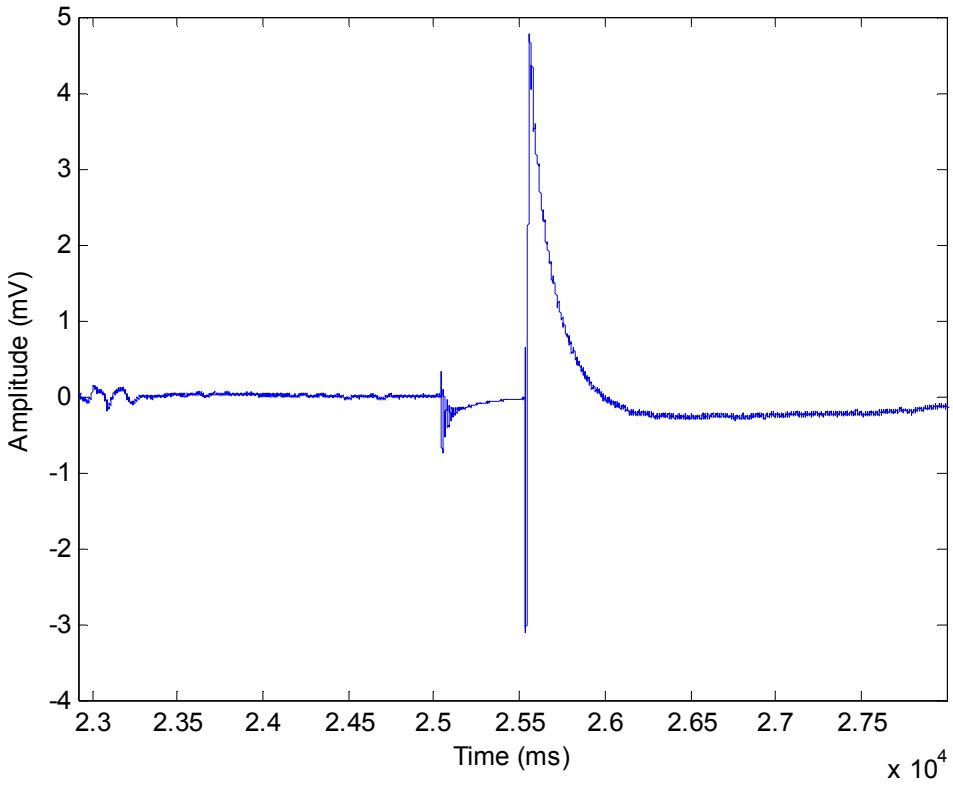

Figure 14: A MATLAB plot of an input referred recording showing that blanking over the entire pulse train is necessary in order to eliminate the artifact. The blanking introduces a recovery time artifact, which is seen at 2.55ms. This is not a perfect solution to eliminate artifacts.

5.2.2 In vivo non human primate testing at Mass General Hospital

A series of tests performed on non human primates demonstrated the difficulties on trying to record in vivo. The recording process was tedious due to grounding issues and noise issues. The electrode used for recording and stimulation was chronically implanted for over two years, and the performance of the electrode decreased over time due to degradation and tissue growth surrounding the contacts. The extensive troubleshooting performed during both stimulation and recording testing demonstrated how much of a challenge in vivo

recordings can be due to several factors. The main factors causing problems recording were electrode degradation/incomplete return paths, and artifacts.

The first test was stimulation on CH0+ and return on CH0- with no recording. The oscilloscope was used to take a screenshot of the stimulation pulse, shown in **Figure 15**. This screenshot shows that the stimulation pulse is saturating the Intan amplifier channel. The stimulation pulse amplitude was made small enough so that it would not saturate the input, so the saturation could be caused by a degraded electrode. It was decided to move on to the electrode configuration for stimulation test 2, which is shown in **Error! Reference source not found.,** to determine if there was any saturation on other channels.

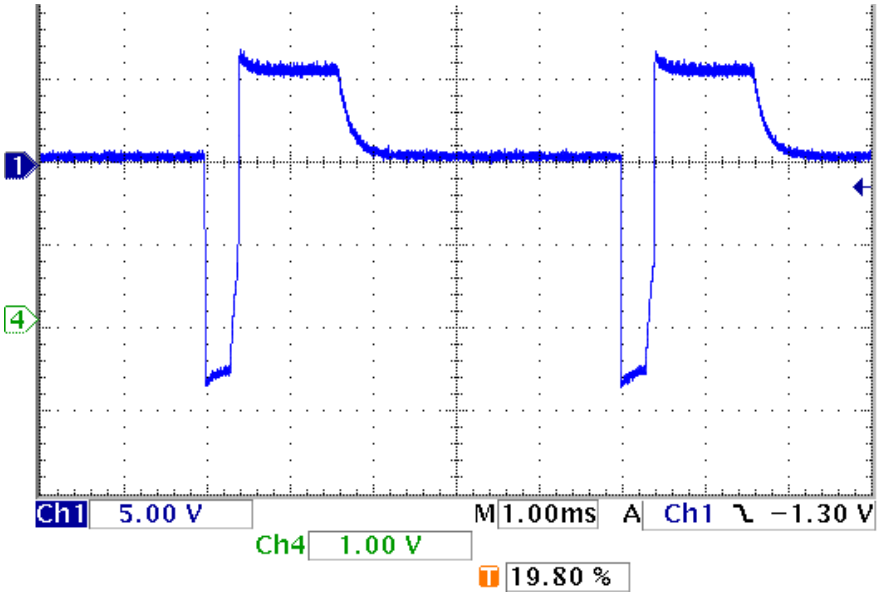

Figure 15: Stimulation during test 1 in NHP shows saturation of stim pulse (blue) when the top and bottom of the waveform are almost square, as shown above.

The second test showed a similar saturation of the stimulation pulse when using CH2+ for stimulation and returning on CH1+. Recording without stimulation

(test 3) was also unsuccessful, so impedance tests were performed in order to determine which electrode contacts might be broken. These impedance tests (tests 4 and 5) were performed using equipment provided by MGH. The results of the impedance test at both the electrode contacts and at the connectors on the board are shown in **Table 2**. The results showed that electrode contacts 2 and 3 were unusable because they have impedances much higher than the other contacts. This meant that CH0- of the Intan could not be used. The broken electrodes explained the stimulation pulse saturation when trying to stimulate on these electrodes, because there was no return path for the current, causing it to saturate the amplifier inputs.

A plot of the electrode impedance along with the impedance at the corresponding channel on the amplifier is shown in Figure 16**.** In the case of electrode 1, 5, and 8, the impedance measurements were not the same at the electrode and the amplifier channel. This means that the connection was not good, and explains why the stimulation in test 2 using CH1+ as a return was saturating. Since the stimulation return path to the board was not completed, the stimulation pulse was saturating.

Table 2: Impedance testing to determine where broken electrode contacts were.

impedance measured at electrode contact	**impedance measured at connector on board**

electrode contact number	impedance (kΩ)	Channel	impedance (kΩ)
1	50	0+	175
2	200	0-	175
3	175	NC	N/A
4	15	2+	40
5	15	1+	100
6	25	3+	35
7	40	1-	35
8	40	2-	175

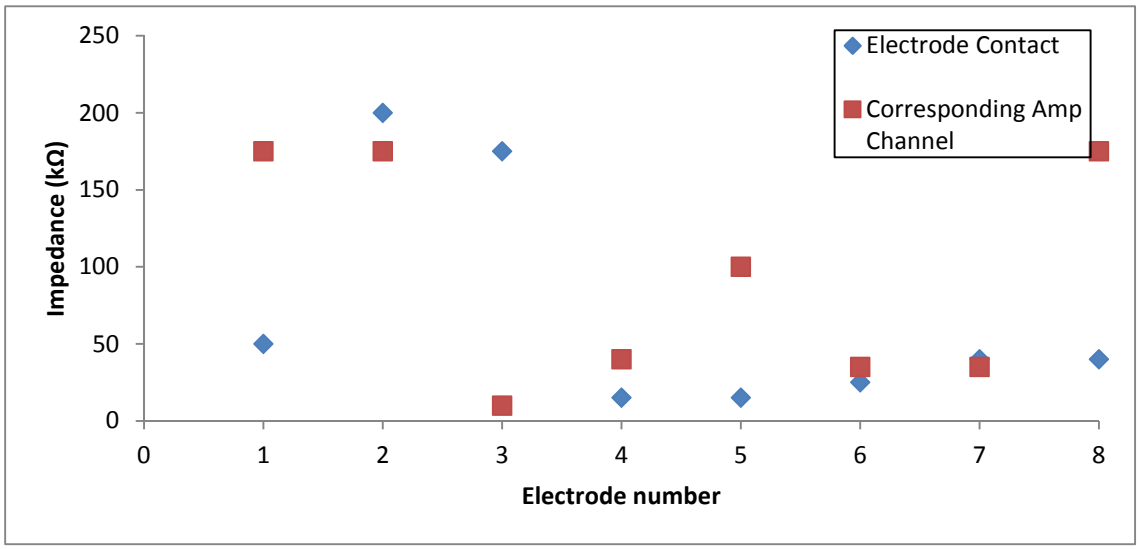

Figure 16: Electrode impedance and impedance on corresponding amplifier channels.

After the impedance tests, the connector between the board and the implanted electrode was removed and re-connected in order to fix the bad connection. Electrodes were then stimulated on CH3+ with a return on CH1+, and no recording (test 6). The

voltage excursion was measured to be about 2.0 Vpp. The screenshot from the oscilloscope in **Figure 17** shows that there was no saturation so the stimulation loop was being properly closed with a current return path.

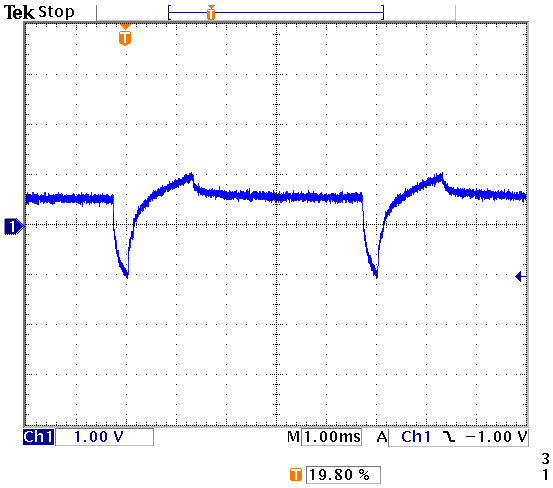

Figure 17: Test 6 stimulation pulse shows what no saturation looks like.

Single-ended recording was used for test 9, with a full bandwidth of 3Hz to 7.5kHz and no blanking. There was no stimulation during this testing. **Figure 18** shows a portion of the recorded signal in the time domain. The time between the two peaks is about 0.003 seconds, which is a frequency of about 300Hz. This shows that although the 60Hz noise is filtered out using a notch filter in the Intan software, the harmonics are still present in the recording. This is also apparent in the FFT. **Figure 19** shows a zoomed in portion of the FFT, and there is a peak at 180Hz, which is the 3rd harmonic of 60Hz. These harmonics are all considered artifacts during recording.

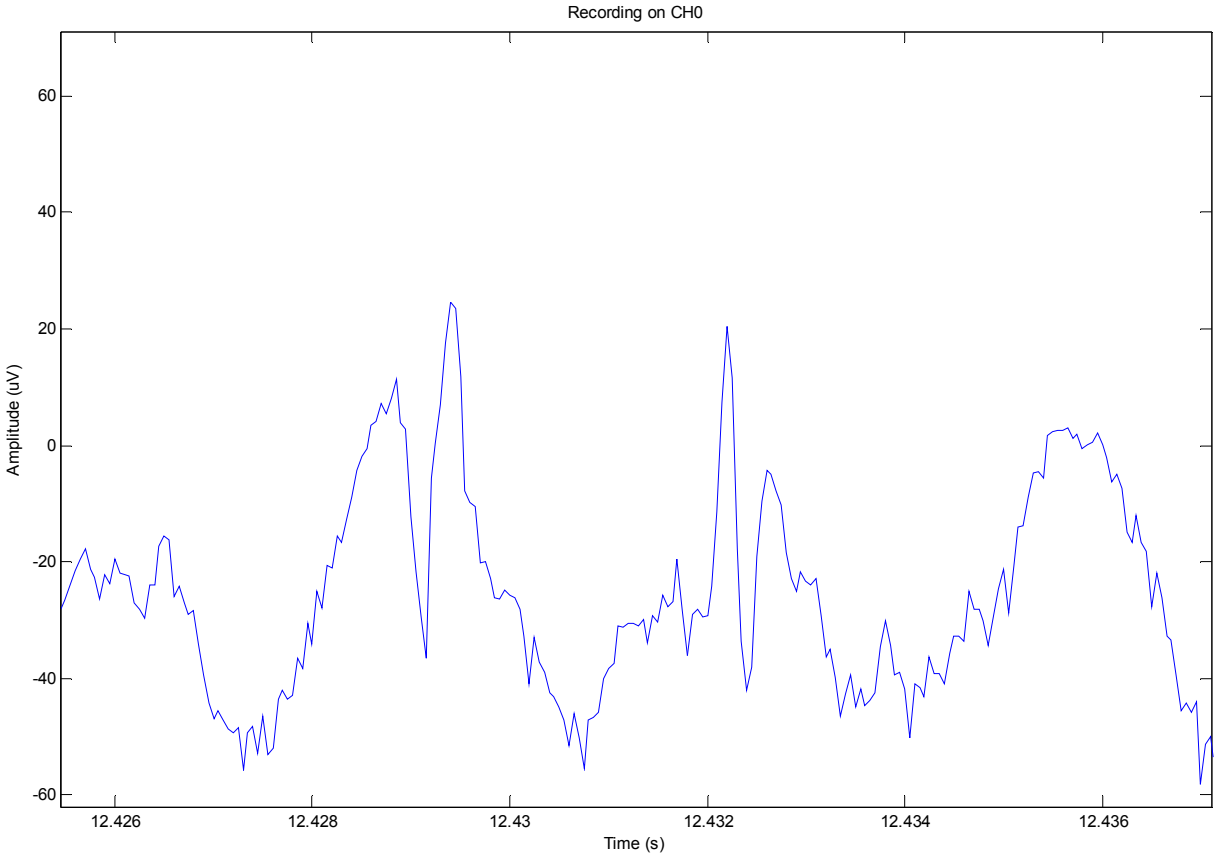

Figure 18: Zoomed in on the time scale of plotted data to examine the frequency of the data in order to determine what types of signals or noise are present.

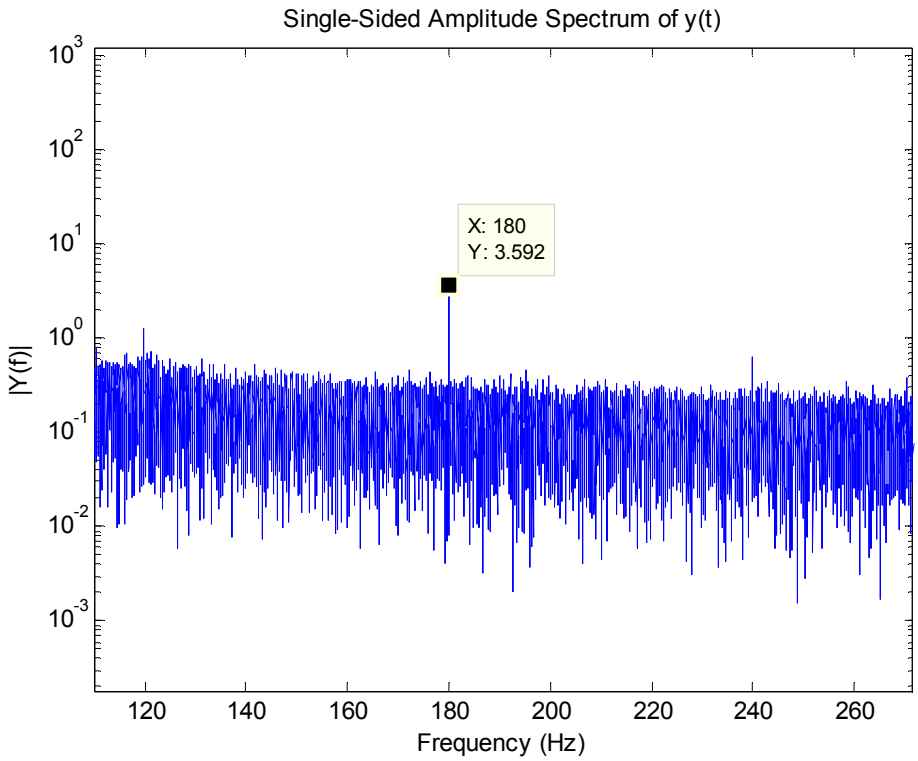

Figure 19: Portion of FFT showing the 3rd harmonic of 60Hz noise and confirming its presence from the previous plot.

For test 10, the recording parameters were the same, and the board was configured to stimulate on CH3+ and return on CH1+. The stimulation pulse was picked up during recording and saturated the amplifier channel, which can only handle ±5mV, as seen in **Figure 20 .** In **Figure 21,** it is shown that the stimulation frequency (200Hz) and its harmonics are seen in the FFT. A screenshot of the stimulation pulse at the output of the stimulation chip was captured with the oscilloscope and is shown in **Figure 22.** The voltage excursion was measured to be about 3.2 Vpp at stimulation amplitude of 1 mA, which matched with the excursion measurements in test 8.

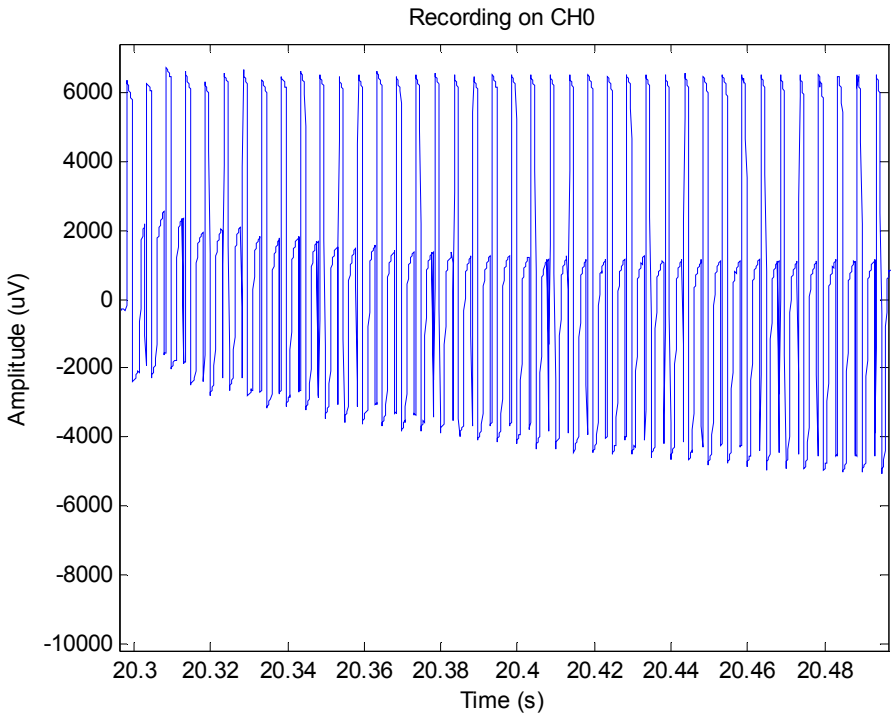

Figure 20: Zoomed in time domain signal, recorded during stimulation. This is showing that the stimulation pulse is saturating the recording amplifier which can only handle up to 5mV.

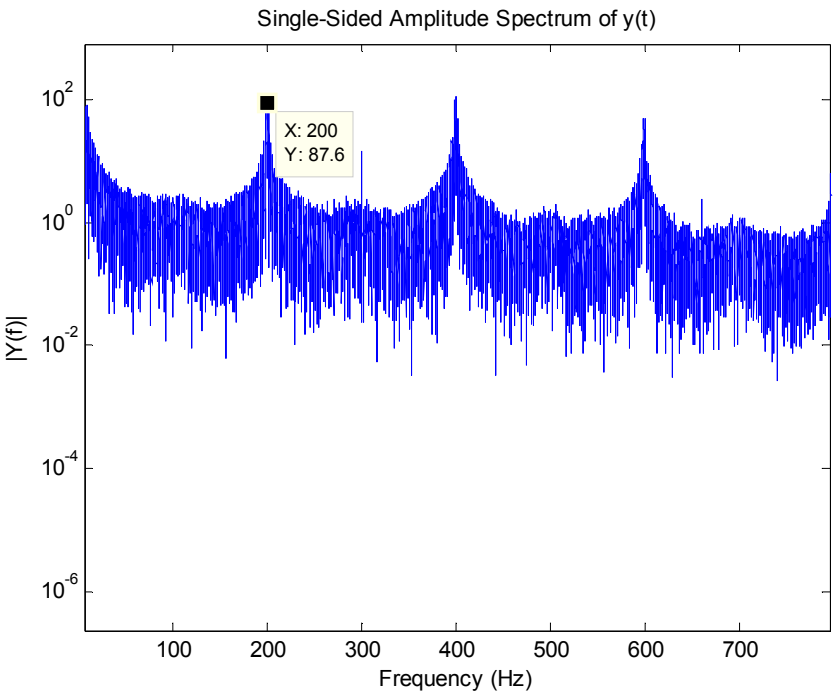

Figure 21: Stimulation frequency (200Hz) and harmonics are present in FFT, confirming the previous figure.

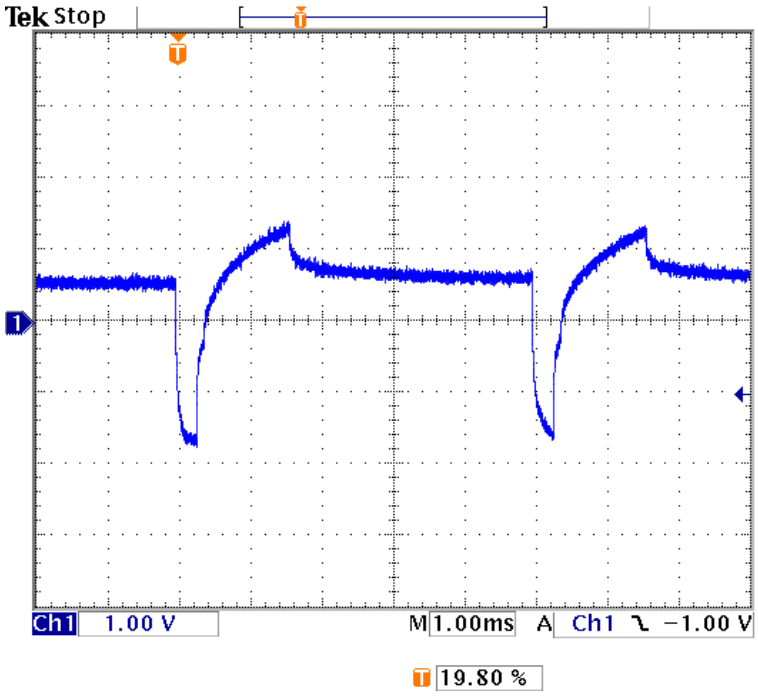

Figure 22: Stimulation pulse captured on the oscilloscope shows the stimulation pulse being delivered.

For test 11, the recording and stimulation parameters were the same. Blanking was enabled over the entire pulse train. **Figure 23** shows the recording during the blanking period, and no stimulation pulse is recording during this time. The “fast settle” feature of the Intan is used for blanking, and it was measured to have a recovery time of about 200 ms, with a recording bandwidth of 3Hz – 7.5kHz, which means neural data during that time period would not be recorded.

Figure 24 shows that the stimulation frequency (200Hz) is not present in the FFT; the 60Hz noise harmonics are still there. This shows that the fast settle capability of the Intan is successful in rejecting the artifact; however the slow recovery time shows that this method of artifact rejection has a negative aspect, because this could overlap potential neural signals that are being recorded as responses to the stimulation pulses.

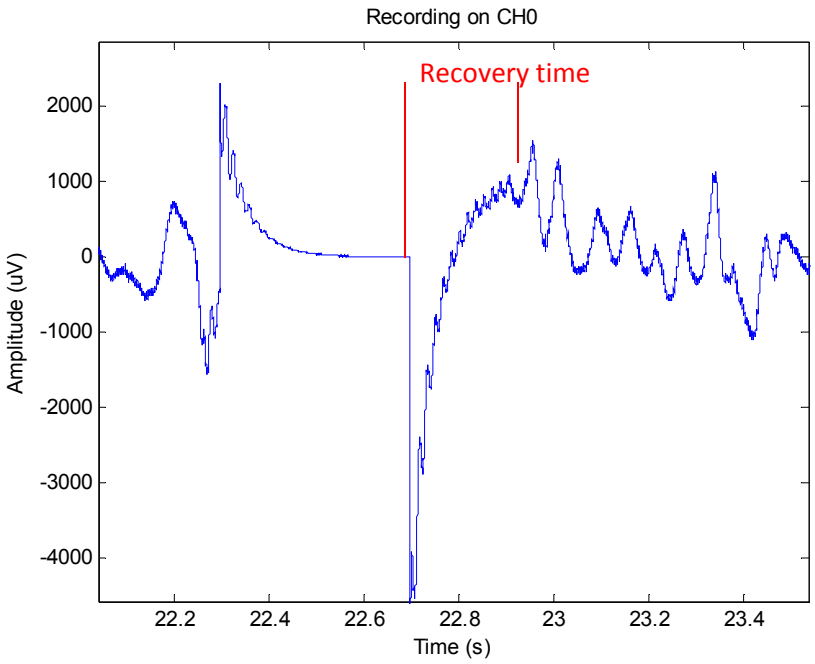

Figure 23: Blanking portion of time domain signal showing the fast settle spike and recovery time of almost a second, which means the neural response is masked by this recovery time.

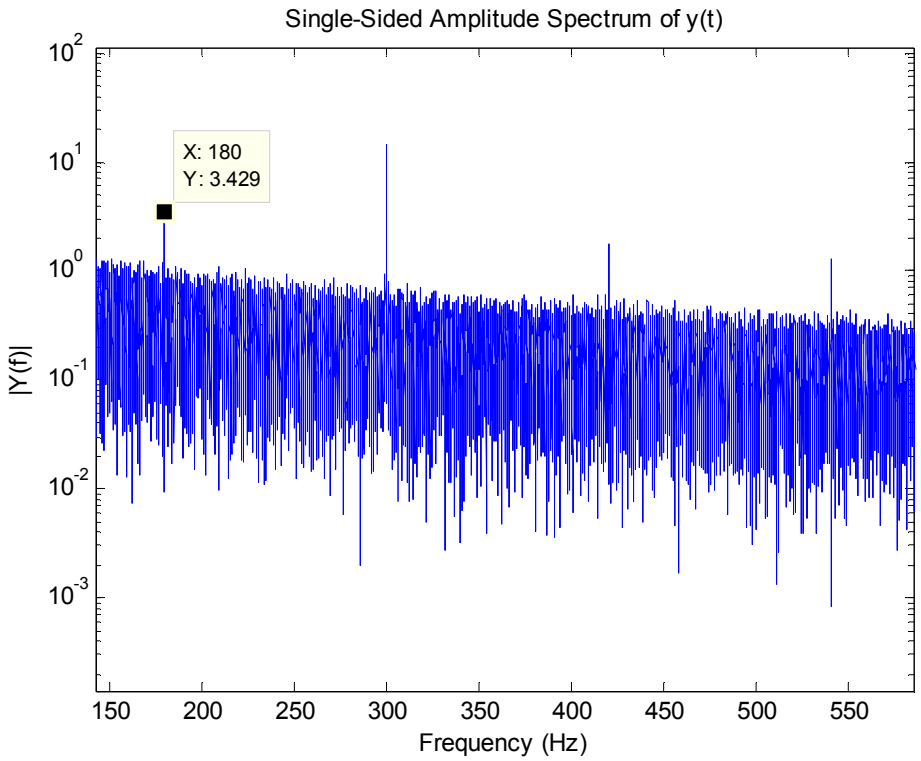

Figure 24: Harmonics of 60Hz noise present in FFT.

For test 12, blanking was enabled over each stimulation pulse instead of over the whole train of pulses. The portion of the recording during stimulation (with the specified blanking) is shown in **Figure 25**. This recording shows that the blanking over each individual pulse is not successful in artifact rejection because it does not recover fast enough. Figure 26 shows that the stimulation frequency (200Hz) and its harmonics are present in the FFT. This also proves that blanking over each individual pulse is not successful at removing the artifact because there is not enough time for the pulse to recover from the fast settle in between pulses, and is resulting in a separate, blanking artifact that occurs at the stimulation frequency.

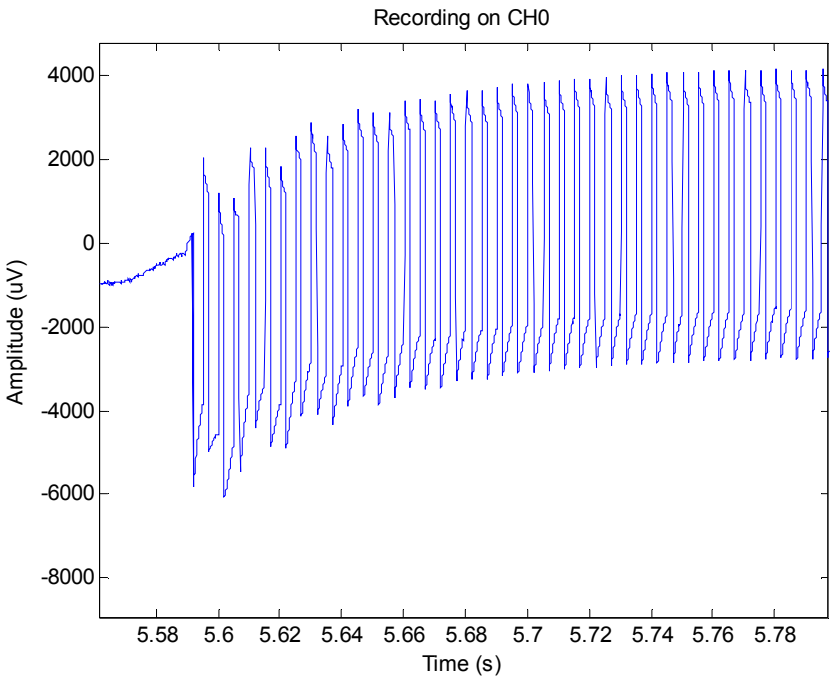

Figure 25: Blanking portion of time domain signal (blanking for each individual stimulation pulse) shows that the amplifier does not recover in time from blanking to record anything between each individual pulse.

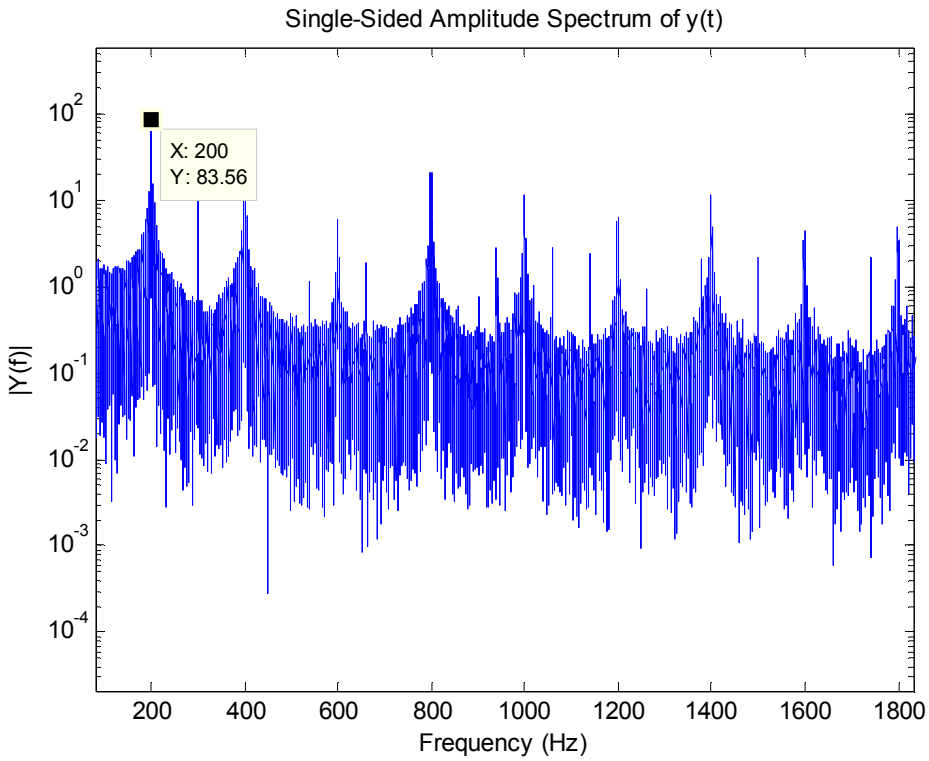

Figure 26: Stimulation frequency (200Hz) and harmonics are present in FFT.

5.2.2.1 Electrode Impedance Measurements

The in vitro impedance of the four-contact electrode measured in saline at 1kHz and a sampling rate of 20kS/s was 1.07kΩ.

Before performing impedance measurements on the resistors, their resistance was measured using a handheld digital multimeter. The following resistor values were used for impedance measurements: 100 Ω, 1.019kΩ, 9.75 kΩ, 97.6 kΩ, and 499.7 kΩ. The impedance measurements for these resistors were recorded and the results are shown in **Table 3**, as well as in **Figure 24.** The figures show the measured impedance plotted vs. the different frequencies. These initial tests verified the functionality of the impedance measurements made with the

Intan chip because the impedances measured were accurate and met the expected values.

Table 3: Impedance measurement of resistors confirm that the impedance test on the Intan chip is accurate.

Measured R with DMM (kΩ)	Measured R with Impedance Measurement (kΩ)	Frequency (kHz)
0.1	0.89	0.1
	0.61	0.5
	0.59	1
	0.57	2
	0.56	5
1.019	1.5	0.1
	1.52	0.5
	1.5	1
	1.43	2
	1.4	5
9.75	10.3	0.1
	10.3	0.5
	10.1	1
	9.65	2
	10.3	5

97.6	105	0.1
	98.2	0.5
	97.8	1
	95.8	2
	98.3	5
499.7	501	0.1
	898	0.5
	589	1
	531	2
	461	5

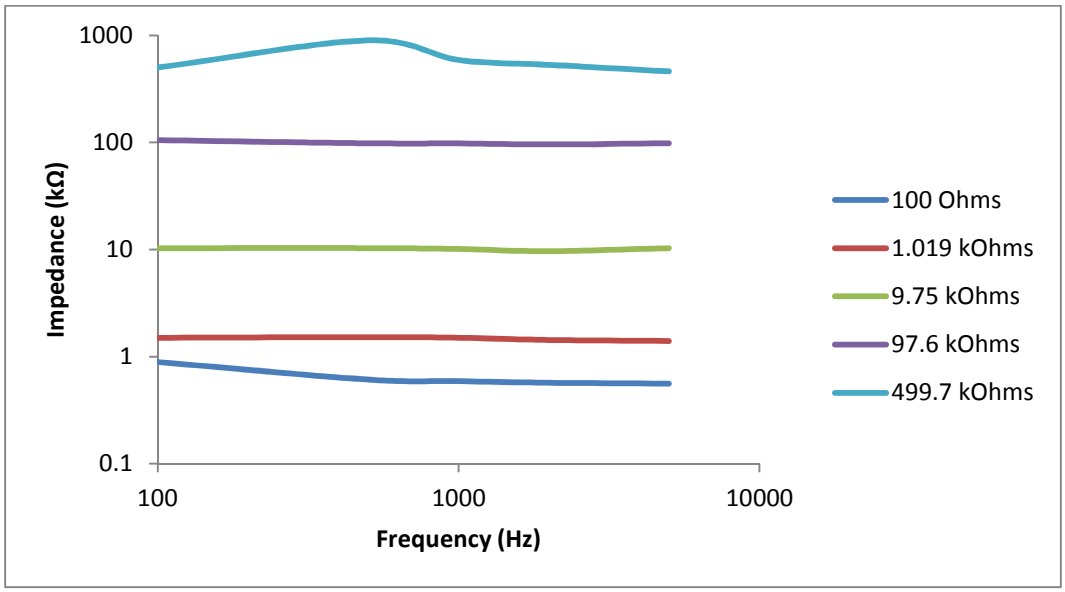

Figure 43: All impedance measurements for resistors on the same plot in a loglog scale.

Since the previous testing verified the functionality of the Intan impedance measurement testing, the test was used in vivo. At MGH, the impedance

measurements were made on the chronically implanted DBS electrode in the NHP. The impedances were measured and the average electrode impedance at each frequency was plotted in **Figure 27.** These impedance measurements show that electrode contact numbers 1, 2, 3, 5, and 7 have higher impedances with their averages falling around 1MΩ or higher at 1kHz. These electrodes potentially would produce a bad signal because the impedance was so high. This was speculated to be a result of chronic implantation of the electrodes and tissue growth around the contacts, resulting in broken contact between the electrode and the targeted neurons.

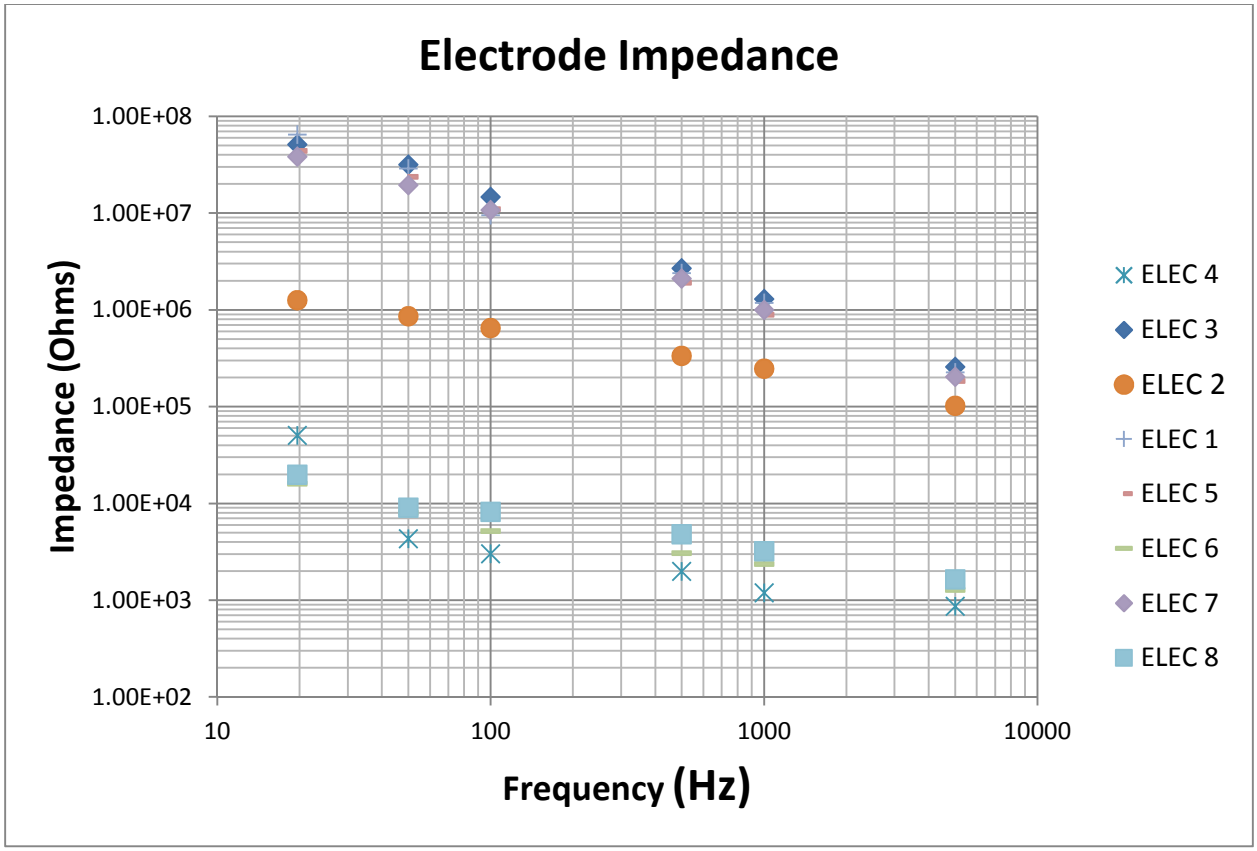

Figure 27: Electrode impedances measured at MGH in chronically implanted electrodes in an NHP to determine which electrode contacts could not be used due to high impedances.

5.3 Layered approach to artifact rejection recording board

Before the amplifier board (LTC6087) came in from production, the MATLAB code and the XMEGA code to get data from the ADC were tested. Because there was no amplifier connected to the board, the test was just observing the noise on the input of the ADC in real time. To start off, a sampling frequency of 2kS/s was used. The top plot in **Figure 28** shows the output voltage of the ADC, which is noise. The bottom plot in the figure shows the power spectral density, calculated by using Welch's averaging estimator for a changing signal. The signal was verified as accurate by looking at the datasheet for the LTC6087 and it was determined that the voltage output offset from the datasheet (0.75mV) was observed in the top plot. In the bottom plot, a small spike at 60Hz can be seen, which shows that 60Hz noise is present in the environment and is being picked up by the ADC. (using 4.096V ref)

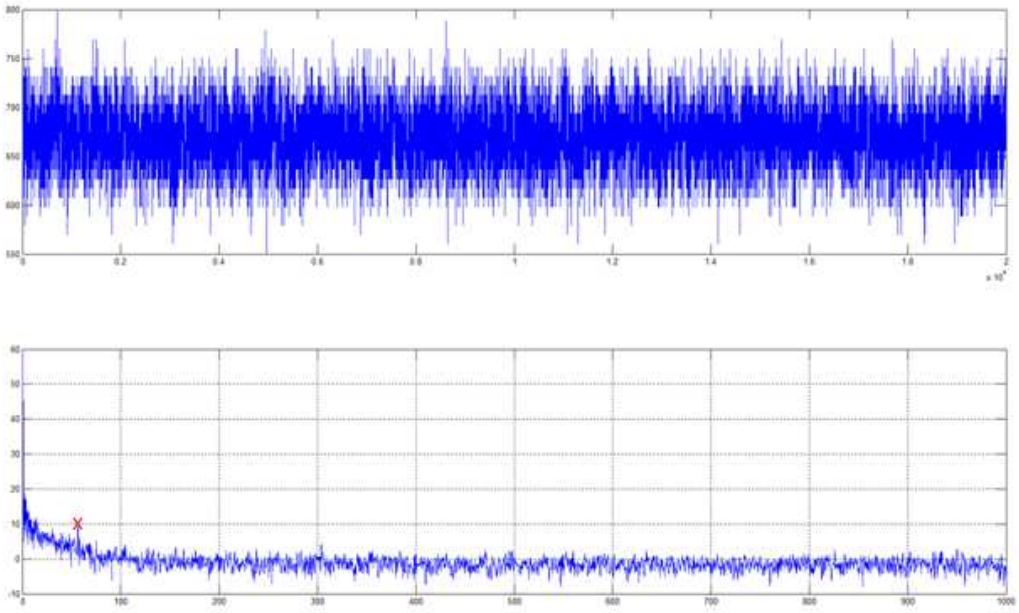

Figure 28: (Top) raw voltage output of the ADC in uV. (Bottom) Welch power spectral density estimate of the signal. The spike at 60Hz found in the bottom plot is marked with a red 'x'.

Once initial setup testing was complete, the blanking of the board was tested using a 2kHz sine wave which was output from a function generator and directly connected to the recording inputs of the board. No stimulation pulse was present, the blanking was just tested to make sure no inputs were leaking through during the blanking period. The inputs to the second stage amplifier were successfully pulled to AC ground when triggered, as seen in **Figure 29.**

The amplifier was then tested with stimulation pulses by connecting the recording inputs to wires in saline. A stimulation pulse was played into the saline and blanking on the second stage input amplifier was triggered. The blanking was successful and the stimulation artifact was not recorded, as shown in Figure 30**.**

The timing of the trigger for blanking is shown with the output of the amplifier cascade on an oscilloscope in Figure 31**.**

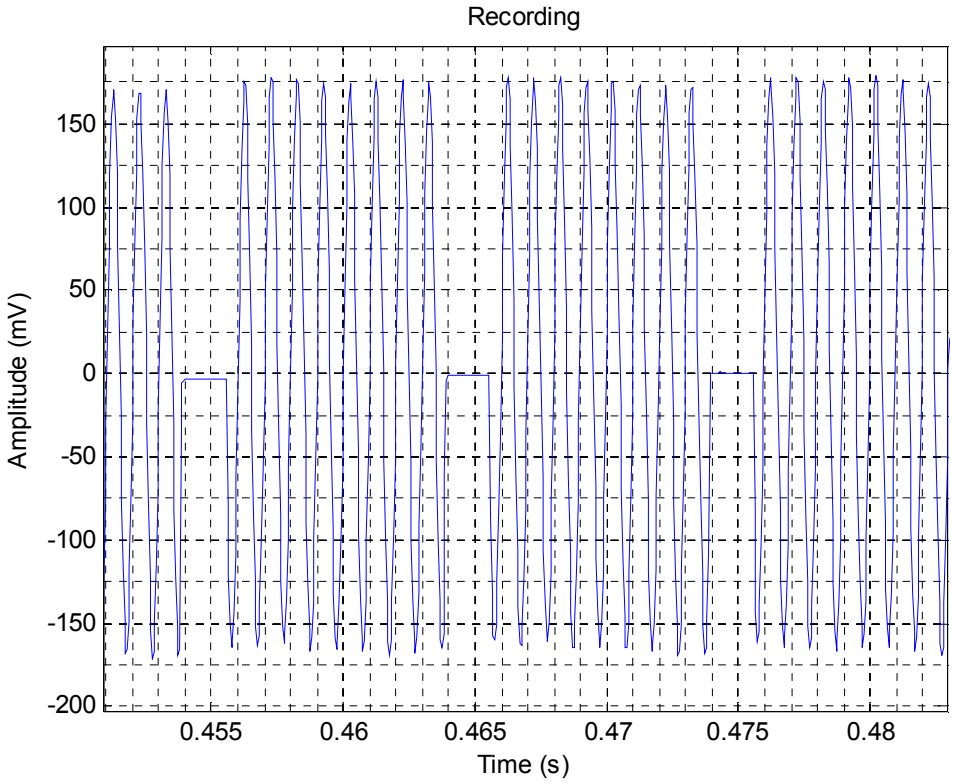

Figure 29: Sine wave used to test amplifier blanking with no stimulation pulse present shows that blanking is working, because there is not output during the blanking periods.

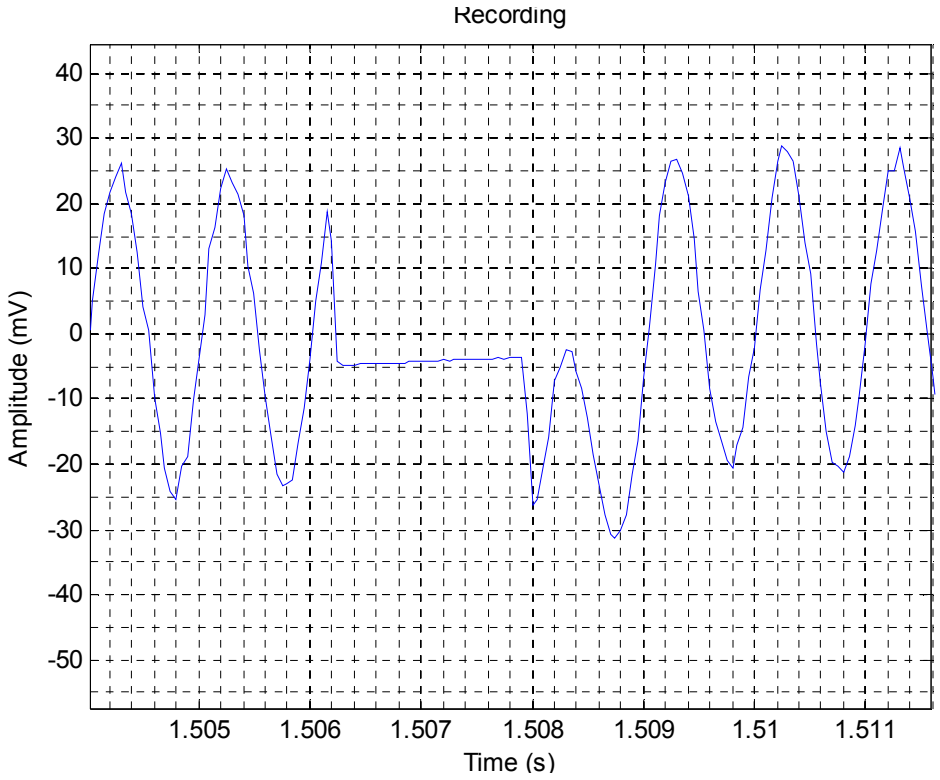

Figure 30: Blanking during stimulation eliminates the artifact and recovers to continue recording the signal quickly.

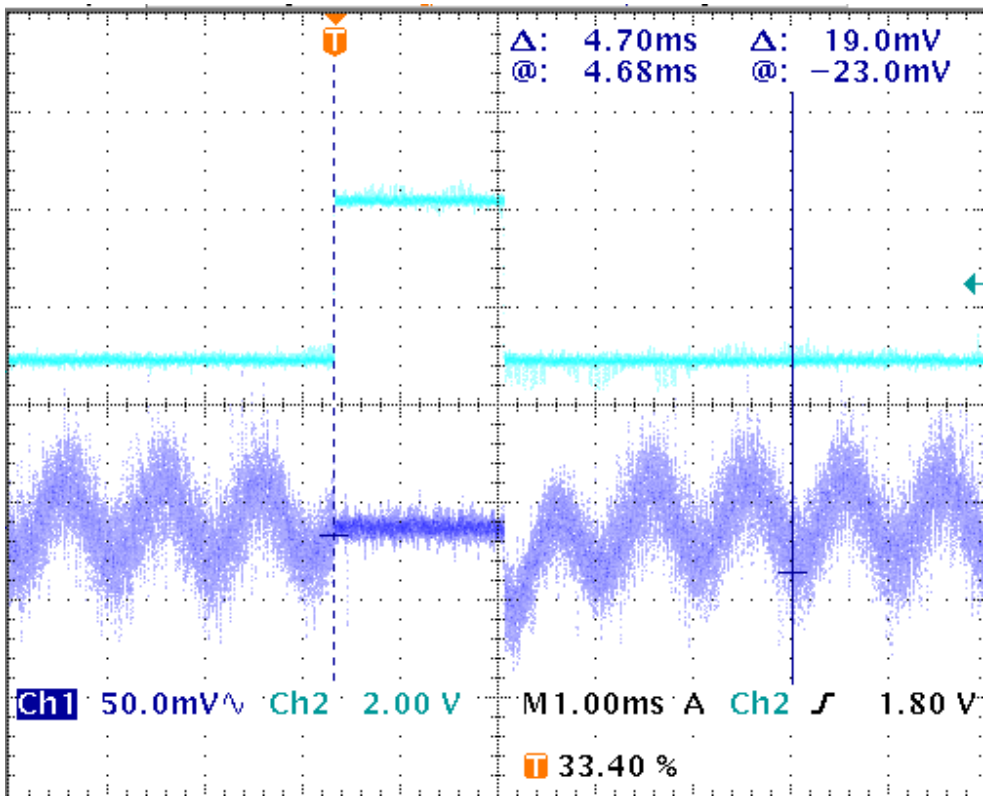

Figure 31: Amplifier output and trigger for blanking during a stimulation pulse to demonstrate that the timing of the blanking is accurate.

Previously recorded neural signals were acquired to use for more realistic benchtop testing. These signals were already noisy since they were pre-recorded, so they introduced an element of noise into the testing.

5.3.1 Artifact rejection board and Intan recovery time comparison

This testing was comparing the post-blanking recovery time of my board to that of the Intan. The testing was done using saline, and the stimulation pulse amplitude was 1mA, with a 0.3ms duration. The overlay of 20 recovery time samples collected with the artifact rejection board is shown in **Figure 32**, and the average of these signals is shown in Figure 33**.** The overlay of 20 samples from the Intan is shown in Figure 34**,** and the average of these signals is shown in Figure 35**.**

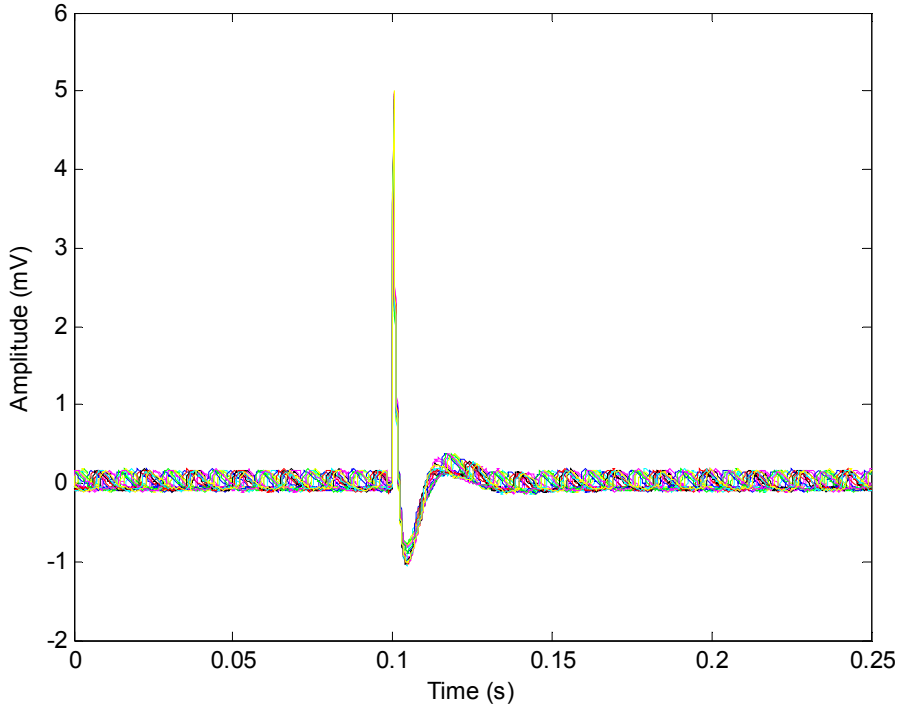

Figure 32: Overlay of artifact rejection amplifier board (my board) recording during stimulation with blanking enabled to examine the recovery time.

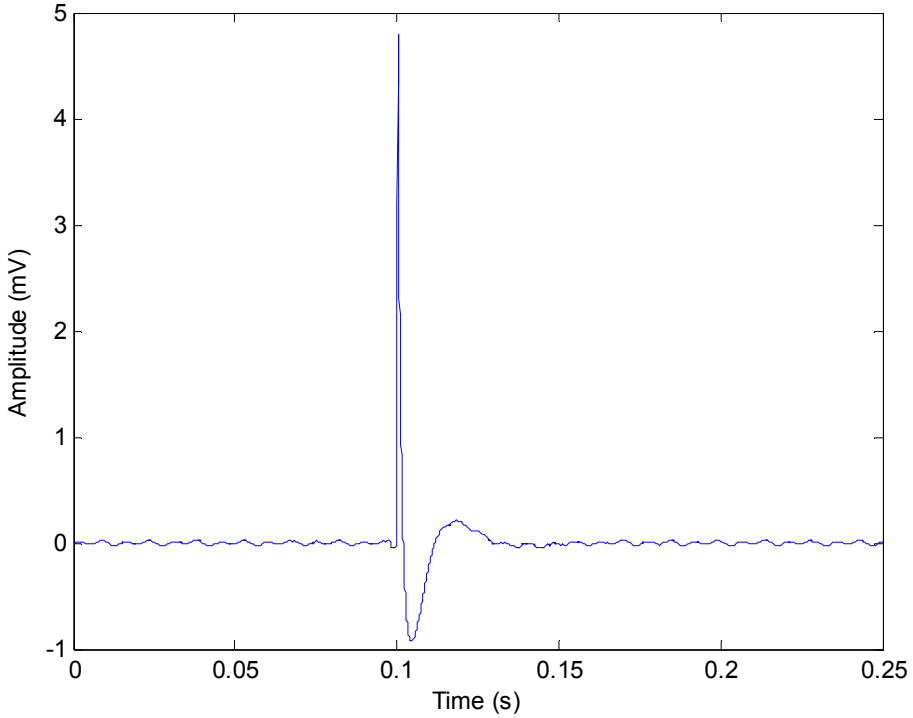

Figure 33: Average of 20 amplifier board recordings during single stimulation pulses to examine the recovery time.

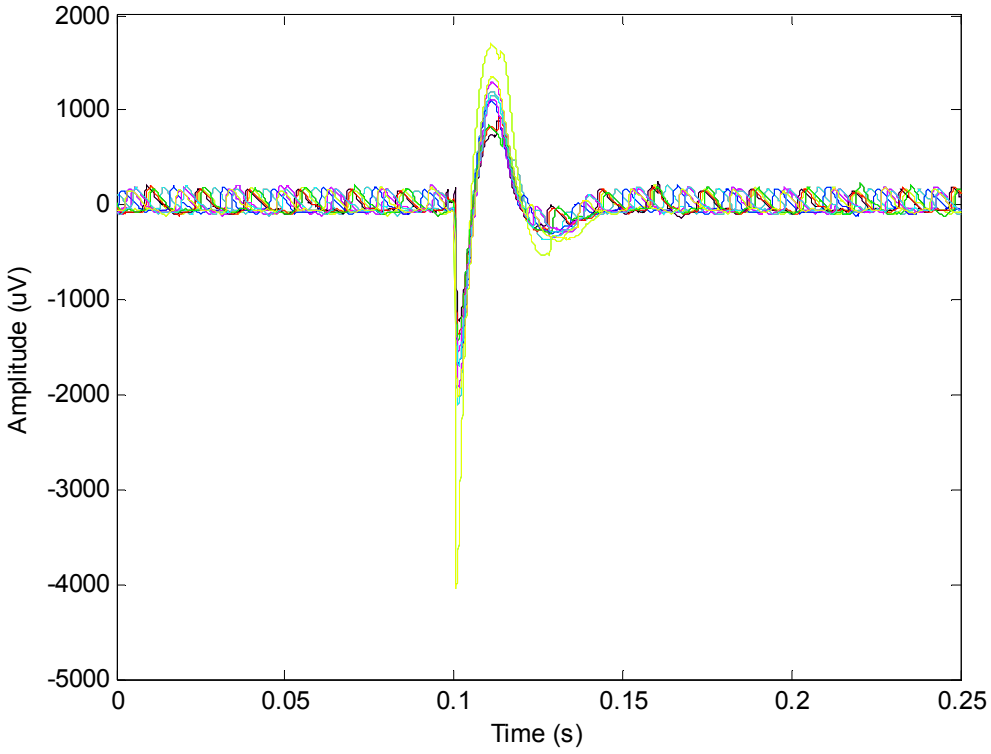

Figure 34: Overlay plot of Intan recording during stimulation with blanking enabled to examine the recovery time.

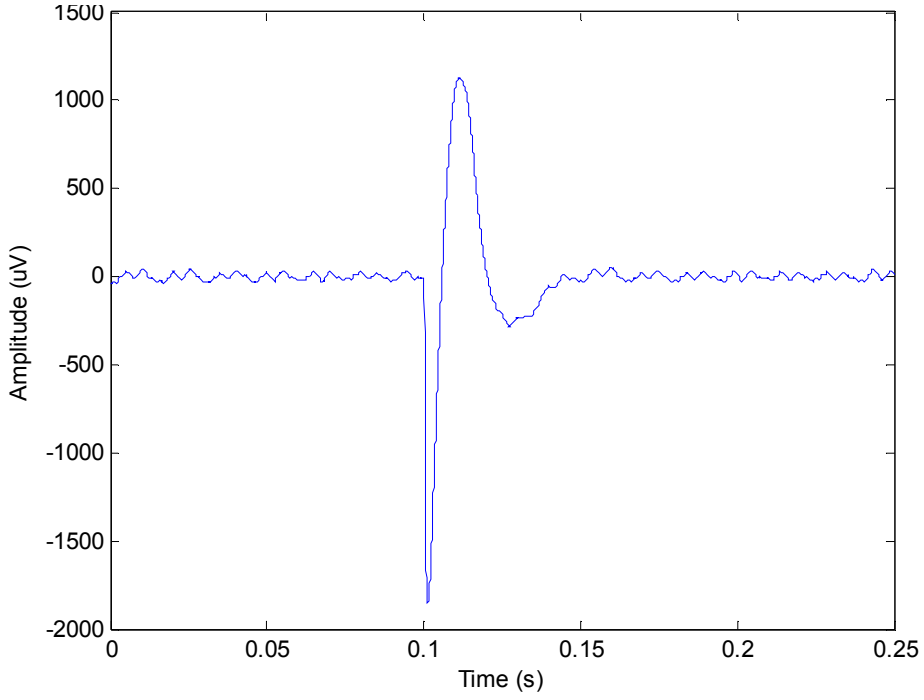

Figure 35: Average of 20 Intan recordings during a single stimulation pulse to examine the recovery time.

The average recovery time of my board was 23.005 ± 1.932 ms, and the average recovery board of the Intan board was 42.3 ± 2.642 ms, as seen in **Figure 36.** A t-test was performed using MATLAB, with the null hypothesis that the means were equal. The null hypothesis was rejected at the 5% significance level. The calculated confidence interval was [17.8089, 20.7811], the degree of freedom was 34.7956, and the p value was less than 0.0001.

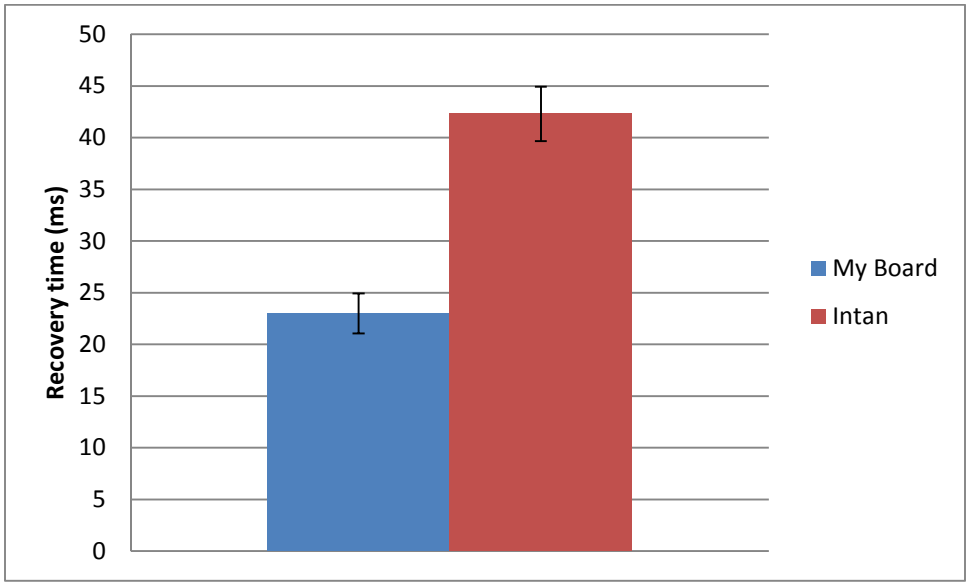

Figure 36: Comparison of the average recovery time post-blanking of the Intan board and my board to show graphically that my board has twice as fast of a recovery time using blanking at the input to the second amplifier stage.

5.3.2 Lowered gain testing

It was found that with the amplifier cascade gain of 100, a stimulation pulse of 1.4mA saturated the amplifier inputs. When the gain was decreased to 45, 1.4mA of stimulation current did not saturate the amplifier; it took 2.2mA to cause saturation. When there is saturation, there is a recovery time as a result, and this makes it so that the neural response to stimulation is lost in the recovery period. **Figure 37** shows that with no amplifier saturation, it is possible to record

a neural signal right after stimulating. **Figure 38** shows that this is not possible when the amplifier saturates; the immediate neural response is lost due to the recovery period back to the normal recording level.

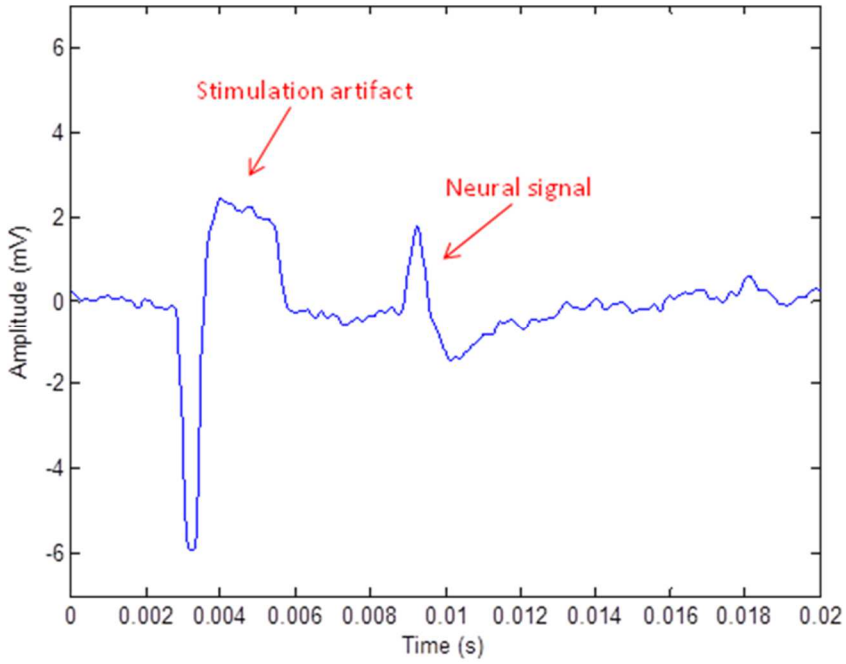

Figure 37: A neural signal can be recorded right after the stim pulse when there is no recovery time resulting from saturation.

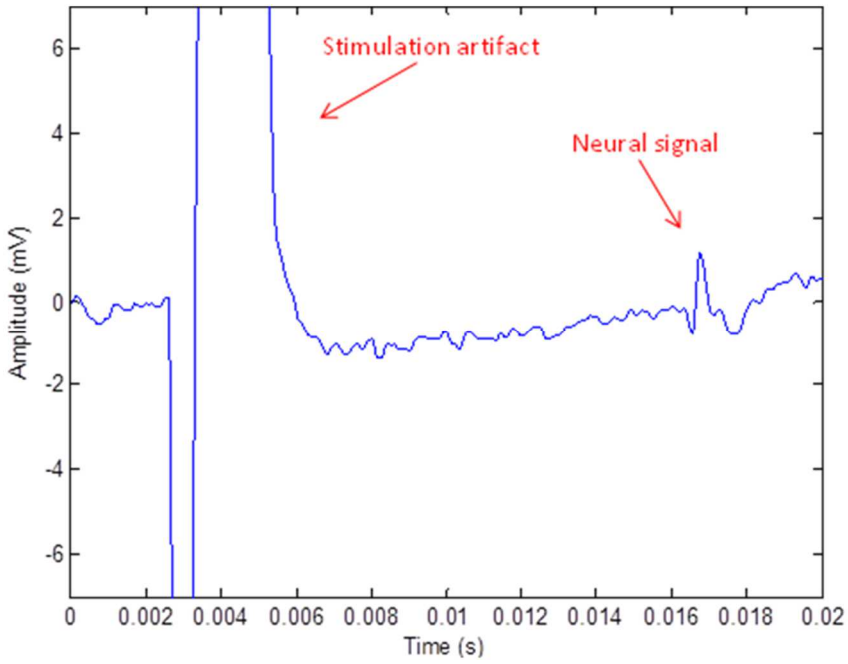

Figure 38: When the amplifier saturates, the result is a recovery time which makes it so that the amplifier cannot record the neural response immediately after stimulation.

5.4 Layered approach to artifact rejection amplifier IC testing

5.4.1 In vitro testing using saline

The data saved from the oscilloscope for the artifact rejection amplifier IC showed that the amplifier had a fast recovery time of 2ms after blanking. This eliminates amplifier saturation. In the case of saturation, the recovery time is much longer, which can lead to missing the neural response for stimulation. Three different cases were tested using the amplifier. Results from case 1, case 2, and case 3 are shown in **Figure 39, Figure 40, and Figure 41**, respectively.

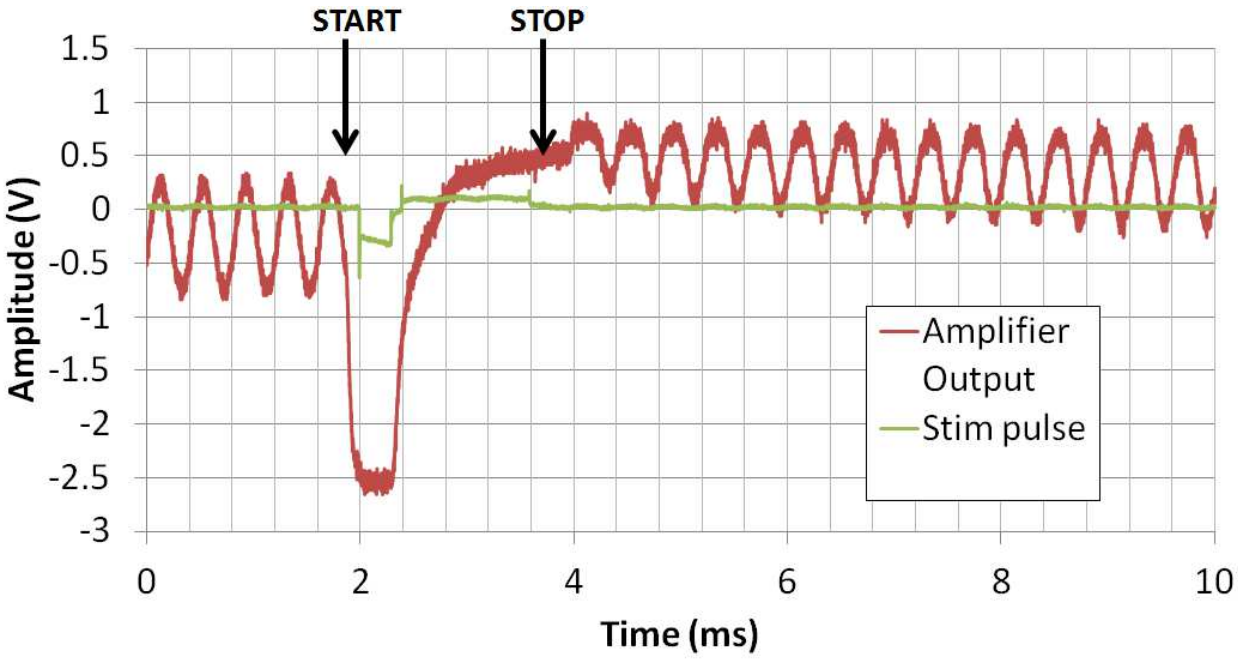

Figure 39: Case 1 results (stimulation and recording on the same electrode with artifact rejection blanking enabled) show the fast recovery time with blanking enabled. Start and stop show the beginning and end of the stimulation pulse.

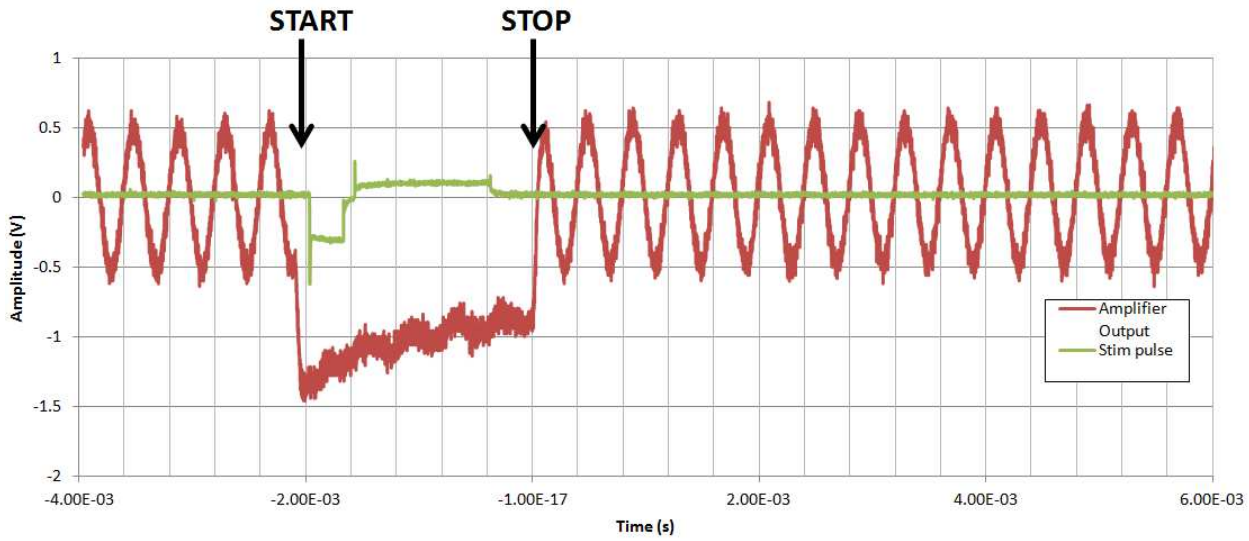

Figure 40: Case 2 results (stimulation and recording on adjacent electrodes with artifact rejection blanking enabled) show a fast recovery time with blanking enabled. Start and stop show the beginning and end of the stimulation pulse.

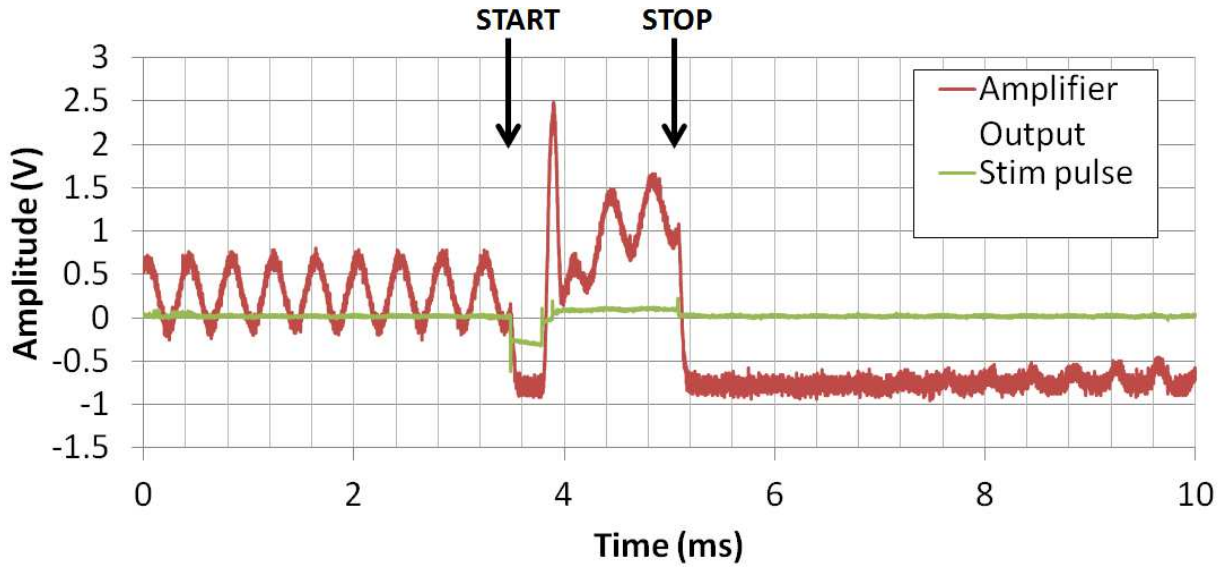

Figure 41: Case 3 results (stimulation and recording on same electrode with artifact rejection blanking disabled) show a longer recovery time due to amplifier saturation resulting from the stimulation pulse amplitude. Start and stop show the beginning and end of the stimulation pulse.

5.4.2 In vivo testing at Boston University

During the testing at Boston University, neural spikes were recorded using the amplifier. **Figure 42** shows an overlay of 10 recordings of spikes from the anesthetized bird at Boston University, which shows that the amplifier can successfully record in vivo.

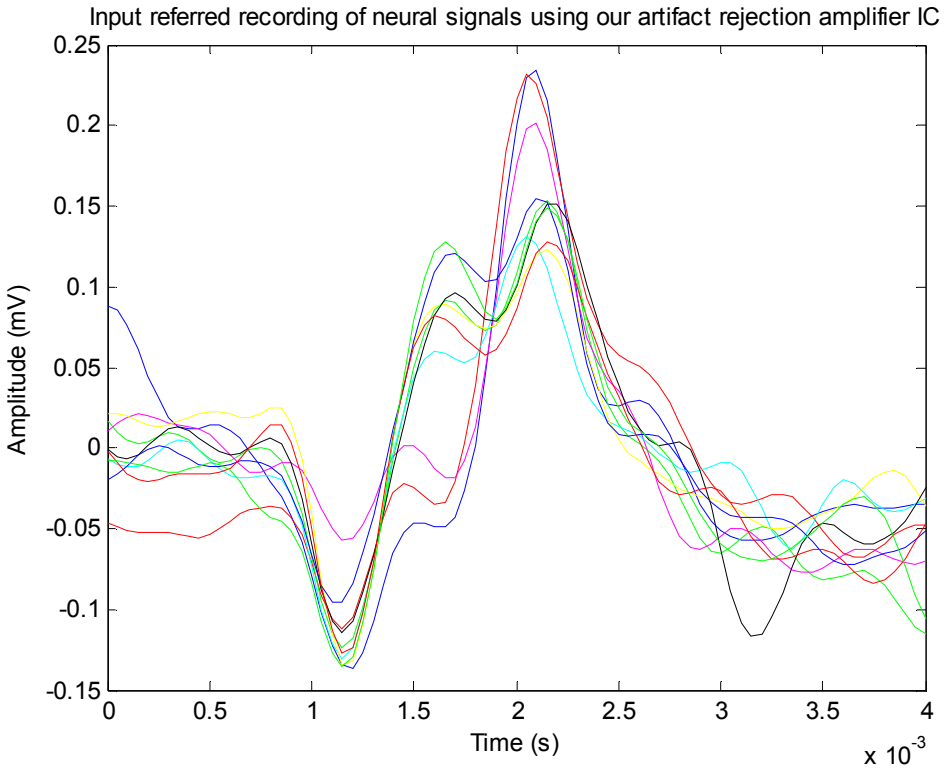

Figure 42: Input referred recording from a bird at Boston University.

6 Conclusion

Neural stimulation and recording is a growing field being used for disease treatment and research. The presence of a stimulation artifact in the recording makes it hard to examine the neural response to stimulation, in turn making it hard to create a closed-loop, implantable, adaptable stimulation and recording

system. The artifact is much larger than the neural signal of interest, and can cause amplifier saturation. Current research in the field uses single techniques, such as template subtraction or filtering, for artifact removal. These methods of artifact rejection do not completely reduce the artifact or avoid saturation.

The idea of a layered approach to artifact rejection is examined in the thesis, and incorporates several different techniques, including lowering the amplifier gain, increasing the dynamic range, and blanking of the amplifier inputs. The goal of this approach is to reduce the artifact enough in order to be able to record during stimulation without causing amplifier saturation or having a long recovery time after stimulating.

The artifact rejection board designed to implement parts of the layered approach had blanking and lowered amplifier gain, and it worked to reduce the artifact using blanking with a recovery time of about 20 ms. This recovery time is faster than a commercially available neural recording amplifier, but still not ideal to record the direct neural response to stimulation. The recovery time of the blanking technique used in the artifact rejection amplifier IC is improved at around 2ms. Taking a layered approach toward artifact rejection is a step in the direction of being able to record through stimulation in order to observe the direct neural response to stimulation.

Future work includes collecting more data in vivo using the artifact rejection amplifier IC. This data could be compared to a commercially available recording amplifier also used in vivo, in order to assess the level of artifact

rejection compared to a currently used amplifier in the field. Also, future work includes collecting in vivo data using the artifact rejection IC with blanking enabled in order to examine the effect of this blanking technique in vivo.

Bibliography

Aksenova, T., Nowicki, D., & Benabid, A.-L. (2008). *Patent No. US8620420 B2.* United States of America.

Al-ani, T., Cazettes, F., Palfi, S., & Lefaucheur, J.-P. (2011). Automatic removal of high-amplitude stimulus artefact from neuronal signal recorded in the subthalamic nucleus. *Journal of Neuroscience Methods* 1, 135-146.

alzforum.org. (n.d.).

Andrews, C., Kermani, B. G., Cascio, W. E., & Nagle, H. T. (1994). Controlling electrical side effects of cardiac stimulus pulses due to high impedance electrodes. *IEEE* 2, 960-961.

Anikeeva, P. O., Jia, X., Lu, C., Canales, A., Froriep, U. P., Tringides, C. M., et al. (2013). *Patent No. US20140371564 A1.* United States of America.

Blum, R. A., Ross, J. D., Brown, E. A., & DeWeerth, S. P. (2007). An Integrated System for Simultaneous, Multichannel Neuronal Stimulation and Recording. *IEEE Transactions on Circuits and Systems* 54, 2608-2618.

Blum, R. A., Ross, J. D., Das, S. K., Brown, E. A., & DeWeerth, S. P. (2004). Models of Stimulation Artifacts Applied to Integrated Circuit Design. *Proceedings of the 26th Annual International Conference of the IEEE EMBS* , 1-5.

Brown, E. A. (2008). Stimulus-Artifact Elimination in a Multi-Electrode System. *Journal on Biomedical Circuits and Systems* 2, 10-21.

Brown, E. A., Ross, J. D., Blum, R. A., Nam, Y., Wheeler, B. C., & DeWoorth, S. P. (2008). Stimulus-Artifact Elimination in a Multi-Electrode System. *IEEE Transactions on Biomedical Circuits and Systems* 2, 10-21.

Chew, K.-M., Sudirman, R., Seman, N., & Yong, C.-Y. (2013). Human Brain Phantom Modeling: Concentration and Temperature Effects on Relative Permittivity. *Advanced Materials Research* 646, 191-196.

DipTrace. (2015).

Gosselin, B. (2011). Recent Advances in Neural Recording Microsystems. *Sensors* 11, 4572-4597.

Harrison, R. R., Watkins, P. T., Kier, R. J., Lovejoy, R. O., Black, D. J., Greger, B., et al. (2007). A Low-Power Integated Circuit for a Wireless 100-Electrode Neural Recording System. *IEEE Journal of Solid-State Circuits* 42, 123-133.

Hashimoto, T., Elder, C. M., & Vitek, J. L. (2002). A template subtraction method for stimulus artifact removal in high-frequency deep brain stimulation. *Journal of Neuroscience Methods* 113, 181-186.

Heffer, L. F., & Fallon, J. B. (2008). A Novel Stimulus Artifact Removal Technique for High-Rate Electrical Stimulation. *Journal of Neuroscience Methods* 170, 277-284.

Hofmann, L., Ebert, M., Tass, A. T., & Hauptmann, C. (2011). Modified pulse shapes for effective neural stimulation. *Neuroengineering* 4.

Intan Technologies, LLC. (2014). *RHD2000-Series Amplifier Evaluation System.* Retrieved 2014 November from intantech.com: http://www.intantech.com/files/Intan_RHD2000_eval_system.pdf

Junghofer, M., Elbert, T., Tucker, D. M., & Rockstroh, B. (2000). Statistical control of artifacts in dense array EEG/MEG studies. *Psychophysiology* 37, 523-532.

Kuncel, A. M., & Grill, W. M. (2004). Selection of stimulus parameters for deep brain stimulation. *Clinical Neurophysiology* 115, 2431-2441.

Libbus, I., & Boon, S. C. (2012). *Patent No. US 8200332.* United States of America.

Limnuson, K., Lu, H., Chiel, H. J., & Mohseni, P. (2013). Real-Time Stimulus Artifact Rejection Via Template Subtraction. *IEEE Transactions on Biomedical Circuits and Systems* 8, 1932-4545.

Lo, Y.-K., & Liu, W. (2013). *Patent No. 20140180052 A1.* United States of America.

Lopez, C. M., Prodanov, D., Braeken, D., & Gligorijevic, I. (2012). A Multichannel Integrated Circuit for Electrical Recording of Neural Activity, With Independent Channel Programmability. *IEEE Transactions on Biomedical Circuits and Systems* 6, 101.

McConnell, G. C., So, R. Q., Hilliard, J. D., Lopomo, P., & Grill, W. M. (2012). Effective Deep Brain Stimulation Suppresses Low-Frequency Network Oscillations in the Basal Ganglia by Regularizing Neural Firing Patterns. *The Journal of Neuroscience* 32, 15657-15668.

McGill, K. C., Cummins, K. L., Dorfman, L. J., Berlizot, B. B., Luetkemeyer, K., Nishimura, D. G., et al. (1982). On the Nature and Elimination of Stimulus Artifact in Nerve Signals

Evoked and Recorded Using Surface Electrodes. *IEEE Transactions on Biomedical Engineering* BME-29, 129-137.

Miller, C. A., Abbas, P. J., Robinson, B. K., Rubinstein, J. T., & Matsuoka, A. J. (1991). Electrically evoked single-fiber action potentials from cat: responses to monopolar, monophasic stimulation. *Hearing Research* 130, 197-218.

Montgomery, E. B., Gale, J. T., & Huang, H. (2005). Methods for isolating extracellular action potentials and removing stimulus artifacts from micrelectrode recordings of neurons requiring minimal operator intervention. *Journal of Neuroscience Methods* 144, 107-125.

Nagel, J. H. (2000). *The Biomedical Engineering Handbook: Second Edition.* Boca Raton: CRC Press LLC.

Nam, Y., Brown, E. A., Ross, J. D., Blum, R. A., Wheeler, B. C., & SP, D. (2009). A retrofitted neural recording system with a novel stimulation IC to monitor early neural responses from a stimulating electrode. *Journal of Neuroscience Methods* 178, 99-102.

Nikolic, Z. M., Popovic, D. B., Stein, R. B., & Kenwell, Z. (1994). Instrumentation for ENG and EMG Recordings in FES Systems. *IEEE Transactions on Biomedical Engineering* 41, 703-706.

Nowicki, D. V., Benabid, A. L., & Aksenova, T. I. (2007). Adaptive Model for Filtering of Stimulation Artifacts in Multichannel Recordsd of Neuronal Activity. *AIP Conference Proceedings* (pp. 382-386). AP Publishing.

Nowicki, D. V., Piallat, B., Benabid, A.-L., & Aksenova, T. (2008). Artifact Processor for Neuronal Activity Analysis during Deep Brain Stimulation. *ICANN* 5164, 508-516.

Nurmikko. (2015). *Patent No. case 2032.* United States of America.

O'Keeffe, D. T., Lyons, G. M., Donnelly, A. E., & Byrne, C. A. (2001). Stimulus artifact removal using a software-based two-stage peak detection algorithm. *Journal of Neuroscience Methods* 109, 137-145.

Olson, R. H., Buhl, D. L., Sirota, A. M., & Buzsaki, G. (2005). Band-Tunable and Multiplexed Integrated Circuits for Simultaneous Recording and Stimulation With Microelectrode Arrays. *IEEE Transactions on Biomedical Enigneering* 52, 1303-1306.

Perelman, Y., & Ginosar, R. (2007). An Integrated System for Multichannel Neuronal Recording With Spike/LFP Separation, Integrated A/D Conversion and Threshold Detection. *IEEE Transactions on Biomedical Engineering* 54, 130-137.

Temel, Y., & Jahanshahi, A. (2015). Treating brain disorders with neuromodulation. *Science* 347, 1418-1419.

Temel, Y., Visser-Vandewalle, V., van der Wolf, M., Spincemaille, G. H., Desbonnet, L., Hoogland, G., et al. (2004). Monopolar versus bipolar high frequency stimulation in the rat subthalamic nucleus: differences in histological damage. *Neuroscience Letters* 367, 92-96.

Waddell, C., Porr, B., Pratt, J. A., & Ewing, S. (2009). Deep Brain Stimulation Artifact Removal Through Under-Sampling and Cubic-Spline Interpolation. *International Congress on Image and Signal Processing* (pp. 1-5). Tianjin: IEEE.

Weiland, J. D., Yanai, D., Mahadevappa, M., Williamson, R., Mech, B. V., Fujii, G. Y., et al. (2003). Electrical Stimulation of Retina in Blind Humans. *International Conference of the IEEE EMBS* (pp. 2021-2022). Cancun: IEEE.

Wichmann, T., & Devergnas, A. (2011). A novel device to suppress electrical stimulus artifacts in electrophysiological experiments. *Journal of Neuroscience Methods* 201, 1-8.

Yao, K.-W., Lin, W.-C., Gong, C.-S. A., Lin, Y.-Y., & Shiue, M.-T. (2008). A Differential Difference Amplifier for Neural Recording System with Tunable Low-Frequency Cutoff. *International Conference on Electron Devices and Solid-State Circuits* (pp. 1-4). Hong Kong: IEEE.

Yazicioglu, R. F., Merken, P., Puers, R., & Van Hoof, C. (2007). A 60 uW 60 nV/rtHz Readout Front-End for Portable Biopotential Acquisition Systems. *IEEE Journal of Solid-State Circuits* 42, 1100-1110.

Yoshida, K., & Stein, R. B. (1999). Characterization of Signals and Noise Rejection with Bipolar Longitudinal Intrafascicular Electrodes. *IEEE Transactions on Biomedical Engineering* 46, 226-234.

Zhang, F., Miller, C. A., Robinson, B. K., Abbas, P. J., & Hu, N. (2007). Changes Across Time in Spike Rate and Spike Amplitude of Auditory Nerve Fibers Stimulated by Electric Pulse Trains. *Journal of the Association for Research in Otolayngology* 8, 356-372.

Appendices

Appendix A: Stimulation and recording board and testing at MGH supporting material

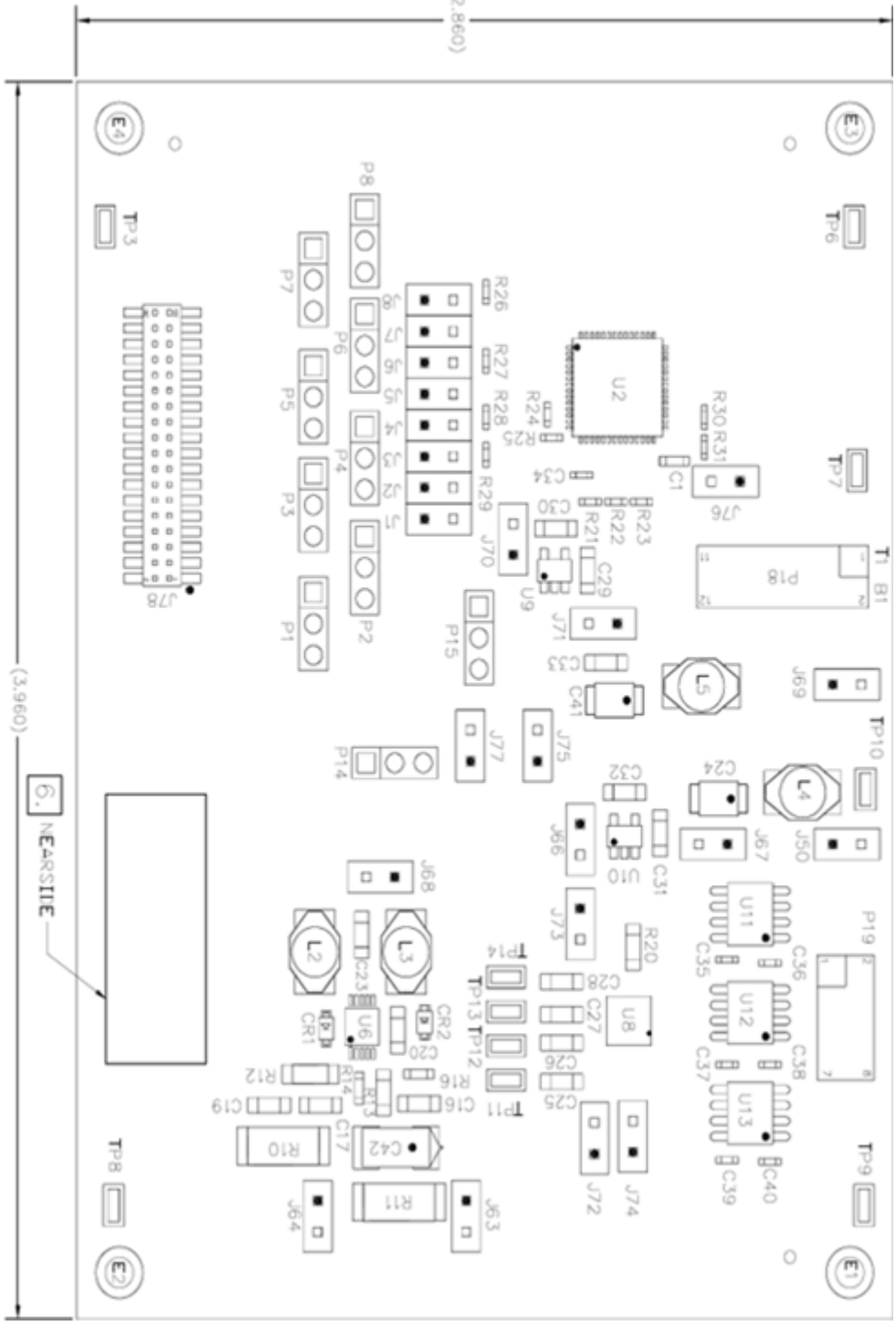

Figure 43: Layout of stimulation and recording board tested at MGH.

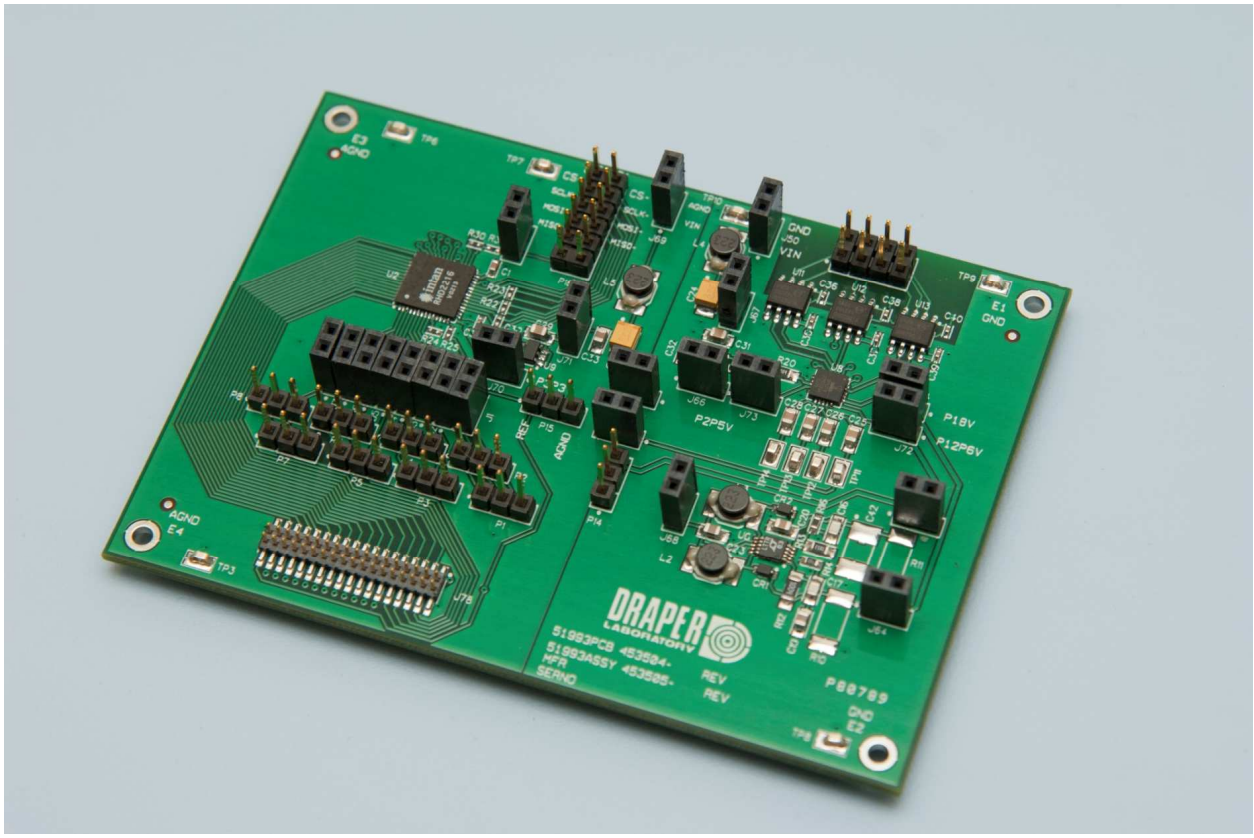

Figure 44: Stimulation and recording board.

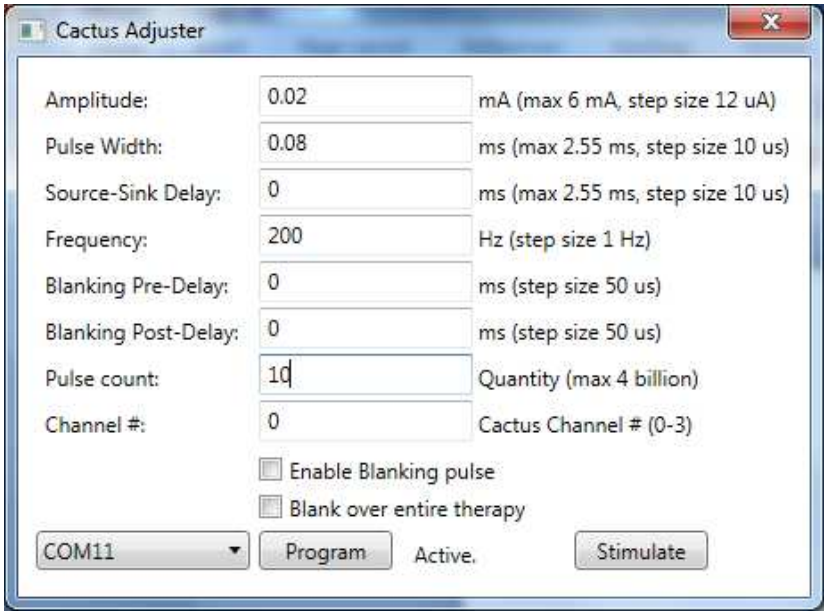

Figure 45: Program used to control the CSI021 and generate stimulation pulses.

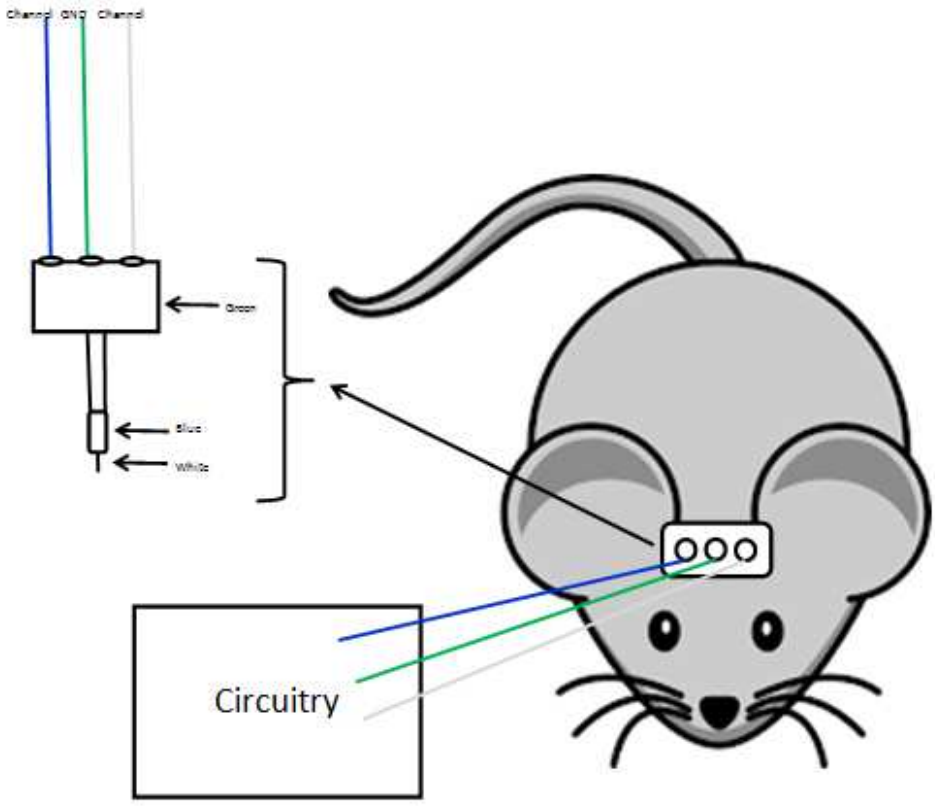

Figure 46: In vivo test setup for stimulation and recording in chronically implanted mice at MGH.

Table 4: In vivo test specifications and parameters.

Test Number	RECORD							STIMULATION
	BW		CONFIG		blanking			
	LFP	Spike	Single ended	differential	none	entire train	single pulses	
1	x		x		x			
2	x		x		x			
3	x			x	x			
4								x
5								x
6								x

7								x
8	x		x		x			x
9	x		x			x		x
10	x		x				x	x
11		x	x		x			x
12	x		x		x			x
13		x	x			x		x
14	x		x			x		x
15		x	x				x	x
16	x		x				x	x

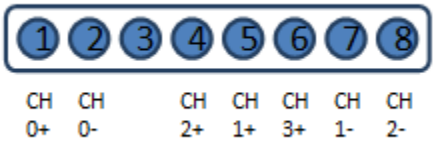

Figure 47: Diagram of the electrode chronically implanted in NHP used for the testing at MGH.

Table 5: Testing parameters for stimulation and recording in NHP.

	Record or stim	**recording parameters**	**Stim parameters**
Test 1	stim		Stimulation on CH0+ and return on CH0-
Test 2	stim		Stimulation on CH2+ and return on CH1+

Test 3	record	single ended recording no blanking	
Test 4	impedance		
Test 5	impedance		
Test 6	stim		stim between CH3+ (stim) and CH1+ (return)
Test 7	stim		stim between CH3+ (stim) and CH1+ (return)
Test 8	stim		stim between CH3+ (stim) and CH1+ (return)
Test 9	record	Single ended recording on CH0+, no blanking	
Test 10	both	Single ended recording on CH0+, no blanking	Stim on CH3+ return on CH1+
Test 12	both	Single ended recording on CH0+,blanking entire train	Stim on CH3+ return on CH1+
Test 13	both	Single ended recording on CH0+,blanking each pulse	Stim on CH3+ return on CH1+

Test 14	both	Single ended recording on CH0+	

Table 6: Stimulation parameters for testing in NHP.

Test	Amplitude (mA)	pulse width (ms)	frequency (Hz)	pulse count
1	0.5	0.3	200	80
2	0.5	0.3	200	80
6	0.5	0.3	200	50
7	0.75	0.3	200	50
8	1	0.3	200	50
10	1	0.3	200	80
11	1	0.3	200	80
12	1	0.3	200	80
13	1	0.3	200	80

Table 7: Electrode mapping to amplifier channels.

electrode number	amplifier CH
1	CH3
2	CH2
3	CH1
4	CH0
5	CH4

6	CH5
7	CH6
8	CH7

Figure 48: Electrode used for in vivo impedance testing.

Appendix B: Artifact rejection ADC board testing support material

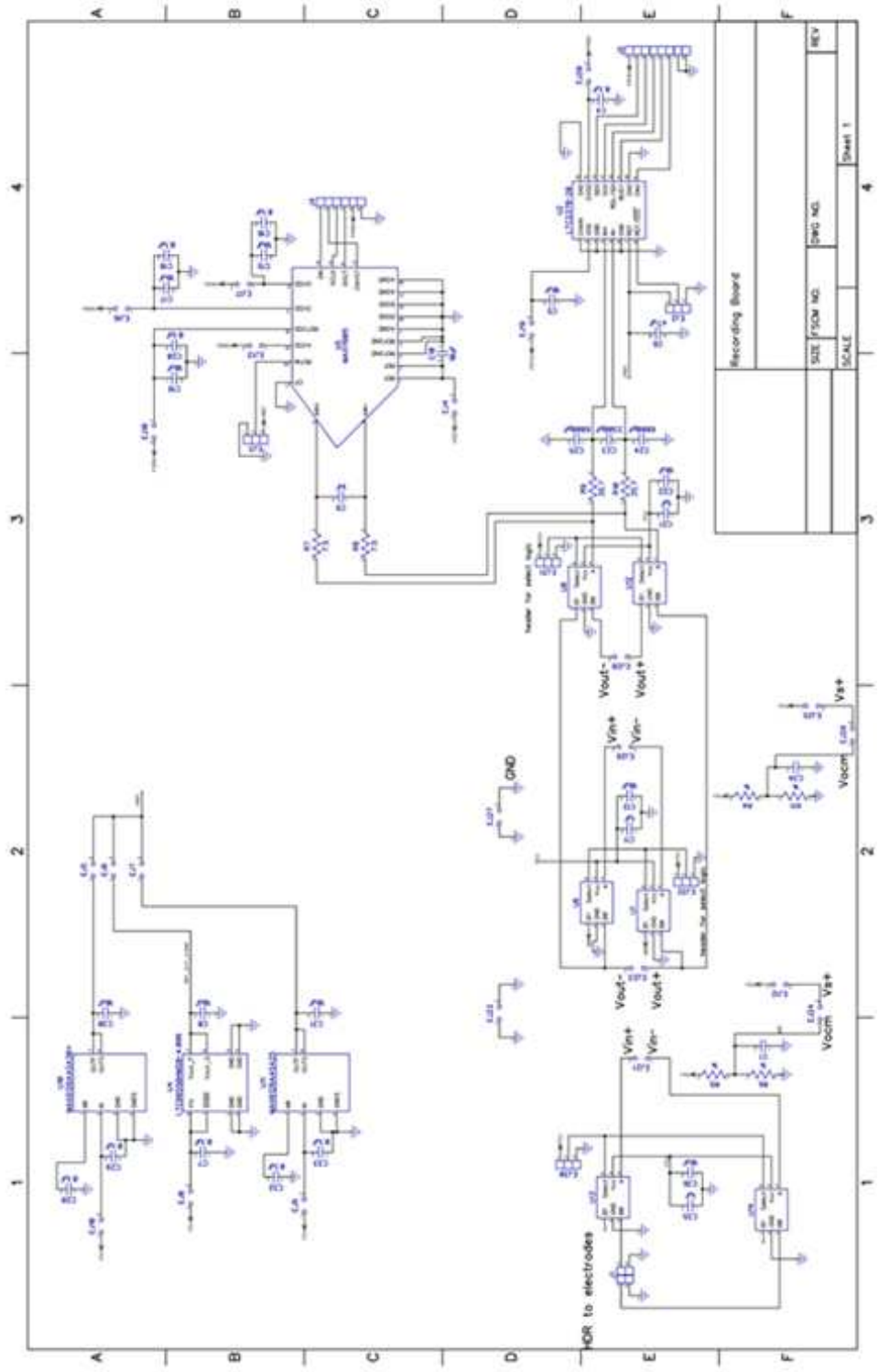

Figure 49: Artifact rejection board schematic 1.

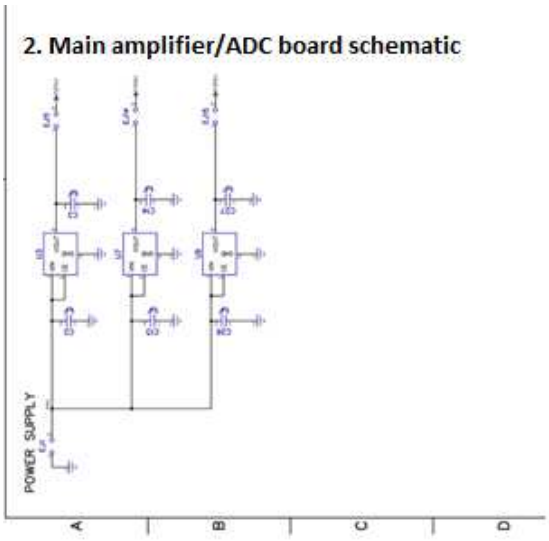

Figure 50: Artifact rejection board schematic 2.

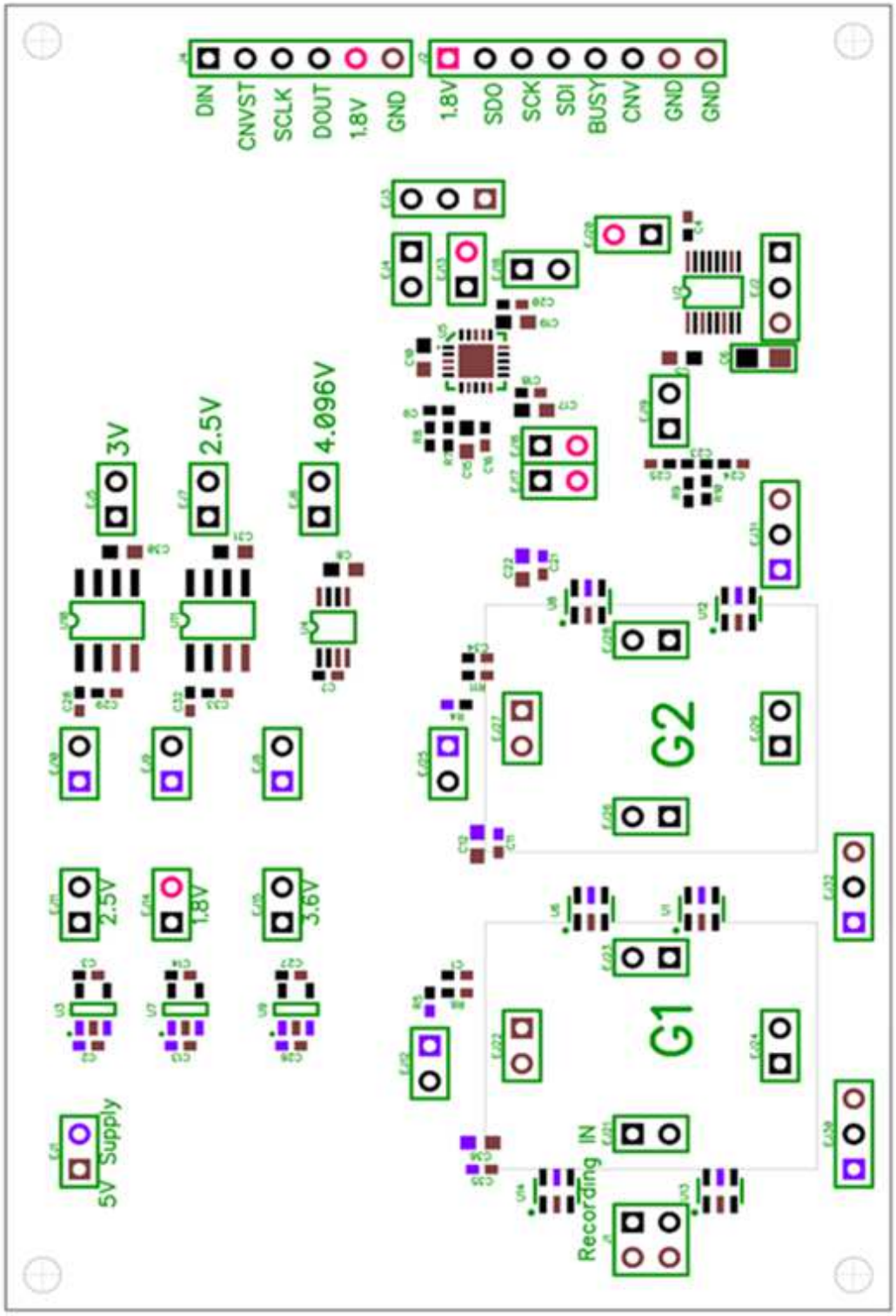

Figure 51: Artifact rejection board layout.

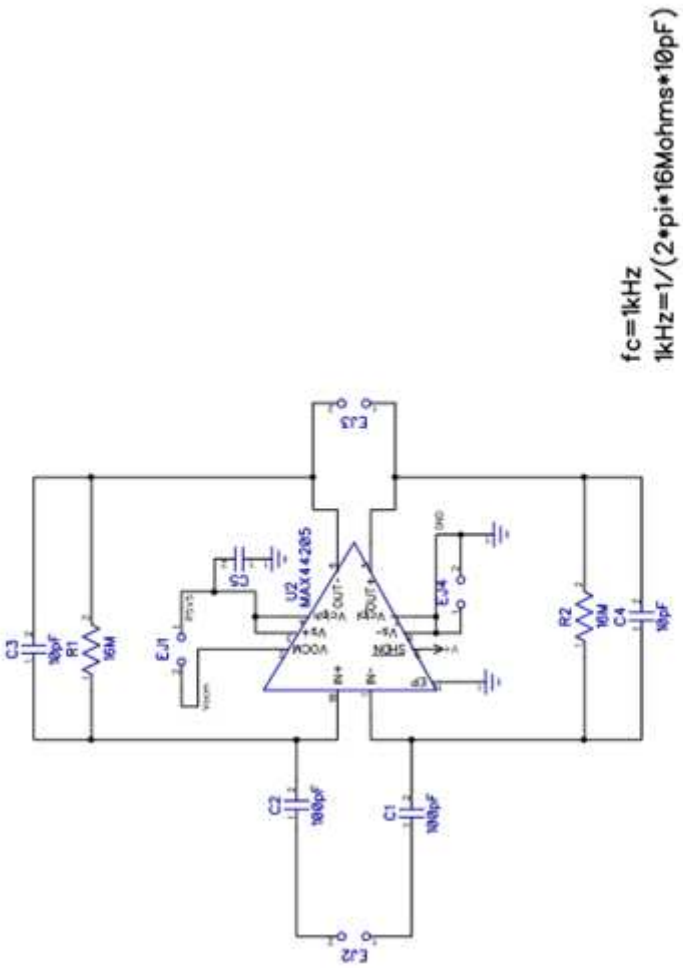

Figure 52: MAX44205 board schematic.

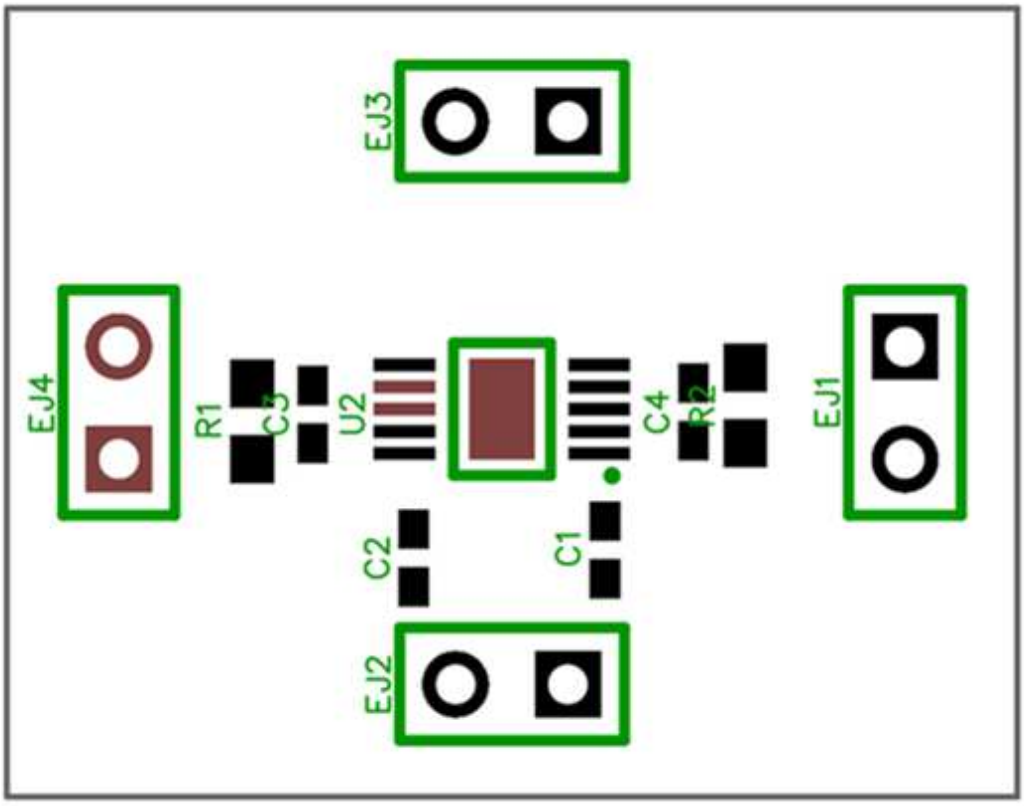

Figure 53: MAX44205 board layout.

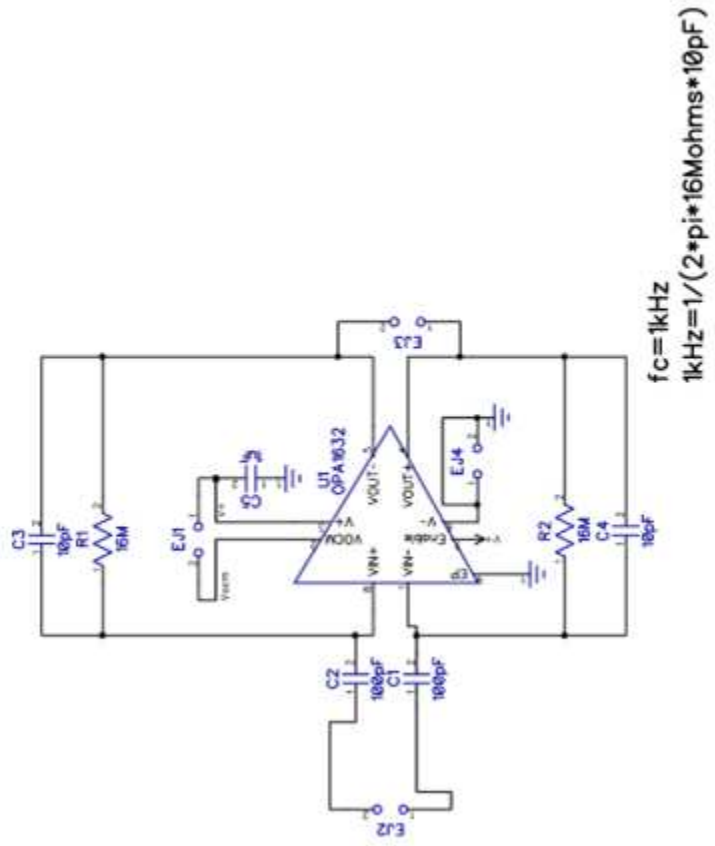

Figure 54: OPA1632 board schematic.

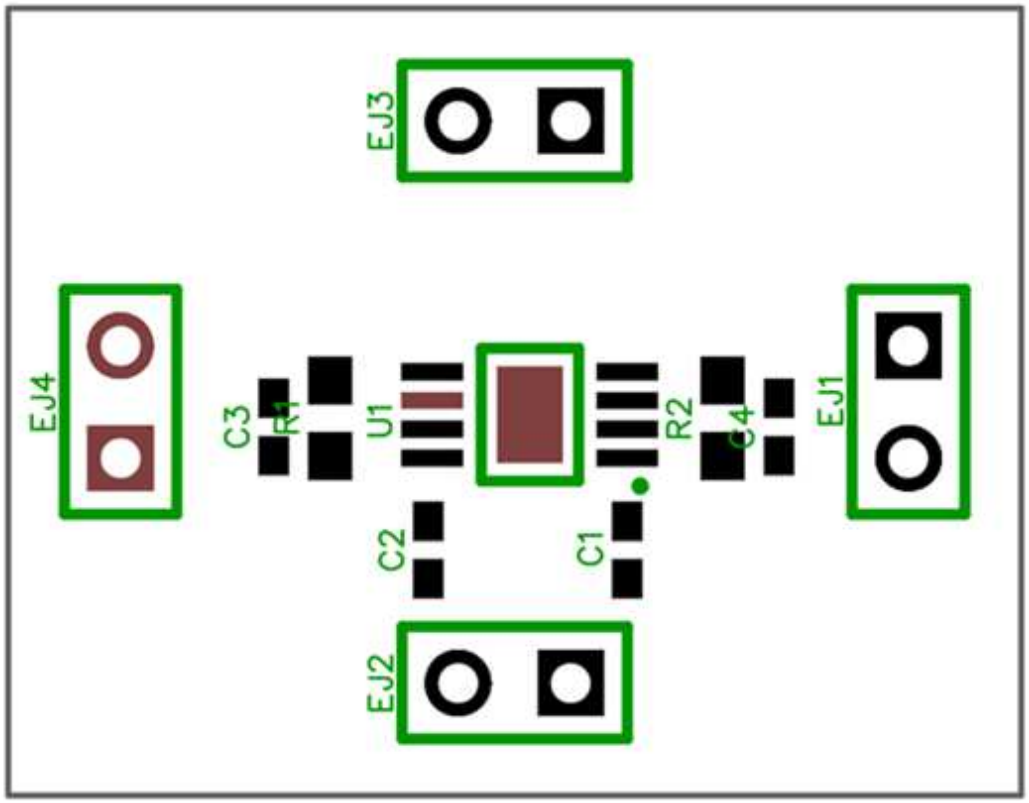

Figure 55: OPA1632 board layout.

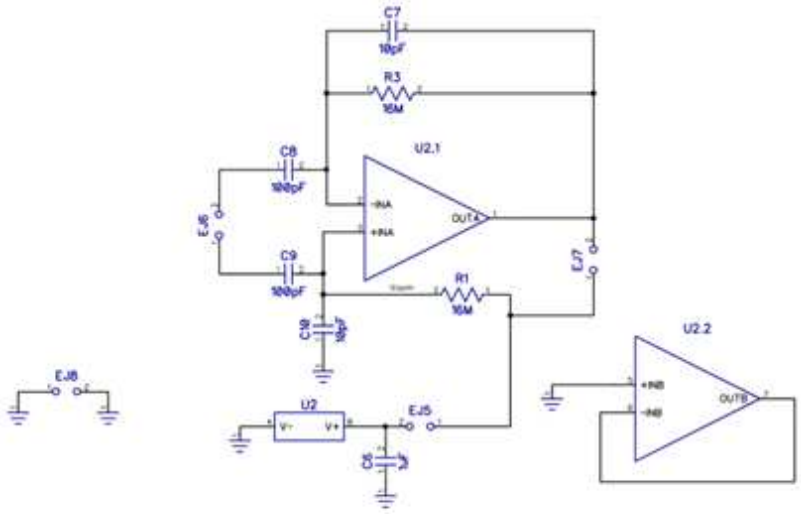

fc=1kHz
1kHz=1/(2•pi•16Mohms•10pF)

Figure 56: LTC6087 board schematic.

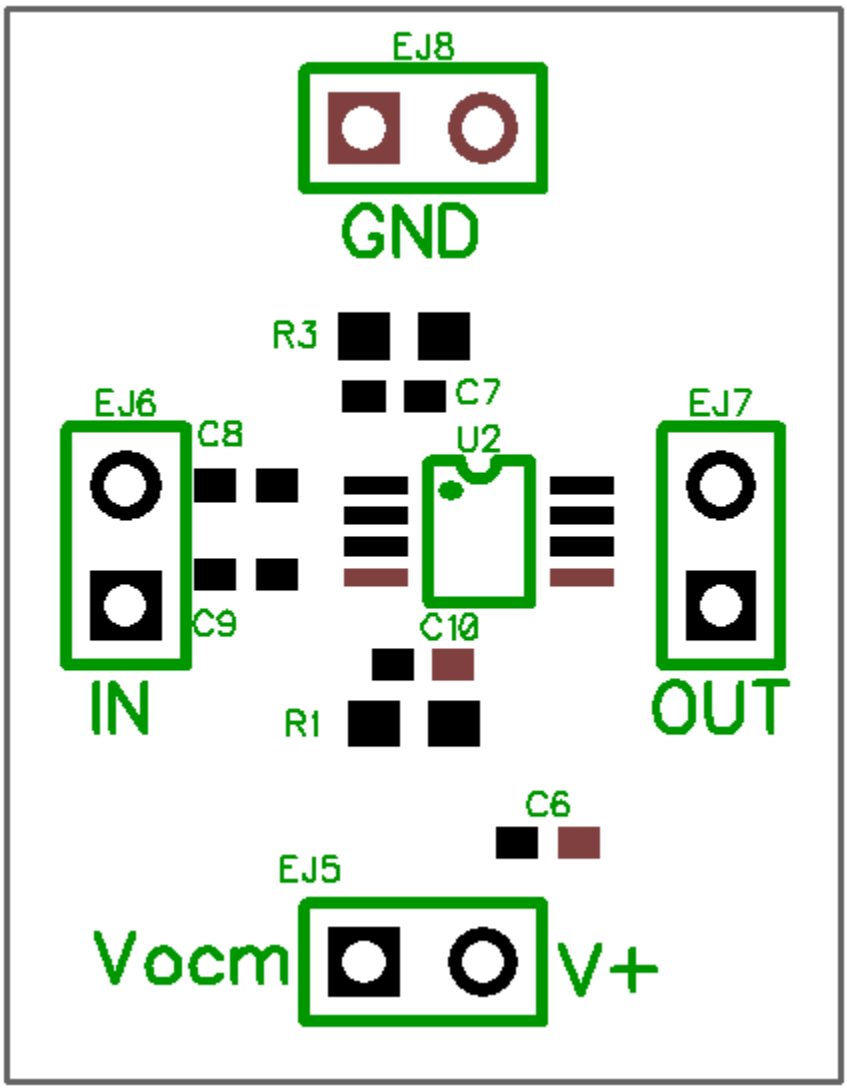

Figure 57: LTC6087 board layout.

Table 8: BOM for artifact rejection board.

RefDes	P/N	Type	Value
C1, C34	587-1227-1-ND	CAP 0402	
C2, C3, C11, C13, C14, C21, C26, C27, C35	490-1320-1-ND	CAP 0402	1uF

C4, C7, C16, C18, C20, C28, C29, C32, C33	587-1227-1-ND	CAP 0402	0.1uF
C5, C8, C10, C12, C15, C17, C19, C22, C30, C31, C36	1276-1119-1-ND	CAP 0603	10uF
C6	490-6469-1-ND	CAP 0805	47uF
C9	490-1303-1-ND	CAP 0402	1nF (1000pF)
C23	1276-1552-1-ND	CAP 0402	3300pF
C24, C25	490-1310-1-ND	CAP 0402	6800pF
EJ1, EJ4, EJ5, EJ6, EJ7, EJ8, EJ9, EJ10, EJ11, EJ12, EJ13, EJ14, EJ15, EJ16, EJ17, EJ18, EJ19, EJ20, EJ21, EJ22, EJ23, EJ24, EJ25, EJ26, EJ27, EJ28, EJ29	header	Jumper	
EJ2, EJ3, EJ30, EJ31, EJ32	header	Jumper 3 Pin	
J1	header	Header 4 Pin	
J2	header	HDR-1x8	
J4	header	HDR-1x6	
R4, R5, R6, R11	P1.0KJCT-ND	RES 0402	1k

R7, R8	P7.5JCT-ND	RES 0402	7.5
R9, R10	P35.7LCT-ND	RES 0402	35.7
U1, U6, U8, U12, U13, U14	NLASB3157DFT2GOSCT-ND	NLASB3157DFT2	
U2	LTC2378IMS-20#PBF-ND	LTC2378-20	
U3	NCP4688DSN33T1G	NCP4688DSN25TCG	
U4	LTC6655BHMS8-4.096#PBF-ND	LTC6655BHMS8-4.096	
U5	MAX11905ETP+-ND	MAX11905	
U7	NCP4688DSN18T1G	NCP4688DMU18TCG	1.8 V
U9	NCP502SN36T1G	NCP502SN36T1G	3.6 V
U10	MAX6126AASA30+-ND	MAX6126AASA30+	
U11	MAX6126AASA25+-ND	MAX6126AASA25	

Table 9: MAX44205 board BOM.

RefDes	Type	Value	P/N
C1, C2	CAP 0402	100pF	709-1123-1-ND
C3, C4	CAP 0402	10pF	399-1011-1-ND
C5	CAP 0402	1uF	490-1320-1-ND
EJ1, EJ2, EJ3, EJ4	Jumper		DNP
R1, R2	RES 0603	16M	P15MGCT-ND

U2	MAX44205		MAX44205AUB+

Table 10: OPA1632 board BOM.

RefDes	Type	Value	P/N
C1, C2	CAP 0402	100pF	709-1123-1-ND
C3, C4	CAP 0402	10pF	399-1011-1-ND
C5	CAP 0402	1uF	490-1320-1-ND
EJ1, EJ2, EJ3, EJ4	Jumper		DNP
R1, R2	RES 0603	15M	P15MGCT-ND
U1	OPA1632		296-17008-ND

Table 11: LTC6087 board BOM.

RefDes	Type	Value	P/N
C1, C2	CAP 0402	100pF	709-1123-1-ND
C3, C4	CAP 0402	10pF	399-1011-1-ND
C5	CAP 0402	1uF	490-1320-1-ND

EJ1, EJ2, EJ3, EJ4	Jumper		DNP
R1, R2	RES 0603	15M	P15MGCT-ND
U2	LTC6087		LTC6087CMS8#PBF-ND

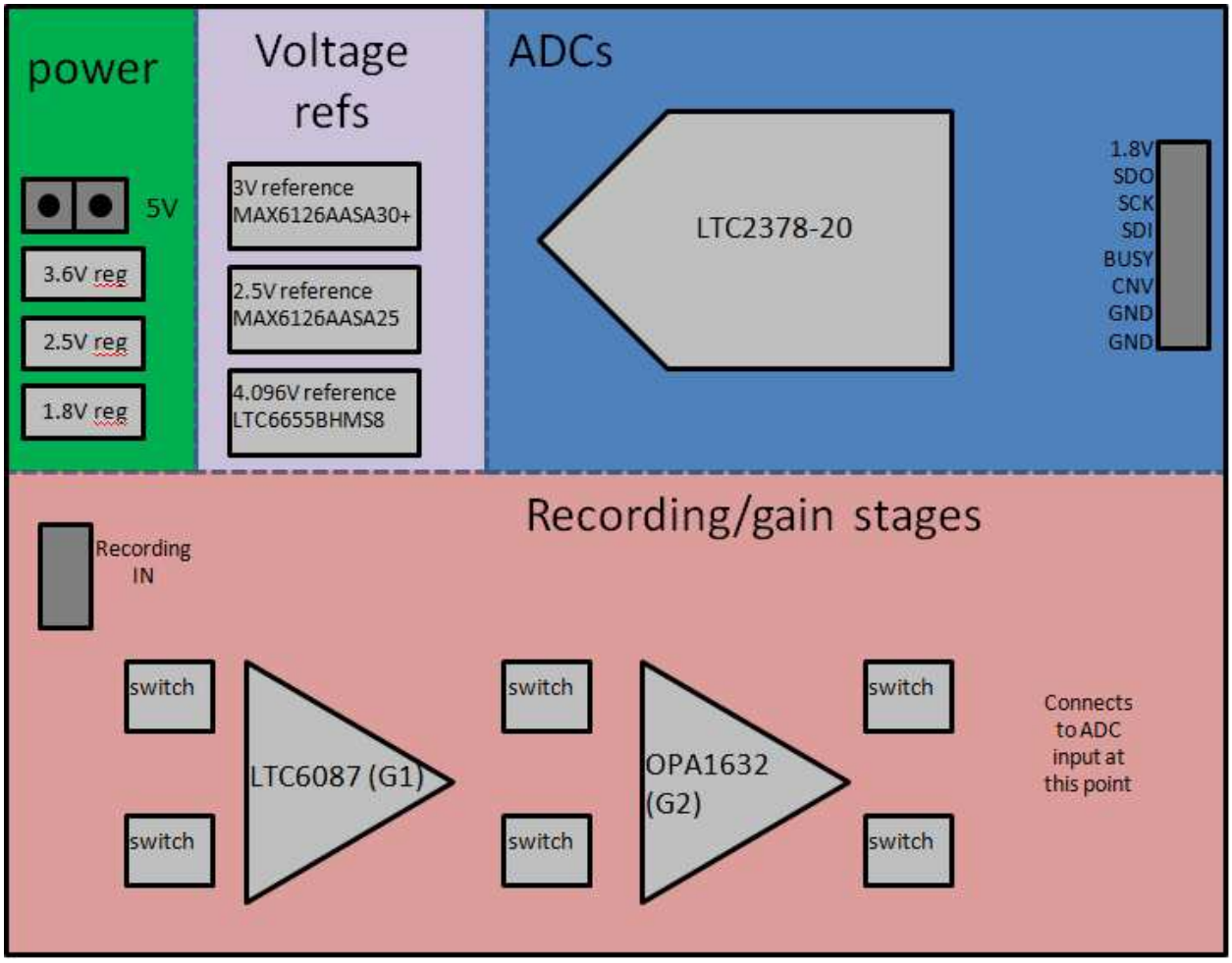

Figure 58: Block diagram of artifact rejection board.

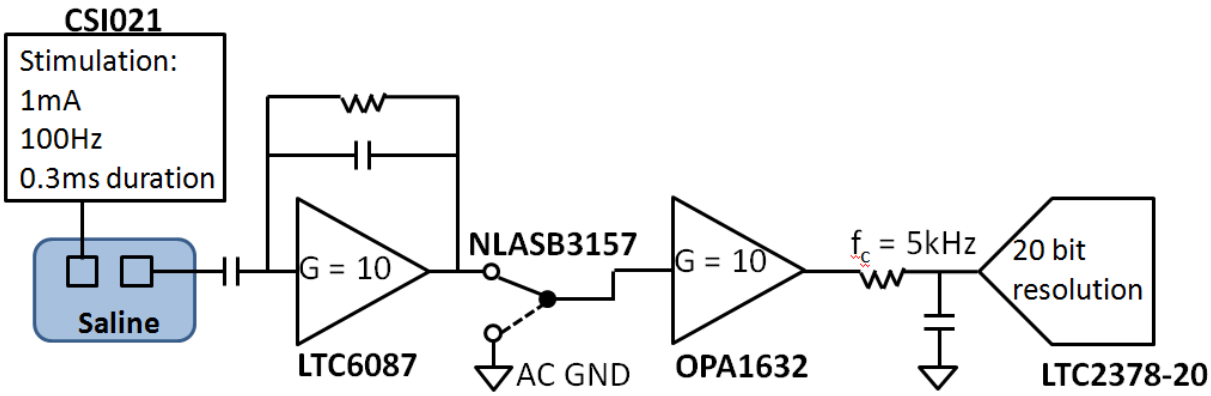

Figure 59: Block diagram of artifact rejection circuitry including stimulation portion of test setup.

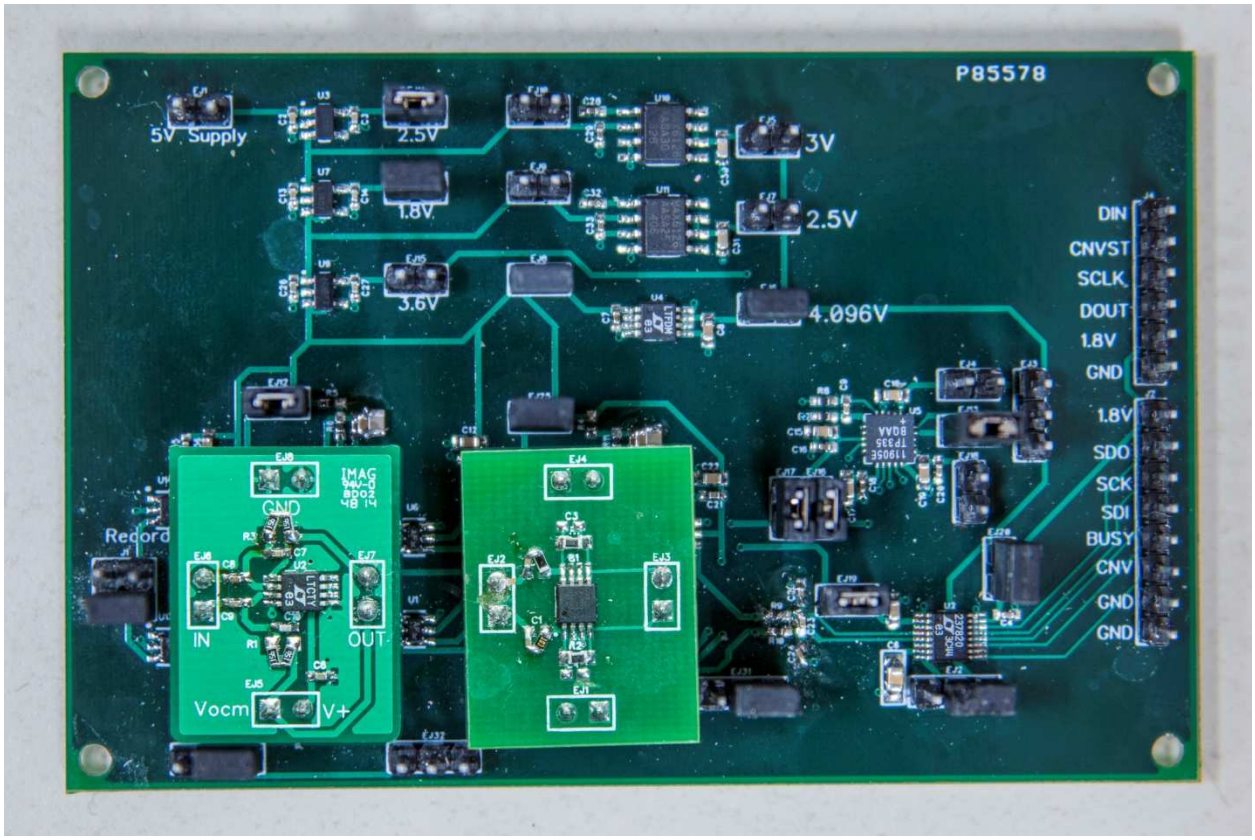

Figure 60: Two-stage artifact rejection board post-fabrication and assembly.

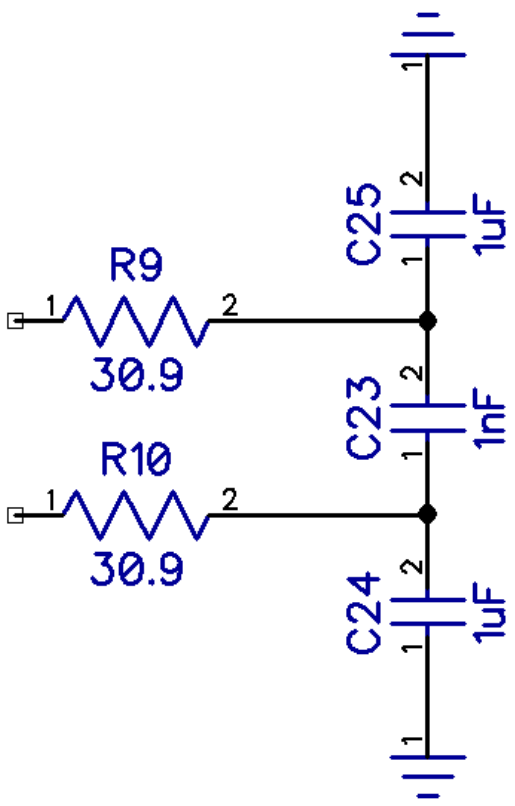

Figure 61: Low pass filter designed to create upper bandwidth of recording, set to capture neural spikes.

Table 12: Pin mapping for header on the XMEGA evaluation board.

Pin number (XMEGA)	Port (for coding uses)	Function(mapping to main board)
Pin1	PC0	CLK
Pin3	PC2	BUSY
Pin7	PC6	MISO
Pin8	PC5	SCK

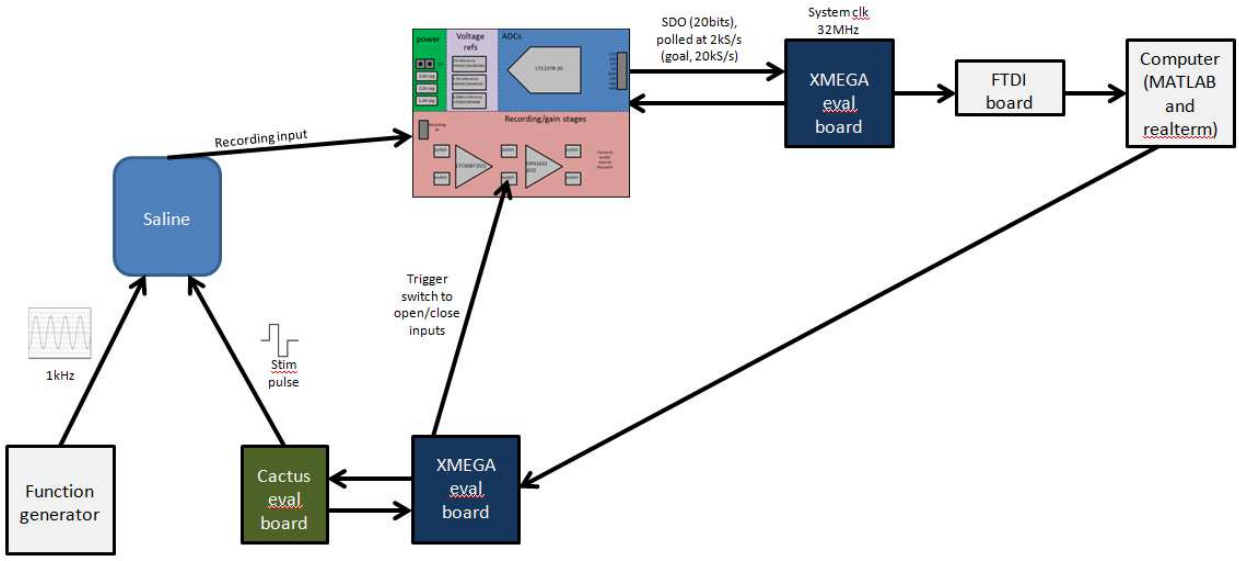

Figure 62: Artifact rejection board test setup to examine the response time resulting from artifact blanking. The setup includes the microcontrollers used to set the stimulation parameters and read the ADC data.

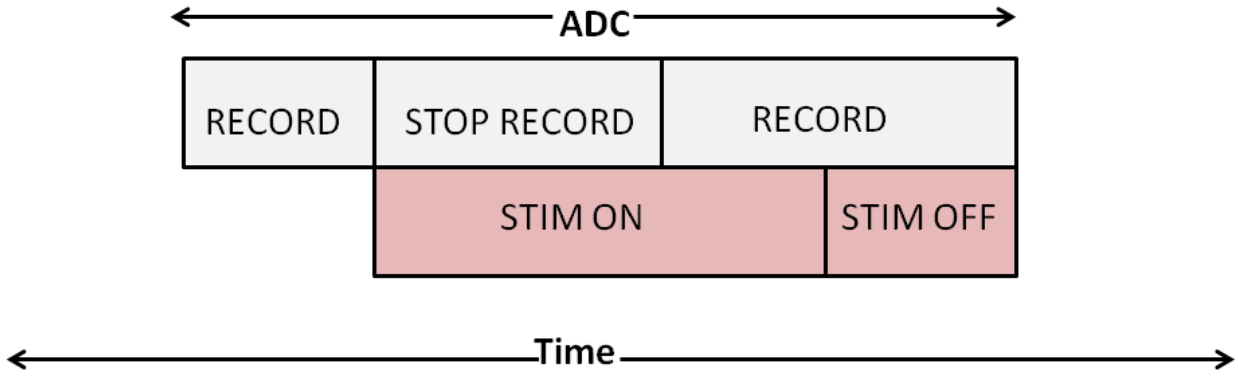

Figure 63: Timing diagram for data collection during board testing using the ADC.

Figure 64: Electrode used for in vitro stimulation and recording during lowered gain testing and blanking.

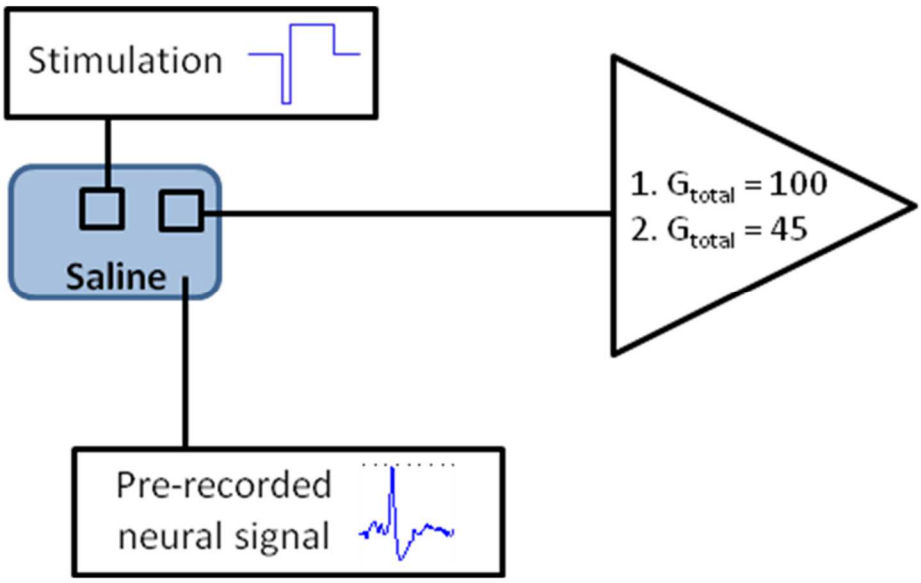

Figure 65: Test setup for lowering gain to avoid amplifier saturation.

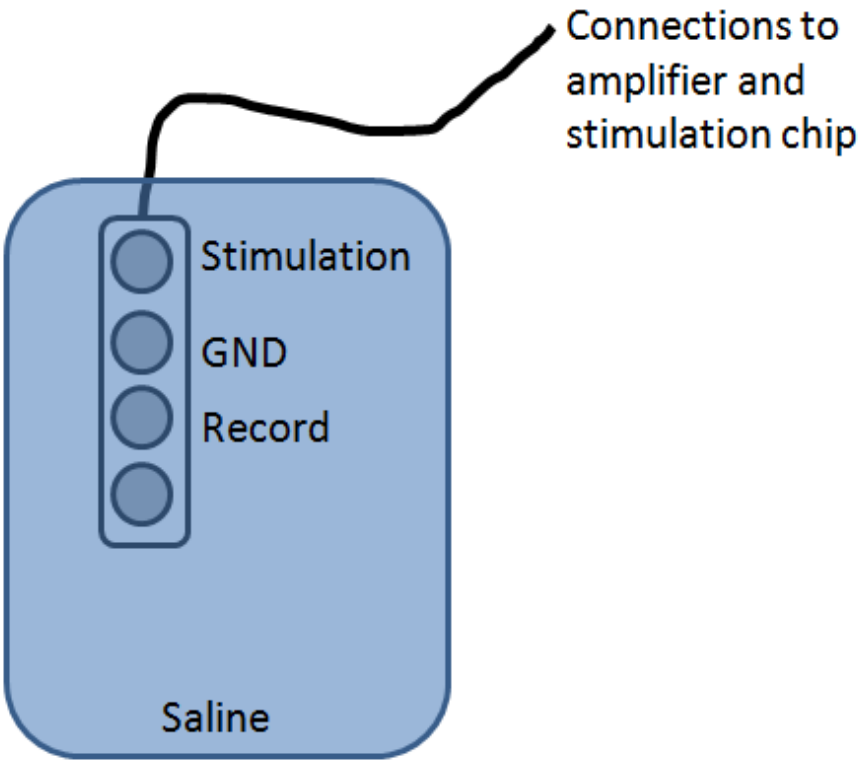

Figure 66: Electrode placement in the saline and connections used for the testing.

Appendix C: Artifact rejection amplifier IC board testing support material

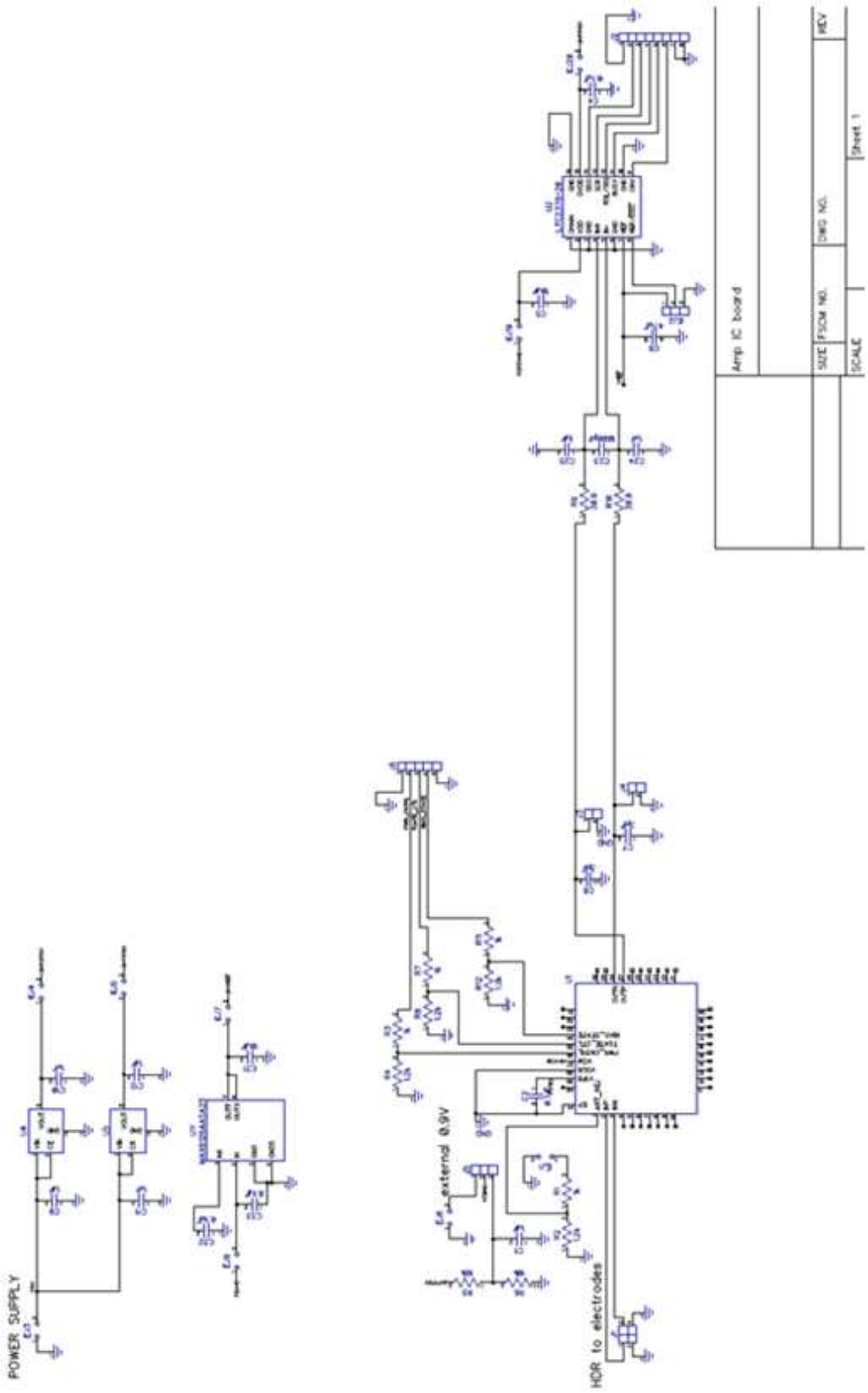

Figure 67: Updated schematic to test artifact rejection IC.

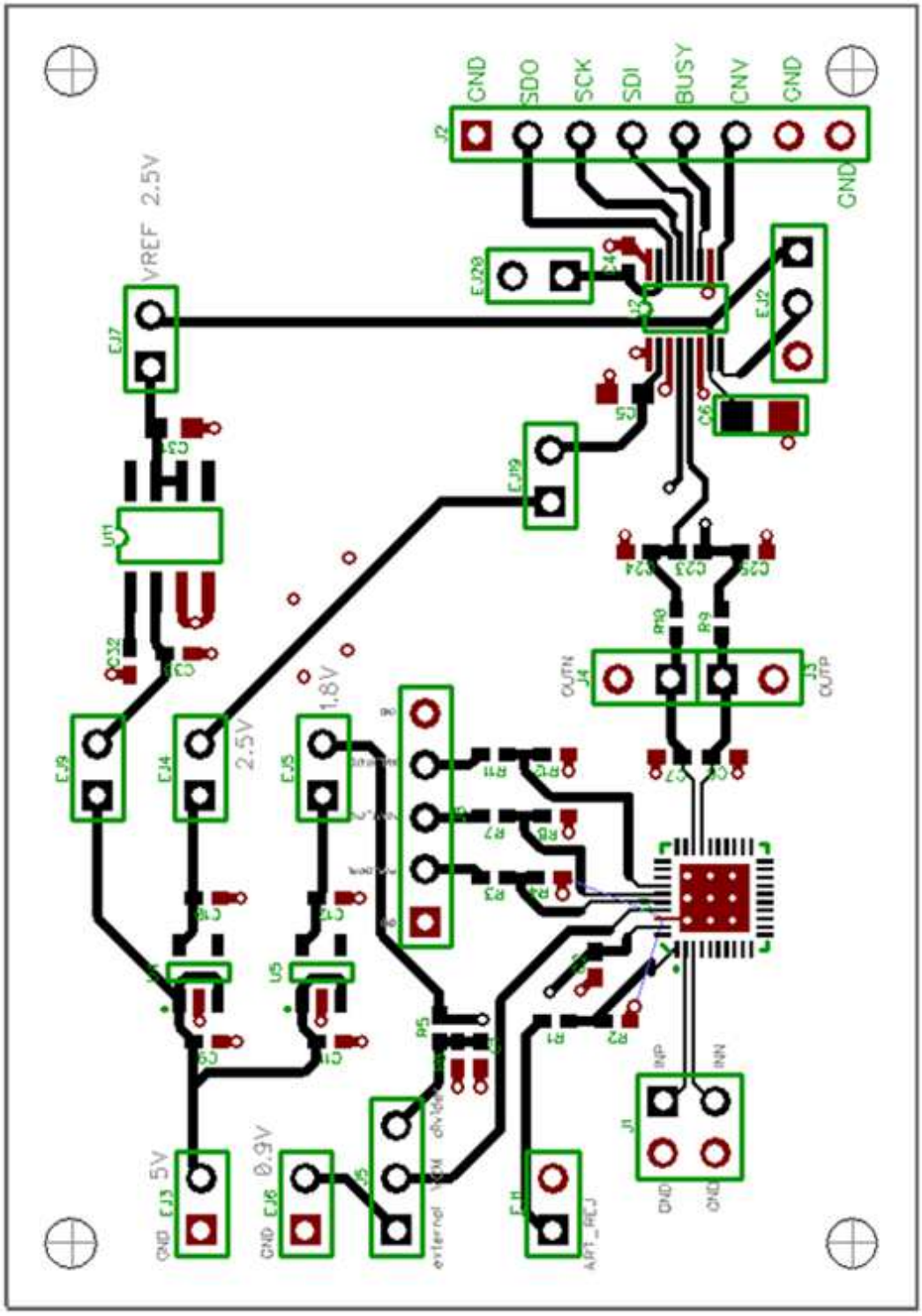

Figure 68: Updated layout to test artifact rejection IC.

Table 13: Updated PCB BOM to test Artifact Rejection Amplifier IC.

RefDes	P/N	Type	Value
C1, C9, C10, C11, C12, C24, C25	490-1320-1-ND	CAP 0402	1uF
C2, C4, C32, C33	587-1227-1-ND	CAP 0402	0.1uF
C5, C31	1276-1119-1-ND	CAP 0603	10uF
C6	490-6469-1-ND	CAP 0805	47uF
C7, C8	712-1283-1-ND	CAP 0402	3.3pF
C23	490-1303-1-ND	CAP 0402	1000pF
EJ1, EJ3, EJ4, EJ5, EJ6, EJ7, EJ9, EJ19, EJ20	header	Jumper	
EJ2	header	Jumper 3 Pin	
J1	header	Header 4 Pin	
J2	header	HDR-1x8	
J3, J4	header	HDR-1x2	
J5	header	HDR-1x3	
J6	header	HDR-1x5	
R1, R3, R7, R11	P1.0KJCT-ND	RES 0402	1k
R2, R4, R8, R12	P1.2KDBCT-ND	RES 0402	1.2k
R5, R6	541-10.0KABCT-ND	RES 0402	10k
R9, R10	P30.9HTR-ND	RES 0402	30.9
U1		Artifact Rejection IC	

U2	LTC2378-20	LTC2378-20	
U4	NCP4688DSN25TCG	NCP4688DSN25TCG	2.5V
U5	NCP4688DMU18TCG	NCP4688DMU18TCG	1.8V
U11	MAX6126AASA25	MAX6126AASA25	2.5V

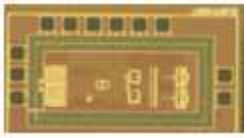

Figure 69: Picture of the artifact rejection amplifier IC.

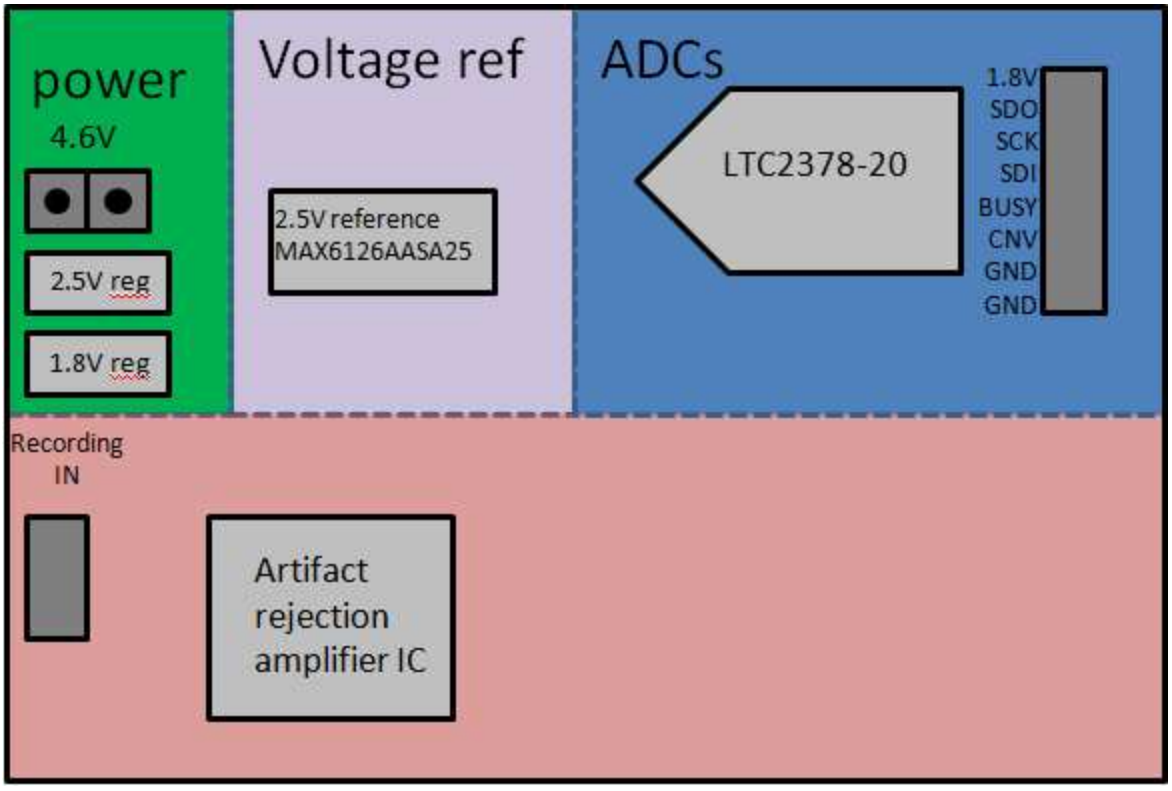

Figure 70: Block diagram of updated board to include the artifact rejection amplifier IC instead of off the shelf recording parts.

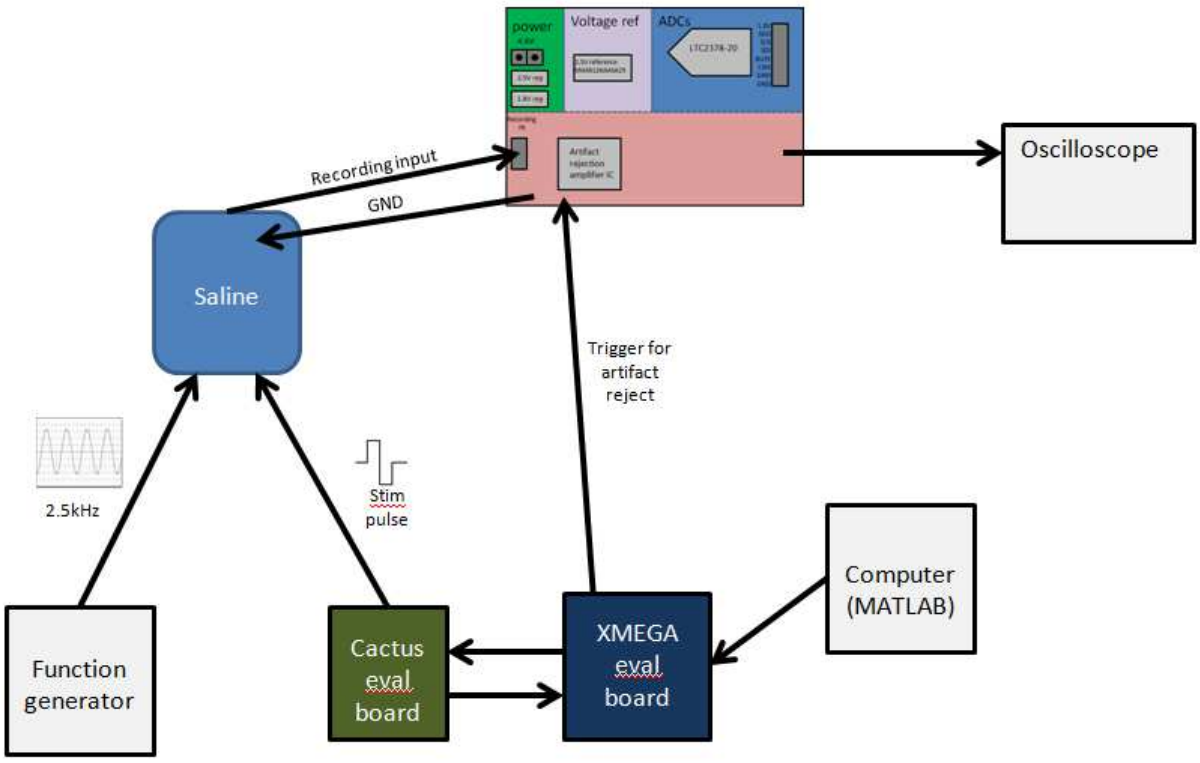

Figure 71: Test setup to examine the ability of the artifact rejection amplifier IC to reduce artifacts using blanking.

Appendix D: MATLAB Processing Code

```
clear all; clc; close all;
read_Intan_RHD2000_file;
CH0 = amplifier_data(1,:);      %CH0 data
% CH1 = amplifier_data(2,:);      %CH1 data
Fs = 20000;                     % Sampling frequency
T = 1/Fs;                       % Sample time
L = length(CH0);                % Length of signal
t=(0:L-1)*T;
figure (1)
plot(t, CH0)
```

```
xlabel('Time (s)')
ylabel('Amplitude (uV)')
title('Recording on CH0')
NFFT = 2^nextpow2(L);           % Next power of 2 from length of y
Y = fft(CH0,NFFT)/L;
f = Fs/2*linspace(0,1,NFFT/2+1);
mag=2*abs(Y(1:NFFT/2+1));
figure (3)
loglog(f,2*abs(Y(1:NFFT/2+1)))
title('FFT of single ended recording on CH0')
xlabel('Frequency (Hz)')
ylabel('|Y(f)|')
```